2017

Shear Stress Modulates Gene Expression in Normal Human Dermal Fibroblasts

Zabinyakov, Nikita

UNIVERSITY OF CALGARY

Shear Stress Modulates Gene Expression in Normal Human Dermal Fibroblasts

by

Nikita Zabinyakov

A THESIS

SUBMITTED TO THE FACULTY OF GRADUATE STUDIES

IN PARTIAL FULFILMENT OF THE REQUIREMENTS FOR THE

DEGREE OF MASTER OF SCIENCE

GRADUATE PROGRAM IN BIOMEDICAL ENGINEERING

CALGARY, ALBERTA

JANUARY 2017

Abstract

Applied mechanical forces, such as those resulting from fluid flow, trigger cells to change their functional behavior or phenotype. However, there is little known about how fluid flow affects fibroblasts. The hypothesis of this thesis is that dermal fibroblasts undergo significant changes of expression of differentiation genes after exposure to fluid flow (or shear stress). To test the hypothesis, human dermal fibroblasts were exposed to laminar steady fluid flow for 20 and 40 hours and RNA was collected for microarray analysis. Gene expression data was processed using gene network analysis, pathway analysis, and gene functional analysis with comparison to data from publicly available data sets. Additional treatment with PI3K/mTOR pathway inhibitor, PI-103, was performed to evaluate pathway involvement in flow modulation of gene expression. Results from overall transcription analysis demonstrated that fluid flow modulated many genes in fibroblasts including those related to differentiation, development and TGF-β pathway regulation.

Acknowledgments

I would like to express my respect and gratitude for my supervisor Dr. Kristina D. Rinker for her advice, suggestions, guidance and encouragement throughout my research. I would also like to thank the members of my thesis committee, Dr. Roman Krawetz, and Dr. Derrick Rancourt, for their great input and feedback during our meetings. Special thanks to Dr. Deborah Studer for being always a remarkably patient and understanding mentor and for her time spent helping me with the research design and methodology. I am thankful to Dr. Robert Shepherd for the training and guiding me through time- and labor-consuming lab techniques.

Moreover, I want to recognize program director, Dr. Michael Kallos, and program coordinator, Lisa Mayer for their help in receiving administrative and financial support.

Finally, to my friends and colleagues from Cellular and Molecular Bioengineering Research Lab, Maria Juliana Gomez, Christopher Sarsons, Linda Tamez, Hagar Labouta, and Kenneth Fuh for backing me up along the way.

Table of contents

List of Tables

List of Figures

List of Symbols, Abbreviations, Nomenclatures

5-AZA	5- Azacitidine
7C, 9C	7 compound or 9 compound medium
AA	Acetic acid
ACTA2	Alpha smooth muscle actin
ADM	Adrenomedullin
AKT	Protein kinase B (PKB)
BMP4	Bone morphogenetic protein
BRN4/POU3F4	Protein coding gene POU Class 3 Homeobox 4
C.AM	Calcein, AM
CAV1	Caveolin 1
CD1	Cluster of differentiation 1
CDH1	Cadherin 1
cDNA	Complementary DNA
CDS	Coding sequence
CM	Cardiomyocytes
CO_2	Carbon dioxide
COL1A1	Protein coding gene Collagen Type 1 Alpha 1
COX-2	Prostaglandin-endoperoxide synthase 2
CPDB	ConsensusPathDB-human
cTnT	Troponin T
DMEM	Dulbecco's Modified Eagle Medium
DMSO	Dimethyl sulfoxide
DNA	Deoxyribonucleic acid
E47/TCF3	Transcription Factor 3
EC	Endothelial cells
ECM	Extra-cellular matrix
EDTA	Ethylenediaminetetraacetic acid
EMT	Epithelial–mesenchymal transition
ERK	Extracellular signal-regulated kinases
ESC	Embryonic stem cells
FASTA	Bioinformatics text-based format
FB	Fibroblasts
FBS	Fetal bovine serum
FGM	Fibroblast Growth Medium
GATA4	Protein coding gene GATA Binding Protein 4
GEO	Gene Expression Omnibus (GEO), a database repository
GFP	Green fluorescent protein
GO:BP	Gene Ontology: Biological Process
GOI	Gene of interest
GTM	GATA4, TBX5, MEF2C
IL-1	Interleukin-1
iPSC	Induced pluripotent stem cells
ITGA2	Integrin, Alpha 2 (CD49B, Alpha 2 Subunit of VLA-2 Receptor)
KIT	KIT Proto-Oncogene Receptor Tyrosine Kinase
KLF4	Protein coding gene Kruppel-like factor 4

KROX20	Early growth response protein 2 (EGR2)
L929	Mouse C3H/An connective tissue L929 cell line
LIF	Leukemia inhibitory factor
LIN28	RNA-binding protein Lin-28 Homolog A
MAPK	Mitogen-activated protein kinases
ME2016	Microsoft Excel 2016
MEF2C	Protein coding gene Myocyte Enhancer Factor 2C
MET	Mesenchymal–epithelial transition
MMP	Matrix metalloproteinases
MSC	Mesenchymal stem cells
mTOR	Mechanistic target of rapamycin
NADPH	Nicotinamide adenine dinucleotide phosphate
NANOG	Transcription factor NANOG
NF-kB	Nuclear factor kappa-light-chain-enhancer of activated B cells
NHDF	Human normal dermal fibroblasts
NK	Natural killers
NOX4	NADPH oxidase 4
OCT4	Protein coding gene Octamer-binding transcription factor 4
OKSM	OCT4, KLF4, SOX2, NANOG
PBS	Phosphate-buffered saline
PMMA	Polymethylmethacrylate
PDGFRA	Platelet-derived growth factor receptor α
PDMS	Polydimethylsiloxane
PEGS-1	Prostaglandin E synthase
PFA	Paraformaldehyde
PI	Propidium iodide
PI3K	Phosphatidylinositol-4,5-bisphosphate 3-kinase
PM	Personalized medicine
PRL13A	Housekeeping gene PRL13A
PRLP0	Gene encodes 60S acidic ribosomal protein P0
PSC	Pluripotent stem cells
PSCLP	Patient-specific cell line production
PTX3	Pentraxin-related protein PTX3, TNF-inducible gene 14 protein (TSG-14)
qPCR	Real-time polymerase chain reaction
RIN	RNA integrity number
RNA	Ribonucleic acid
ROCK	Rho-associated protein kinase
ROS	Reactive oxygen species
RPOL2A	DNA-directed RNA polymerase II subunit RPB1, also known as RPB1
RUNX2	Runt-related transcription factor 2
SB431542	Inhibitor of the activin receptor-like kinase (ALK) receptors
SCX	Basic helix-loop-helix transcription factor scleraxis
SD	Standard deviation
SEM	Standard error of the mean
SMAD2/3	Mother against decapentaplegic homolog 2/3
SMC	Smooth muscle cells

SNAI1	Snail Family Zinc Finger 1
SOX4	Transcription factor SRY (sex determining region Y)-box 4
SRY	Sex-Determining Region Y
SSB	Stirred suspension bioreactor
TBX5	Protein coding gene T-Box 5
TFR	Transferrin receptor
TGFBR3	TGF-β receptor 3
TGF-β	Transforming growth factor beta
UV	Ultraviolet
c, φ	Concentration
D	Diffusion coefficient
Q	Volumetric flow rate
μ	Fluid viscosity
P	Permeability
τ	Shear stress
χ	Position, the dimension of which is length
ω	Channel width

Chapter 1. Introduction

Cell trans-differentiation techniques bear significant potential for converting terminally differentiated cells into cells of a different origin. Theoretically, under the influence of certain factors and manipulations, any cell type (A) can be transformed into any other cell type (B) and vice versa. Practically, the ability of some cell types is higher than others in this regard. While some cell types are relatively easy to harvest and expand, other ones are not. Thus, some cell types are utilized to increase their potential value for further implications. For example, fat tissue–derived mesenchymal stem cells are widely used for regenerating cartilage and ligament cells [1], keratinocytes are employed to obtain nerves [2], and fibroblasts are used in the generation of induced pluripotent stem cells [3,4]. Unfortunately, the methodology of cell line production contains many disadvantages. The cell yield of trans-differentiation techniques is relatively low. Purification requires many different medium compositions and frequent routine medium changes that result in impairment of scale-up production and increased cost. Viral transfection methods are currently inappropriate for human therapeutic purposes. Therefore, new paths and efficient practices of cell generation are an active area of research.

Fluid flow exposure is a relatively simple yet effective approach to modulate cell function that may be able to help address these issues. This approach may become a valuable tool to prevail some of the disadvantages and increase the efficacy of cell line trans-differentiation techniques. It was demonstrated that application of shear stress to murine embryonic stem cells modulated and maintained expression of genes responsible for pluripotency [5,6]. Hypothetically, if shear stress or mechanical stimuli modulate pluripotency then they might also be capable of modulating de-, re- or trans-differentiation. However, the literature does not provide the evidence of how shear stress could affect the potential of fibroblasts to differentiate.

The cell type of normal human dermal fibroblasts were chosen for this work because they satisfy the criteria to be considered for de-differentiation based on the existing literature. Criteria were as follows: 1) cell line subjected to shear stress (fluid flow) must be responsive to flow and possess a significant plasticity to de-differentiate, 2) cell type should be easy to grow and expand in culture, and 3) cell acquisition should be the least invasive from its residing site in the body. Thus, the hypothesis is formulated below based on found scientific gap, appropriate fluid flow subject, and practical approach and perspective application.

1.1. Hypothesis.

The hypothesis was formulated as following: shear stress modulates gene expression, including expression of differentiation genes, in normal human dermal fibroblasts. This hypothesis addresses some remarks that were not fully elucidated in the literature:

1) Dermal fibroblasts are subjected to low levels of fluid flow, interstitial flow, under normal conditions. Although the level of shear stress may increase in the site of injury (for more information refer to section 5.1.), it is unknown if higher levels of shear stress would induce genes involved in differentiation without causing cell detachment.

2) The large scale gene expression study of gene expression profile of flow-induced fibroblasts is not available.

3) Although fibroblasts were used in many flow models and modulation of various responses was highlighted, modulation of de-differentiation by flow was not found to be reported yet (refer to Table 1 in section 2.4.).

4) Which signaling pathways are involved if fluid flow modifies the phenotype of fibroblasts? Literature suggests that shear stress modulates TGF-β pathway. Previous studies also reported PI3K/AKT pathway involvement in flow modulation of gene expression.

1.2. Thesis Objective.

Three objectives were derived from statements above. Each objective refers to one of the main sections from Results chapter:

1) Establish a flow protocol to expose normal human dermal fibroblasts (NHDFs, FBs) to fluid flow and evaluate its effect on cell morphology and viability – Section 4.1.

2) Perform a microarray study and analyze the expression of genes of interest – Section 4.2.

3) Evaluate the mechanism of flow-induced expression by treating fibroblasts with PI-103, a dual PI3K/AKT/mTOR pathway inhibitor – Section 4.3 (for additional information refer to section 5.6.).

1.3. Thesis Overview.

Chapter 2 provides a literature background of key aspects of the project. The potential impact in the field of cell therapies, methods of FB differentiation into a different cell type, the reason of FBs utilization and their plasticity regarding similarities with mesenchymal stem cells, FB role in physiological processes in the body and their response to mechanical stimuli are observed in Chapter 2. Methods and materials are provided in Chapter 3. Specifically, routine procedures of cell seeding, passaging, and expansion, cell transfer from the plastic surface onto glass slides, set-up of parallel plate flow chamber, sample selection, qPCR, primer design, $2^{-\Delta\Delta C_T}$

analysis, microarray analysis, GO category and pathway analysis, and data set comparison from GEO repository. Chapters 4 and 5 include results and discussion, leaving some of the questions open for future work. Additional information is presented in the Appendix.

Note. Name of human genes are spelled out in all capital letters (e.g. SMAD3), and rodent gene names are in lowercase with the first letter in uppercase (Nox4). Generic gene names without specifying species are presented with all capital letters. Proteins are presented with their assigned names in a traditional way (e.g. GFP, Bmp4).

Chapter 2. Background and Literature review

Dermal fibroblasts are easily obtained and retain enough plasticity to be reprogrammed and are responsive to mechanical stimuli, such as shear stress. Fluid flow (or shear stress) possesses significant potential to improve existing techniques of fibroblast reprogramming. This would be advantageous for future applications, such as cell therapy for personalized medicine and drug-screening platforms. The idea of cell production through de-differentiation is not new. Nonetheless, it has many roadblocks, which require new efficient and improved approaches.

2.1. Production and expansion of cell lines through de-, re- and trans-differentiation.

Cell potency or potential for differentiation is the capability of a cell to differentiate into specialized cell types, including terminally differentiated cells. Cells undergo different stages of potency during their development. Totipotent cells originate from a zygote and can form a complete organism. Cells from a zygote remain totipotent during first few divisions only and lose some of their potential with the formation of the three germ layers. At this stage, cells possess the ability to differentiate into any cell of three germ layers and are called pluripotent. The difference between totipotent and pluripotent cells is that the former can form both placenta and embryo, while the latter participate in embryo development only. Pluripotent cells are true stem cells (PSCs – pluripotent stem cells) and characterized by three main properties: self-renewal, differentiation, and the absence of specialization. Less potency is assigned to multipotent cells. This type of cells can differentiate mostly within their germ layer of origin. Oligopotent cells form only a few cell types, e.g. lymphoid line within blood cell lineage. Unipotent cells are restricted to produce one cell type only e.g., adipose tissue progenitors and epithelial progenitors. The main difference between unipotent stem cells and terminally differentiated ones is self-renewal properties of stem

cells. During self-renewal cell may undergoes one of three paths as following: (1) one stem cell divides into two daughter stem cells without specialized properties, (2) one stem cell divides into one stem cell and one specialized cell or progenitor, (3) one stem cell divides into two specialized cells or progenitors. Path selection is determined by cell fate and is based on a number of internal and external cell communication signals. Normally, only terminally differentiated cells are produced during cell proliferation while self-renewal may give rise to both unspecialized stem cells and specialized ones [7].

Conrad Hal Waddington, the British developmental biologist, created a series of diagrams and presented the concept of epigenetic landscape. One of his modified drawings, created in 1957, is demonstrated in Figure 1. The landscape is a metaphor representing embryonic development. The landscape consists of 'hills' and 'valleys' or grooves and slopes. Small balls or marbles are rolling down towards the spectator's view and stop at the lowest point. So, it represents cell developmental path coordinated by diverse orchestrated signals and communications [8,9].

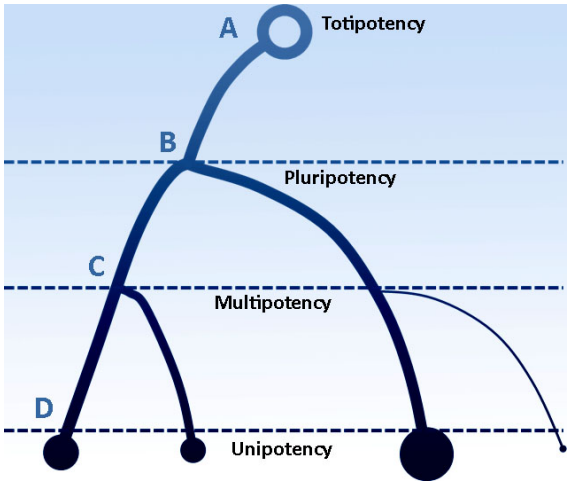

Figure 1. Conrad Hal Waddington's classical epigenetic landscape. In the original landscape, marble or cell is held at the highest point (A) with assigned totipotent properties. As it starts to roll down the hill, it approaches the first stop (point B) where it is pushed to choose its fate towards differentiation into one of three germ layers. After crossing point B, the potential of a cell to differentiate into a cell of different germ layer decreases significantly. The second stop (point C) defines multipotency of a cell. Crossing point C will make it harder for the cell to differentiate into a cell of a different

tissue within the germ layer of the same origin, and even harder to differentiate into a cell of another germ layer. At the lowest point (D), the cell remains unipotent.

The term ‘terminally differentiated’ indicates that a certain cell has reached its developmental potential to be able to proliferate without producing progenitor cells. In fact, not every terminally differentiated cell turns off its potency entirely. Differentiation of one specialized cell type into another one is called trans-differentiation. Although trans-differentiation is a naturally occurring process and is common for the living organism, it is usually activated under certain conditions. For example, cardiac fibroblasts keep their fibroblastic state until heart tissue is damaged. Cardiac FBs within the site of injury become activated and transdifferentiate into contractile cardiomyocytes (CMs) to restore the loss of function. The efficiency of this process is less than 5% in the case of mending heart tissue [10].

Trans-differentiation according to epigenetic landscape concept follows: if the landscape with a marble at point D, Figure 1, is exerted by external force, e.g. landscape is tilted to the right-hand side, the marble moves to point E. Naturally, cells transdifferentiate in the boundaries of similar cell types within the germ layer of origin. The main reason for that is to prevent a possible cell malfunction such as unstoppable division. Thus, a balance of different signaling pathways controls it. For instance, fibroblasts can undergo osteogenesis or chondrogenesis and transdifferentiate into osteocytes or chondrocytes respectively [11]. However, as the current literature suggests, they may never become FB-derived blood cells.

Specialized cells, however, can be redirected to change their phenotype and increase potency. This process is called de-differentiation. De-differentiation leads to the production of pluripotent or multipotent cell lines from unipotent or specialized cells. They are induced pluripotent stem cells – iPSCs. Takahashi and Yamanaka demonstrated the first successful

transformation of murine fibroblasts into iPSCs in 2006 [3,4]. They showed that overexpression of four transcription factors was sufficient to reprogram FBs, which are considered a terminally differentiated cell type, into ESC-like cells or iPSCs [3,12]. Yamanaka introduced induced PSCs by reprogramming murine embryonic FBs. These cells closely mimic embryonic stem cells (ESCs) regarding pluripotency [4]. Reprogramming involves the overexpression in a cell of pluripotency-related transcription OKSM markers [4,13]. Later, Dr. Yamanaka showed that the same set of genes, when overexpressed in human FBs, could also generate iPSCs [4,13]. Dr. Thomson also reported successful reprogramming based on different combination of four factors (OCT4, SOX2, NANOG, and LIN28) [13,14]. One of the major drawbacks is the use of viral transduction to introduce genes to cells, leaving viral traces in de-differentiated cells. These FB-derived iPSCs may be used to produce any favorable cell type or 're-differentiated' into any other cell of the organism by existing methods through viral transfection, siRNA treatment, or chemically defined medium. While the yield of iPSCs or redifferentiated cells remains relatively low, there are purification and expansion techniques available to increase the cell output; for example, combination of episomal vectors and spinning flask bioreactors to produce a large number of iPSCs followed by treatment with starvation medium in static cultures to increase the percentage of iPSCs in the final culture. These methods with protocols are described elsewhere.

Trans-differentiation and de-differentiation are two main methods of cell reprogramming. The combination of both these methods may also lead to a production of partially reprogrammed cells. Cells can be treated to express some of the pluripotency markers to become iPSCs-like cells followed by suitable treatment to obtain another cell type. Figure 2 summarizes the main reprogramming methods.

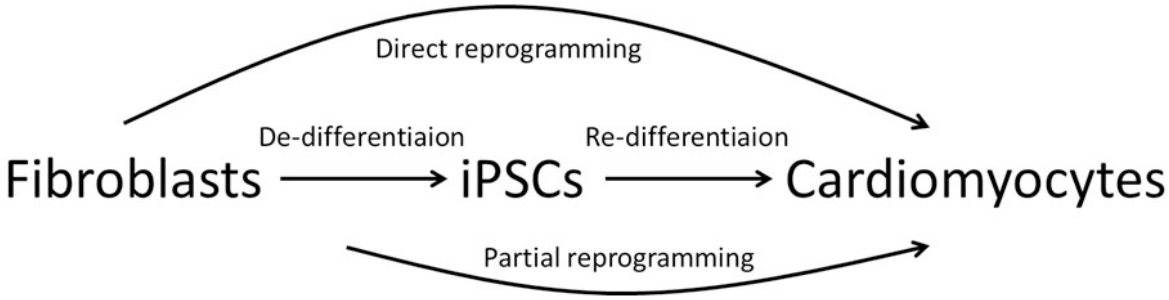

Figure 2. Common reprogramming methods. Specialized cell type (A) (e.g. FBs – fibroblasts) can be reprogrammed into another specialized cell type (B) (e.g. CMs – cardiomyocytes) through direct reprogramming without producing intermediate pluripotent cells (iPSCs – induced pluripotent stem cells). (A) cells may also be forced to undergo reprogramming to become an intermediate cell type – iPSCs that could be further treated to produce cell type (B), this process includes two phases: de-differentiation and re-differentiation. Partial reprogramming is a less used term. However, the production of iPSCs may include several intermediate progenitors or production of multipotent stem cells expressing mesenchymal stem cell (MSC) – like activity, which is used for further reprogramming needs.

Reprogramming methods provide a solid and promising background for patient-specific medicine. Reprogramming of these cells will make it possible to create a drug-screening platform to study specific drug response (Figure 3). Moreover, these cells, as they do not cause ethical issues, may be considered for re-injection for regenerative or tissue-replacing purposes as they carry patient-specific genotype. However, obstacles such as low efficiency of the process, viral traces, acquisition of damaged tissue phenotype by injected stem cells at the site of injury, and teratoma development due to the high number of re-injected pluripotent stem cells, should be overcome first.

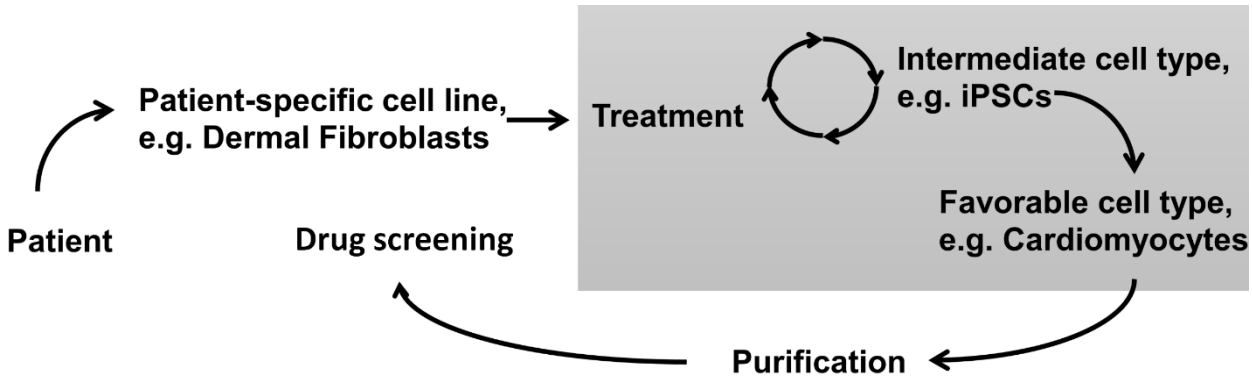

Figure 3. Simplified example of cell-based therapy. Chosen cell type is obtained from a patient for further treatment. Under certain reprogramming conditions, cells begin to transform into a different cell type or intermediate cell type or both. During the next phase, cells are purified and expanded to use as a drug-screening platform. Part of the figure with a gray background in the upper right-hand corner indicates the focus of current thesis and represents annotations in Figure 2.

The mechanism of fibroblast nuclear reprogramming by four OKSM (OCT4, KLF4, SOX2, CMYC) transcription factors (or Yamanaka factors) is described in the original papers [3,4,12]. Primarily, when reprogrammed cells reach a state of full or partial pluripotency driven by overexpression of core transcription factor in the DNA, they can be differentiated into any another desirable cell type, such as adipocytes, osteocytes, chondrocytes, muscle cells, cardiomyocytes, neurons, specialized organ cells, and their progenitors and derivatives.

2.2. Fibroblasts possess a significant plasticity to de-differentiate.

Fibroblasts are a preferable cell type to use for reprogramming [15]. Neuronal, chondro/osteocyte, and cardiomyocyte (CM) differentiation are three major directions of application of stem cell medicine, which may significantly contribute to regenerative therapies, maintenance of the degenerative process, and prevention of autoimmune disease progression. FBs can be reprogrammed into neurons, osteocytes or chondrocytes by defined factors. Han et al. (2012) used five transcription factors Brn4/Pou3f4, Sox2, Klf4, cMyc, and E47/Tcf3 to force

mouse FBs to obtain neural stem cell phenotype [16]. Other studies reported successful FB trans-differentiation into functional neurons [2,17–21]. Outani et al. (2013) were able to induce chondrogenic cells directly from mouse dermal fibroblasts by transduction of three transcription factors: cMyc, Klf4, and Sox9, and later they reported the generation of the same cells from human dermal fibroblast by using lentiviral COL11A2-reporter vectors [1]. GTM transcription factors (Gata4, Mef2c, and Tbx5) were reported to directly reprogram mouse cardiac and dermal fibroblasts into cardiomyocyte-like cells [22]. Fu et al. (2015) provide an overview of all existing techniques for FBs to CMs direct reprogramming [23]. The number of beating CMs in all published studies for human models is indicated as very low or rare [24–26].

To produce cardiomyocytes, 5-azacytidine (5-aza) alone [27] or in combination with other factors [28] remained the main inducer of stem cell reprogramming. Interestingly, human adipose-derived stem cells responded differently to 5-aza treatment by impaired expression of the main cardiac markers troponin T (cTnT) and cardiac actin [29]. In 2016, Cao et al. published a large study of the conversion of human FBs into beating CMs by small molecules [30]. They were able to screen a collection of 89 small molecules, which were known to induce or enhance reprogramming (based on existing literature) and found the combination of 7 compounds (so-called '7C cocktail') were sufficient and necessary to induce CMs reprogramming. The addition of two other inhibitors ('9C cocktail') showed the higher efficiency of CMs production [30]. Briefly, 9C includes activator of Wnt pathway, an inhibitor of TGF-β signaling pathway, two histone inhibitors, ERK inhibitor, ROCK inhibitor, epigenetic modulator and two PDGFR inhibitors [30].

FBs can be directed towards endothelial differentiation as well using a partial reprogramming technique. FBs started to express endothelial markers at day four after nucleofection with a plasmid and was able to form vascular-like tubes in vitro [31]. Sayed et al. were

able to show direct FB to endothelial cells (EC) reprogramming by using a chemically defined medium with toll-like receptor agonist and exogenous EC growth factor followed by treatment with TGF-β inhibitor, SB431542, to enhance the expansion of ECs [32]. The same inhibitor was used to produce ECs from mature amniotic cells [33] and induce growth of embryonic stem cell – derived ECs [34].

Fibroblasts can also be directed towards differentiation into other cell types. Szabo and colleagues (2010) demonstrated that partial reprogramming by OCT4 together with cytokine treatment in chemically defined medium turn FBs into hematopoietic progenitors expressing pan-hematopoietic marker CD45 [35]. Junker et al. (2009) demonstrated that one of the most basic cell types in the human body, fibroblasts, retain sufficient plasticity to differentiate into adipocyte-, chondrocyte-, osteoblast-like cells in vitro when subjected to specific induction medium [11]. According to optimized protocols published by Junker et al. (2009), dexamethasone, isobutylmethylxanthine, indomethacin, and insulin are sufficient to stimulate adipogenesis in human FBs, while dexamethasone, glycerophosphate and ascorbate-2-phosphate drive FBs towards osteogenic differentiation. Moreover, ascorbate-2-phosphate and insulin with an addition of TGFβ1 stimulate FBs to transdifferentiate into chondrocyte-like cells [11]. TGFβ1 involvement into cell differentiation and other physiological processes are highlighted in the following sections.

The abovementioned fibroblast potential provides an evidence of inherited high plasticity of human dermal fibroblasts. Plasticity that makes fibroblasts compliant to differentiate into different cell types under certain circumstances in the body. In the following section, dermal fibroblast niche, origin, and flexibility to differentiate in comparison with other stem cell types will be presented.

2.3. Dermal fibroblast niche and origin.

This section presents an overview of existing literature, discussing one of the main properties of dermal fibroblasts – heterogeneity. Commercially available human normal dermal fibroblasts are distributed as a culture with following general specifications: cells are obtained from a single donor, isolated from skin, with spindle-shaped morphology, and often neglecting a source of a specific skin layer or functional condition of fibroblast. 'Dermal fibroblasts' are a broad generic definition which is "oversimplified" [36]. Dermal fibroblasts encompass a very dynamic (based on their stages of development) and diverse (based on their origin) population of cells [36].

Fibroblast heterogeneity is observed in different tissues. Normal human skin consists of three distinct subpopulations of fibroblasts, which arise from different embryonic origin and reside in corresponding niches in the dermis. Dermal fibroblast origin is not the same. Fibroblasts in the face derive from neural crest, mainly, ventral body skin fibroblasts – from lateral plate mesoderm, and fibroblasts in back skin – from dermomyotome [37–39]. Interestingly, fibroblasts from different niches demonstrated certain differences when cultured separately [36,39]. Two subpopulations of fibroblasts occupy superficial papillary dermis and deeper layers of the reticular dermis. These fibroblasts differ from each other and the third subpopulation of fibroblasts associated with hair follicles [40]. Other subpopulations of fibroblasts may potentially exist in hypodermis residing alongside with preadipocytes, adipocytes and mesenchymal stem cells (Fig. 4).

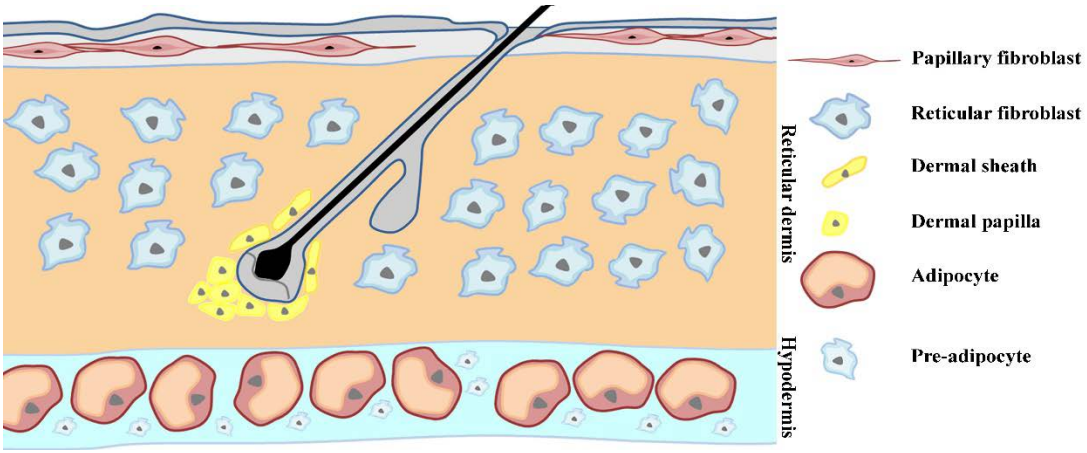

Figure 4. Heterogeneity of fibroblast-like cells in skin layers. Three distinguishable layers are shown. Papillary fibroblasts reside in the papillary dermis, dermal sheath, and dermal papilla derives from the same lineage as the papillary dermis, while reticular fibroblast, preadipocytes, and adipocytes have a common origin (modified from [39]).

Subpopulations of fibroblasts demonstrate certain preferences towards differentiation into a different cell types. Lee & Tumbar (2012) and Sennett & Rendl provided a description of cellular signaling required for hair morphogenesis and hair cycle coordination in a group of fibroblasts forming a base of the hair follicle (dermal papilla) [41,42]. Biernaskie et al. (2009) and Toma et al. (2001) showed that some dermal papilla cells are capable of differentiating into not only hair follicle but also nerve and cartilage [39,43,44]. Both, dermal papilla and dermal sheath, constitute the dermal portion of the hair follicle and are specialized fibroblasts of mesenchymal origin [45,46]. Moreover, dermal papilla cells were found to express neuronal markers suggesting that portion of dermal papilla cells derive from the neural crest and thus have a neural origin [37,47]. Signaling between dermal papilla and dermal sheath involves PI3K-Akt pathway which regulated the transformation of fibroblasts between dermal papilla and dermal sheath and is discussed elsewhere [47,48].

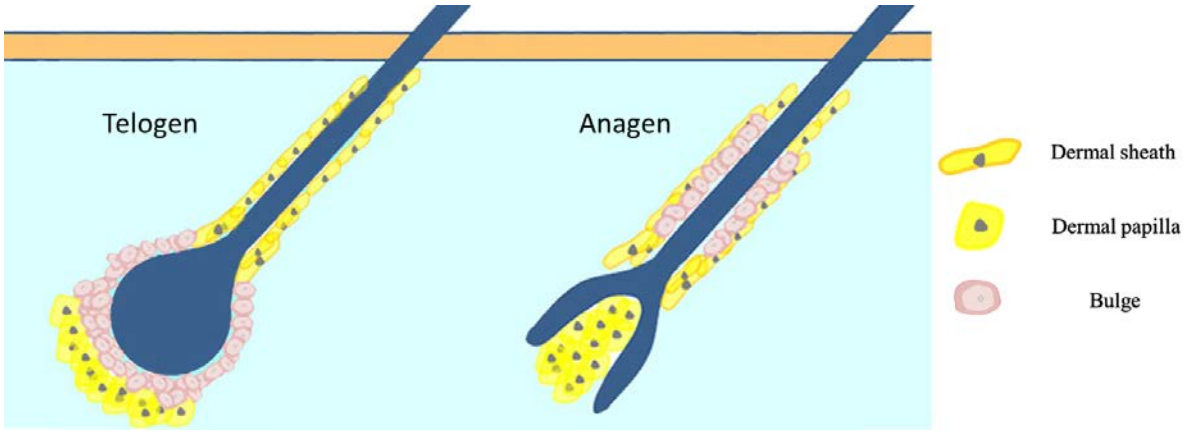

Figure 5. Structure of hair follicle at different stages of development (modified from [47]).

Cells from the hair follicle dermal compartment residing in the bulge area are considered as pluripotent adult stem cells and express nestin, a protein marker for neural stem cells (Fig.5) [49]. These cells, hair follicle pluripotent stem cells (hfPSC), are capable of differentiating into neurons, glial cells, keratinocytes, smooth muscle cells and melanocytes in vitro [50]. These stem cells associated with hair follicle are not homogeneous and represent a mixture of two different population of pluripotent and unipotent types [49,50]. In 2015, Janmaat et al. used fibroblasts as a negative control to perform immunohistochemistry with antibodies for the glial and neuronal marker and were able to demonstrate that dermal fibroblasts express glia-specific markers SOX9, KROX20, and neuronal-specific marker class III β-tubulin, at the protein and RNA level [51].

According to the existing literature, fibroblasts from different dermis layers that are not associated with hair follicles share some markers in common with mesenchymal stem cells, pre-adipocytes, and adipocytes from the hypodermis. Moreover, International Society of Cellular Therapy is not able to distinguish MSCs from fibroblasts with current minimal criteria set for MSCs [52,53]. Jaager and Neuman claim that fibroblasts and adipose tissue-derived mesenchymal stem cells (AdMSCs) are phenotypically indistinguishable cell types [54]. Ali et al. (2013) consider preadipocytes as fibroblast-like cells during the process of adipogenesis [55]. Indeed, MSCs are

defined as cells with fibroblast-like morphology, adherent to plastic surfaces, expressing such markers as CD73 and CD105, negative for the hematopoietic markers CD14, CD34, and CD45, which is also correct for fibroblasts [52,53].

Some papers state that MSCs are distinguished from fibroblasts by the failure of the latter to differentiate into mesenchymal lineages [52,56]. It is also possible to consider that all commercially available primary dermal fibroblast cultures comprise a mixture of fibroblasts, mesenchymal stem cells, and mesenchymal progenitor cells [56]. However, the yield of FBs and MSCs from different tissues spans a wide range and depends on the methodology.

2.4. Mechanotransduction in cells.

Living cells experience a significant amount of mechanical stimuli, such as shear stress, stretch and strain, osmotic force, hydrostatic pressure, thermal influence and so on [57]. Evolutionarily, cells developed certain adaptation mechanisms to sense these stimuli and interact with the environment and neighboring cells [58]. Mechanical sensing carries great importance for normal cell development, differentiation, morphogenesis, cell life cycle, and disease state [59]. Mechanosensitive molecules are widely represented on the cell surface as well as in the cell membrane and capable of converting physical force into biochemical information and triggering a downstream signaling response depending on mechanical influence on the membrane, for instance, bilayer tension, membrane thickness, or local curvature [58,60]. These molecules may include cadherins responsible for cell-cell adhesion, integrins involved in the cell-extracellular matrix (ECM) adhesion, membrane channels, caveolae and receptors, surface glycocalyx, cytoskeleton filaments and ECM molecules such as fibronectin, collagen, proteoglycans [57].

Mechanotransduction is also important in the regulation of physiological functions. Dermal fibroblasts are considered as non-excitable mechanoresponsive cells that produce collagen, growth factors, matrix-degrading enzymes, and cytokines, and play a central role in ECM remodeling and wound healing [61]. According to Davies (1995), forces from the apical surface are transmitted through the cytoskeleton to the focal adhesion points that anchor the cell in place [62]. These forces are sensed by both cell-ECM and cell-cell interaction receptors, mainly by integrins. Thus integrins are key players in mechanotransduction [63]. Initially, cells stiffen integrin contacts when resistance is present. If the shear stress persists, cells activate specific signaling pathways such as MAPK and PI3K affecting adhesion and alignment [60,64–66]. Disturbed flow leads to an activation of NF-kB pathway, which promotes inflammation and cell survival in ECs [67]. Extracellular matrix receptors serve functions beyond a simple anchoring. They can provide phosphorylation sites upon activation, which trigger multiple signaling pathways of cell survival, differentiation, migration, and ECM remodeling [63,68,69].

Cell functions altered by mechanical stimuli can be studied by mimicking the physiological environment. Models simulating stretch and strain are abundant in the literature since fibroblasts are a key component of ligaments and tendons, which are mainly subjected to high tensile loads. These models are described elsewhere [61]. Table 1 summarizes existing models of fluid flow exposure of fibroblasts.

Table 1. Fluid flow simulation models for fibroblast study*.

Reported cells	*Type of load (model)/substrate*	*Flow rate*	*Response*	*Reference*
Human skin fibroblasts	Shear stress in parallel plate flow chamber. Plain glass surface.	Over 90 minutes of 350 dyn/cm^2	Cells gradually withdraw their borders showing filamentous extrusions.	T. van Kooten et al. (1992) [70]
Dupuytren patient fibroblasts	Short-term shear stress in flow chamber; mixed loads. Plain glass surface.	1 minute of 25 dyn/cm^2	Increased cellular proliferation and expression of profibrotic markers.	Gupta et al. (1998) [71]
Murine fibroblasts	Fluid shear stress mechanical stimulation system. PDMS flexible substrate.	24 hours of 6±3 dyn/cm^2	Induced reorganization and recruitment of fibronectin.	Steward et al. (2011) [72]
Rat adventitial fibroblasts	Rotating disk apparatus. Plates coated with growth factor-reduced Matrigel.	4 hours of 1 and 20 dyn/cm^2	Enhanced migration of subconfluent fibroblasts and impaired of confluent ones.	Garanich et al. (2007) [73]
Rabbit tendon cells	Multi-slide flow device. Collagen treated glass coverslips.	6 hours at 1 dyn/cm^2 and 3 hours at 1, 10, 25 dyn/cm^2	Modulated intracellular calcium transient, increased MMPs and IL-1β production.	Archambault et al. (2002) [74]
Human dermal fibroblasts	Interstitial flow chamber. FB-populated collagen gels in porous polyethylene.	0.1-0.3 dyn/cm^2	Modulated TGFβ1 and ACTA2 expression, induced differentiation, induced perpendicular cell alignment.	Ng et al. (2005) [75]
L929 murine fibroblasts	Curved microchannel. Collagen and polyacrylamide gels.	4-16 dyn/cm^2	Enhanced proliferation.	Park et al. (2004) [76]

Rat tendon fibroblasts	Polymethylmethacrylate substrate. PMMA nanopits.	0.4 dyn/cm^2	Impaired cell adhesion to nano pits.	Martines et al. (2004) [77]
Adventitial fibroblasts	Interstitial flow-cell migration system. Collagen gel.	0.05 dyn/cm^2	Increased migration.	Shi et al. (2010) [78]
Human dermal fibroblasts	Microchannel system. Plain glass microchannel.	$1.77 \cdot 10^{-5}$ dyn/cm^2	Improved proliferation.	Korin et al. (2007) [79]

* – for a list of 3D models, spinner flasks bioreactors, suspension flow chambers, and pulsatile flow models refer to Liu et al. (2010) [80].

Fibroblasts observed in the models mentioned in Table 1 demonstrated significant shear stress-dependent functional modulation. However, cellular signaling and gene expression profiles of normal human dermal fibroblasts exposed to shear stress remain unclear.

Interestingly, mechanical cues can alter cellular function by modifying histones and remodeling chromatin, which leads to changes in transcription. Nuclei of cells contain DNA which is packed into chromatin, where DNA is wrapped around specialized proteins, histones [81]. Due to histone structural peculiarities, they can be modified through different signaling [82]. Chen et al. (2013) demonstrated regulation of eNOS gene expression by shear-stress-induced epigenetic modification [82]. They also confirmed that stress-modulated mRNAs play an important role in angiogenesis, proliferation, and atherosclerosis via, mainly, Flk1-PI3K-Akt pathway [82]. Illi et al. (2003) previously confirmed that ECs exposed to shear stress undergo series of chromatin modifications resulting in gene expression [83]. Unfortunately, similar studies have not been done with dermal fibroblasts but were performed with a cell type with relatively same characteristics, to some extent, mesenchymal stem cells. Heo et al. (2015) demonstrated that mechanical perturbation of MSCs resulted in chromatin condensation leading to upregulation of

fibrochondrogenic markers [84]. Moreover, they also reported that chromatin condensation in MSCs remained upregulated with time after loading, so-called 'mechanical memory' [84].

Current literature suggests that several major signaling pathways (MAPK, RhoA/ROCK, PI3K, NF-kB) are triggered with expression of several key genes in fibroblasts both at the RNA and protein level. Wang et al. (2007) categorize them into two large groups: ECM-related (different types of collagen, MMPs, fibronectin, TGFβ1) and inflammation-related genes (COX-2, mPEGS-1) [61]. TGFβ1 gene stands out in many studies suggesting that SMAD signaling pathway is one of the major translators of mechanical force into biochemical signals in fibroblasts. TGFβ1 signaling is propagated through serine/threonine kinase that phosphorylates a family of SMAD proteins that transduce the signal to the nucleus where they facilitate a production of ECM-related (collagen, MMPs) and inflammatory-related (cytokines) transcription [61,85,86].

Different types of mechanical stimuli cause different responses in fibroblasts. Rat fibroblasts under cyclic strain release increased levels of active TGF-β into the medium [87]. TGFβ1 RNA level was upregulated in cyclically stretched human tendon fibroblasts [88]. Heinemeier et al. (2003) reported that mechanical loading of the human tendon during physical activity increases COL1A1 and TGFβ1 production [89]. Maeda et al. (2011) demonstrated that at physiological levels mechanical loads maintain the expression of Scleraxis (Scx), tendon cell specific marker, through TGF-β/Smad2/3-mediated signaling [90]. Loss of Scx leads to a release of TGFβ1 under mechanical stress causing tenocyte death [90]. Interestingly, low flow rate, such as interstitial fluid flow, increases TGFβ1 production playing an important role in wound healing and is required for the expression of α-smooth muscle actin (ACTA2), a myofibroblast specific marker [63,75,80,91,92].

2.5. Fibroblast response to low rate interstitial flow and wound healing.

The effect of low-level interstitial flow on the phenotype of a variety cell types has been studied [93–96]. The majority of studies of interstitial flow effect on fibroblasts was performed on cardiac fibroblasts. Indeed, cardiac fibroblasts comprise nearly half of the heart and are directly exposed to the interstitial fluid flow in the myocardium [97]. Moreover, injuries in the heart are capable of producing additional fluid flow effect [98]. Interstitial flow provides a certain signaling environment between cells distributing biomolecules, facilitating mass exchange, and processing metabolites [80]. It modifies cell morphology in a number of different ways.

One of the main and well-studied response of fibroblasts to injury is trans-differentiation into myofibroblasts, the main feature of scar tissue. It is common for, mostly, all types of fibroblasts including those that are not directly exposed to a different level of fluid flow, such as adventitial fibroblasts [73]. Myofibroblast phenotype is characterized by increased expression of α-smooth muscle actin (ACTA2), secretion of extracellular matrix proteins and increased contractility [97]. Myofibroblasts are distinguishably larger than original fibroblasts they derive from [99]. Myofibroblast microfilaments terminate at the cell surface in a specialized adhesion complex to function as a contractile mechanism, which is reinforced by excessive deposition of collagen, thus they are involved in production and remodeling of the ECM [92]. A significant amount of literature confirms that myofibroblast recruit other cells, such as immune cells, in the site of injury by producing cytokines and other inflammatory mediators [73,80,91,92,97,100]. Myofibroblasts and fibroblasts also participate in autocrine signaling, which stimulates their migration, adhesion, shape changes and production of stress molecules [80,92].

Fibroblasts respond to stimuli through several pathways. Wnt/β-catenin pathway mediates ECM remodeling and facilitates fibrosis [101]. Integrin-mediated pathways such as JNK, FAK-ERK,

p38, as well as AT1R, promote fibroblast activation [97,102–104]. JAK-STAT pathway is involved in the promotion of proliferation and differentiation fibroblasts under certain condition [105]. ILK/PI3K-AKT regulates fibroblast migration and differentiation [106]. TGF-β pathway and its downstream targets may play a central role in the regulation of fibroblast function under shear stress, and interact with many pathways mentioned above [91,97]. Due to a number of interplays between different pathways or their targets, a picture of all signaling pathways modulated by fluid flow in fibroblasts is complex and has not been fully explained yet.

2.6. Exposure to fluid flow influences pluripotency.

Some studies have shown that mechanical stimuli in SSBs dramatically influence the expression of pluripotency genes [5,6,107,108]. It was shown that different cells (mainly, murine endothelial and embryonic stem cells) react differently to shear stress in SSBs.

For example, Gareua et al. (2012) demonstrated that shear stress in SSBs maintains and influences gene expression of certain pluripotency markers in ESCs. Specifically, expression of OCT4, NANOG, SOX2, REX1 were maintained by shear stress [5]. Interesting finding was observed in Shafa et al. paper (2011) of mESCs differentiation into cardiomyocytes [107]. Bioreactor differentiated ESCs confirmed to retain their ability to express pluripotency markers to form ESC-like colonies while differentiation efficiency is suppressed by shear stress [107]. In their 2012 paper, they discuss the property of bioreactors to maintain pluripotency to achieve and accelerate iPSCs expansion in SSBs [108]. Lata et al. (2013) reported fluctuation of expression of pluripotency markers in mESCs in the absence of LIF. Specifically, expression of OCT4 and SOX2 was increased while NANOG was decreased [6]. Thus, shear stress potentially may affect expression of

pluripotency genes in other cells, such as fibroblasts, driving the cells towards their pluripotency counterparts or progenitors.

2.7. Chapter highlights.

There are three major findings in the observed literature that helped us to find a potential gap and formulate our hypothesis:

1) Fibroblasts possess a significant plasticity potential to differentiate, which is similar, to some extent, to mesenchymal stem cells, keratinocytes, adipocytes, adipose tissue progenitors, pre-chondrocytes, pre-osteocytes, and nerve progenitors.

2) Fibroblasts are very responsive to different rates and time of exposure of fluid flow. Fibroblast response to mechanical stimuli is being studied in a limited fashion. More comprehensive studies are needed.

3) Previous studies, including research in our laboratory, provide evidence that fluid flow may become a useful tool to influence the fate of terminally differentiated cell types, such as fibroblasts, to trigger trans-differentiation into another desired cell type. Shear stress may be an initial driving force of trans-differentiation or de-differentiation.

Chapter 3. Materials and methods

3.1. Cell culture.

All experiments for RNA extraction were performed with primary culture of human normal dermal fibroblasts (NHDF) from an adult female donor (Lonza, Walkersville, MD, USA). Initially, NHDF were cultured in FGM™-2 Fibroblast Growth Medium-2 supplemented with 2% FBS (Lonza). Fibroblasts were grown in T-75 filter cap cell culture flasks. Culture flasks were coated with 1% gelatin before seeding. Gelatin 1% working solution was autoclaved, cooled down, filtered through 200nm sterile filter (Drummond Scientific Company, Broomall, PA, USA) and kept at a room temperature.

Cell flasks with NHDF were kept in a humidified 95% air, 5% CO_2 incubator at a temperature of 37°C. Cells were routinely cultured to passage 5 with medium changes every second day. Cells were monitored twice a day for microbial and fungi infections by visualization under the microscope to confirm the absence of contamination and normal medium color and transparency. Cells were frozen in 1 mL cryovials when reached passage 5 and then were placed in a tank with liquid nitrogen to keep them frozen until used. To preserve the viability of NHDF from low-temperature, FGM™-2 Fibroblast Growth Medium-2 was supplemented with 5% DMSO 1:1 v/v. A frozen stock of cells was thawed in a 37°C water bath for approximately two and a half minutes until small ice crystals were left in a vial before being seeded at 12000 cells per cm^2. NHDFs were seeded in T-75 flasks with 17 mL DMEM, high glucose (4500 mg/L) medium (Thermo Fisher Scientific, Grand Island, NY, USA) supplemented with 1% of L-glutamine (Thermo Fisher Scientific) and 1% Penicillin-Streptomycin 5000 Units/mL (Thermo Fisher Scientific). T-75 flasks were coated with 1% gelatin as mentioned previously. DMEM culture medium was changed after 5 hours to remove remaining DMSO and a suspension of dead cells.

Cells were kept growing until they had reached a visualized confluence of 75-80% for the expansion. Culture medium was then aspirated, and cells were washed twice with sterile 1xPBS solution preliminary warmed to 37°C in a water bath. To sterilize PBS, the bottle with working solution was autoclaved. Trypsin-EDTA, 1x0.25% (Corning, New York, NY, USA) solution was used to detach NHDFs. To trypsinize cells, the bottom of the flask was covered with 2 mL of Trypsin and flasks were kept in the incubator for 2 minutes. TBS (Trypsin Neutralizing Solution) was used to inhibit trypsin. Cell suspension was gently aspirated and transferred to 15 mL conical tubes and centrifuged at 250g and 37°C for 5 minutes. Surfactant was removed, and cells were washed twice with 1xPBS. A cell suspension of 100 µL was mixed with 100 µL of Trypan Blue Solution, 0.4% (Thermo Fisher Scientific) to calculate a number of cells for further seeding on glass plates. Cell number in each flask was approximately 1.2 mln. Calculated doubling time for NHDFs at passage 6 was 41.8 hours.

Glass plates, 20x10 cm, were washed and treated in an ultrasonic bath with soap water for 40 minutes to remove proteins. Glass plates were coated with 8 µg/cm^2 collagen I from rat tail (Thermo Fisher Scientific) in a solution of 0.02M acetic acid. After 3 hours, the collagen was aspirated, and glass plates were treated with UV in a biosafety cabinet for another 3 hours. Glass plates were washed with PBS and stored in plastic chambers, 25x25 cm, until needed. NHDFs were seeded at a density of 16000 cells/cm^2 on glass slides. One pair of glass plates with cells was placed in the same plastic chambers and covered with 125 mL of supplemented DMEM medium until the confluence of 90-95% was reached. When confluent, one glass plate with NHDFs was placed in a parallel plate flow chamber; another glass plate left for static control. All experiments were performed at passage 7.

3.2. Flow experiments.

Parallel plate flow chamber consisted of three parts: top acrylic plate, 20x10 cm, a 0.038 cm thick silicon gasket (Specialty Manufacturing, Saginaw, MI, USA), and a glass plate with cell stacked on a metal frame of the same size. Assembled flow chamber is shown in Fig 6.

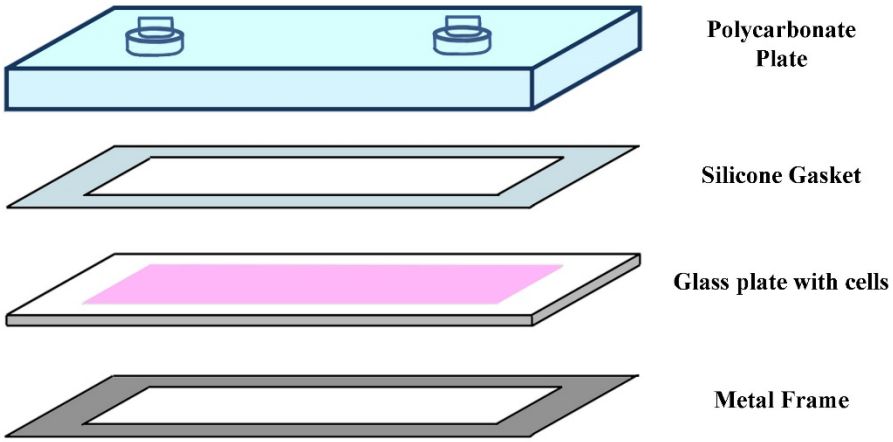

Figure 6. Plate assembly for flow experiments. The cultured glass slide is topped with a silicone gasket that provides the chamber height. A polycarbonate plate sits on top of the system (modified from [109]).

Spring clamps were used to secure all parts of the chamber together. The chamber had inlet and outlet to apply tubes and arrange a closed flow loop with circulating medium. Loop included a peristaltic pump (Cole Parmer, Montreal, QC, Canada) and norprene food tubing MF16 (Cole Parmer, Montreal, QC, Canada) was used. The schematic of a flow loop and flow chamber is illustrated in Fig 7.

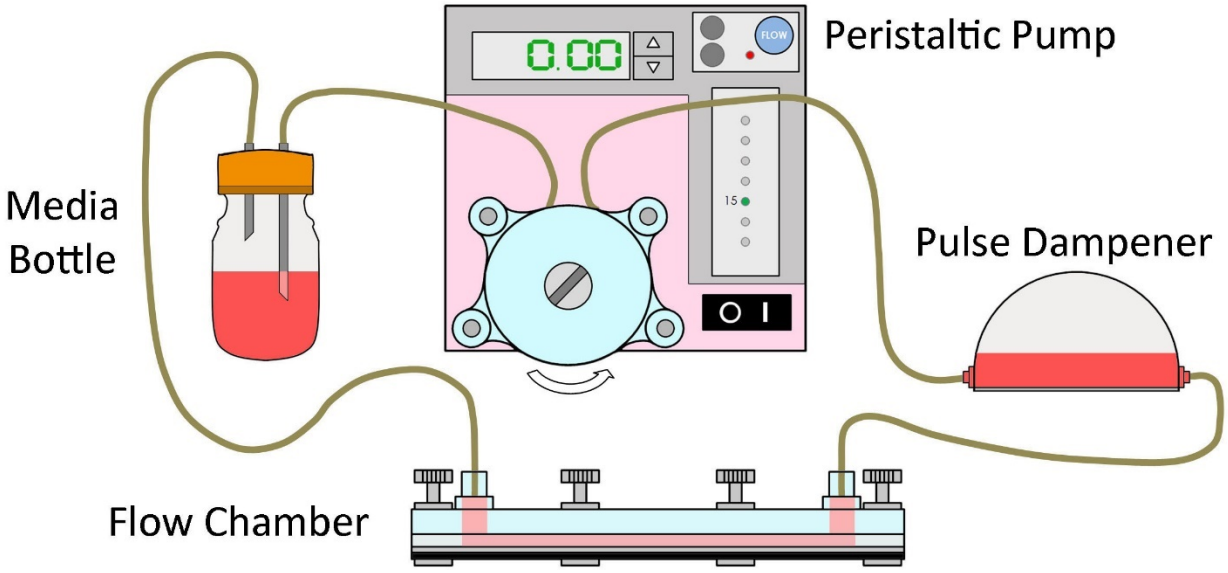

Figure 7. Assembled flow system. Flow medium is taken from the media bottle by a peristaltic pump and pushes through a pulse dampener to reach cells in the parallel-plate flow chamber (modified from [109]).

Flow was initiated at 1 dyn/cm^2 and was increased every 20 minutes by 1, 2, and 2 dyn/cm^2 within an hour to reach the needed shear stress of 6 dyn/cm^2. The system as depicted in Fig 7 was placed in a 95% air, 5% CO_2 incubator at 37°C for 20 and 40 hours for 2 sets of the experiment. The cap of the bottle with medium had several tubes applied to the holes on top with air filters allowing spontaneous air exchange. Flow loop was not pressurized with additional oxygen or CO_2 source. Flow loops and bottles were sterilized in an autoclave before assembling the entire system. The bottle, 150 mL, contained 85 mL of DMEM medium, same used for cell expansion after thawing. Flow loops with leaks or excessive bubbling on top of the medium in the bottle were discharged from the experiment and NHDFs from these samples were not used for RNA harvesting. Chambers were left overnight and monitored several times to assure the absence of leaks, blocked air filters, and excessive bubbling.

Shear stress in the parallel plate chamber was calculated with assumptions that steady laminar flow of a Newtonian fluid was developed in a loop, and length and width of the channel were much greater than height:

$$\tau = \frac{6Q\mu}{\omega h^2}\,, \tag{1}$$

where Q is volumetric flow rate, μ is the fluid viscosity (for DMEM high glucose medium with 10% FBS at 37°C μ was accepted = 0.89 cP [110]), ω – width of the channel (silicon gasket makes ω = 6.2 cm), h – is the channel height (0.036 cm).

The Reynolds number was calculated using the following equation:

$$Re = \frac{QD_h}{\nu A} = \frac{Q(2h)}{\frac{\mu}{\rho}(wh)}\,, \tag{2}$$

where fluid density, ρ=1000 kg/m^3.

The Reynolds number for 6 dyn/cm^2 was ≈3, indicating that flow was in the laminar state. The viscosity of flow medium was not additionally increased. Peristaltic pump generates pulsatile flow, so a pulse dampener was used to achieve a steady flow (Cole Parmer, Montreal, QC, Canada). Static samples were allowed to expand in the same medium on glass plates as mentioned previously for 20hrs and 40hrs in parallel, respectively (Fig. 8).

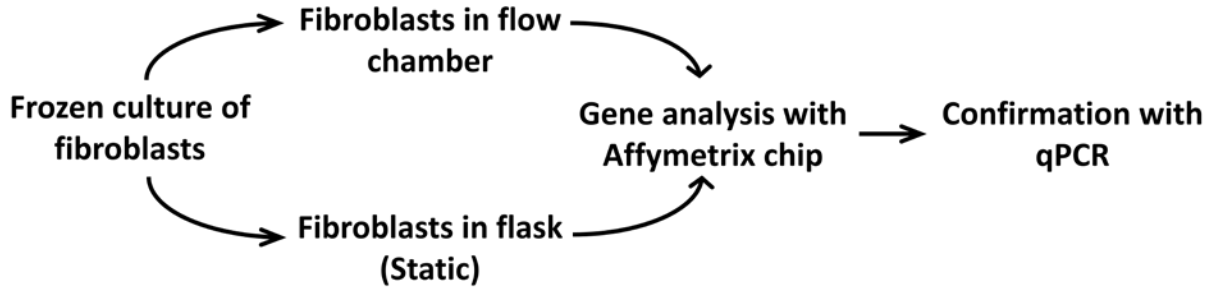

Figure 8. Sequence of methods of the experiment. Fibroblasts were thawed and cultured on gelatin-coated surfaces. After 4-8 days the cells were subcultured for control and flow experiments. Total RNA was isolated using mirVana Kit (Thermo Fisher Scientific) and analyzed on a GeneChip Human Transcriptome Array 2.0 (Affymetrix, Cleveland, OH,

USA). qPCR confirmed the expression of genes of interest. Viability tests were done with live/dead staining with Propidium Iodide (PI) and Calcein AM (C.AM).

The third run of flow experiment was performed with PI-103 (Selleckchem, Houston, USA), a dual PI3K/Akt/mTOR inhibitor. The optimal concentration of PI-103 for human dermal fibroblasts under shear stress was not found in the existing literature and manufacture's protocol. To determine the optimal concentration, a separate experiment was performed on passage 7 of confluent NHDFs in 8-well plates. Seven different concentrations were tested: 0.005, 0.5, 1, 10, 100, 250, and 500 µL/ml. Cell morphology and attachment were monitored every 5 hours. All concentrations above 100 µL/ml were toxic for cells approximately after first 10 hours. Further replication of flow was done with a PI-103 concentration of 100 µL/ml at 6 dyn/cm^2 for 20 hours. The corresponding amount of PI-103 100 µL/ml inhibitor was added into a medium in flow loop and control static in plastic dishes with glass plates. To calculate the final concentration of inhibitor for different amount of medium the following formula was used:

$$C_1V_1 = C_2V_2\ , \tag{3}$$

where C_1 is initial concentration of inhibitor, V_1 is initial volume of inhibitor, C_2 final concentration of inhibitor, V_2 final volume of inhibitor.

3.3. Sample preparation for RNA extraction.

The glass plate was transferred from a disassembled chamber to a 25x25 cm plastic dish, gently washed twice with PBS and visualized under a Nikon inverted microscope with a 10x objective and digital camera (DAGE-MTI, Michigan City, IN, USA) for cell monolayer integrity, areas of disturbed by flow, and contamination. Samples with disrupted areas were discarded. All steps during this phase of the experiment were performed with ice-cold solutions within 15 minutes

until cells were lysed to slow down cellular kinetics. Cells were trypsinized, gently detached with a cell scraper, collected in 15 mL conical tubes, and stored on ice. Cells were pelleted by spinning at 300g in a centrifuge at 4°C for 5 minutes. Surfactant was removed, and spinning was repeated with PBS. RNA was extracted following the mirVana miRNA Isolation Kit with phenol protocol (Thermo Fisher Scientific) with modifications. Briefly, the cells were lysed with a denaturing lysis solution followed by lysed extraction with Acid-Phenol:Chloroform leaving RNA in the water phase of the solution. RNA extraction was done with 100% ethanol and immobilizing RNA on glass-fiber filters. Filter with immobilized RNA was washed three times with salt washing solutions and eluted with RNAse-, DNAse-free water heated to 95°C. The final volume of water with RNA was 100 µL. Samples were stored at -80°C until used for reverse transcription. This protocol also allows collecting total RNA and short RNA separately. Due to the restricted sensitivity of microarray platforms used in the experiment, samples containing short RNA were collected but never analyzed.

3.4. RNA quantification and reverse transcription.

RNA was quantified by using Quant-iT RiboGreen RNA Assay Kit (Thermo Fisher Scientific) according to manufacturer's protocol. First ten samples were handed over to Charbonneau Cancer Centre Microarray Facility at the University of Calgary to analyze RNA quality on Agilent RNA 6000 NanoChip on 2100 Bioanalyzer (Agilent Technologies, Santa Clara, USA). The total number of collected samples from all experimental runs was 36. Based on the highest RNA yield, RIN values, and PCR amplification plots, 15 out of 36 sample were picked for further analysis, one triplicate per five conditions.

The total amount of 20 µL of RNA from each sample was used to make cDNA with a final concentration of 50 ng/µL. RNA to cDNA conversion was achieved with qScript cDNA Synthesis Kit (Quanta Biosciences, Gaithersburg, MD, USA). The amount of 200 µL RNAse-, DNAse-free vials with 20 µL of RNA template were mounted on a heat block of MJ Mini Personal Thermal Cycler (BioRad, Hercules, CA, USA). Cycler ran customized 5 step RNA→cDNA program: step 1 at 22°C for 5 min, step 2 at 42°C for 30 min, step 3 at 85°C for 5 min, step 4 at 4°C for 10 min and step 5 included storing samples at 4°C. Each cDNA sample was diluted 1:10 to a final volume of 200 µL with cDNA concentration of 5 ng/µL.

3.5. Real-time PCR and $2^{-\Delta\Delta C_T}$ analysis.

Fifteen nanograms of cDNA template was loaded into each well of fast 0.2 µL 96-well plate alongside with Fast SYBR Green Supermix (Thermo Fisher Scientific) or TaqMan Fast Advanced Master Mix (Thermo Fisher Scientific). Primers for Cyclophilin H, RPOL2A, PRL13A, RPLP0, TFR, β-actin, OCT4, CDH1, CDH24, PDGFRA, COL1A1, SNAI1 were obtained from Thermo Fisher Scientific. Primers for SOX9, CAV1, SMAD3, NOX4, ITGA2, RUNX2, KIT, PTX3, ADM, and TGFBR3 were designed and purchased from Integrated DNA Technologies (IDT, Coralville, IA, USA). For primer design refer to Appendix. All forward and reverse primers for each gene are listed in the table below.

Table 2. Sequences of designed primers for genes of interest.

Gene	Forward primer	Reverse primer
SMAD3	CGTCTGCAAGATCCCACC	CACATTCGGGTCAACTGGTAG
NOX4	GACTTGGCTTTGGATTTCTGG	CTGAGGGATGACTTATGACCG
CAV1	ACCCTAAACACCTCAACGATG	TTCCAAATGCCGTCAAAACTG
PTX3	TGTTGAGATGGCCACAGGTC	TTCATCAAAGCCACCACCCA

KIT	TGGCACGGTTGAATGTAAGG	CGAAACCAATCAGCAAAGGAG
SOX9	ACTCGCCACACTCCTCC	GCTGCACGTCGGTTTTG
ADM	CGTCGGAGTTTCGAAAGAAG	CCCTGGAAGTTGTTCATGCT
RUNX2	AGTTACAGTAGATGGACCTCGG	CATACTGGGATGAGGAATGCG
TGFBR3	GGACGCCTCGATAATCTGG	GATTTGGTTCCTTCATGCTTGG
ITGA2	ATCACGGTTATTCAGGCTCAC	ACCAAGAGCACGTCTGTAATG

The PCR reaction was carried out by loading 20 μL of cDNA of each well in 96-well plate. Batches of primers were prepared before loading with cDNA template and were as following. For primers with Fast SYBR Green Supermix: 10 μL of SYBR Green mix, 1.25 μL of forward primer, 1.25 μL of reverse primer, 4.5 μL of RNAse-free, DNAse-free water, which made the total amount of 17 μL in a batch to test one gene of interest. For TaqMan Fast Advanced Master Mix: 10 μL of TaqMan mix, 1 μL of primers containing forward and reverse primers, 6 μL of RNAse-free, DNAse-free water to the total amount of 17 μL. These 17 μL from batches of primers were loaded with 3 μL of cDNA (the total amount of cDNA was 15 ng in 3 μL) in each well. All used TaqMan probes had FAM reported and MGB quencher. The system, ViiA 7 Real-Time PCR System (Thermo Fisher Scientific), performed one 10 min cycle at 50°C for 2 minutes, followed by 95°C for 20 seconds for polymerase activation, then 40 cycles of denaturation at 95°C for 1 second for annealing and extension at 60°C for 20 seconds. To verify a single product amplification, a standard melt curve was run. Collected C_T data were analyzed using $2^{-\Delta\Delta C_T}$ method [111] in Microsoft Excel 2016 (refer to Appendix).

3.6. DNA Microarray analysis.

Collected RNA was handed over to Charbonneau Cancer Centre Microarray Facility at the University of Calgary to perform a microarray analysis on a GeneChip Human Transcriptome Array 2.0 (Affymetrix, Cleveland, OH, USA). A portion of RNA from each sample (100 ng) was

labeled with 3' IVT Express Kit (Thermo Fisher Scientific) and hybridized to Affymetrix GeneChip for several hours. Chips then were stained and washed on Affymetrix GeneChip Fluidics 450 and scanned with Affymetrix GeneChip Scanner 3000 7G System to collect fluorescent signal from 67528 genes. Library .CEL files were generated and used for further analysis. Affymetrix Expression Console™ Software[1] was used to run gene level differential expression analysis with Signal Space Transformation (SST) algorithm in conjunction with the regular robust multiple-array (RMA) average normalization method (SST-RMA) [112]. After analysis, .CHP files were generated and analyzed in Affymetrix Transcriptome Analysis Console (TAC) Software v.3.0 [(3)]. To reduce the number of false-positive results, the fold change cut-off between flow and control experiments was 3-fold and *p*-value<0.01.

3.7. Live/Dead and Nuclear/Cytoskeleton staining.

For live/dead staining Propidium iodide (PI) and Calcein, AM (both obtained from Thermo Fisher Scientific) were used. PI is an intercalating agent and a fluorescent molecule that binds to nucleic acids. PI has an emission maximum of 617 nm, and, when the cell is not functional, permeabilizes cell membrane, enters the nucleus and stains DNA into red color. Calcein, AM is a cell-permeant dye. When the dye is present in a living cell, it converts from non-fluorescent into a fluorescent calcein. Nonfunctional cells do not convert the original dye.

For Nuclear/Cytoskeleton staining Hoechst (Thermo Fisher Scientific) and Phalloidin, TRITC (Phalloidin–Tetramethylrhodamine B isothiocyanate)–labeled (Sigma-Aldrich, St. Loius, MO, USA) were used. Hoechst is a fluorescent dye that binds DNA. Phalloidin is a naturally

[1] http://www.affymetrix.com/

acquired toxin that binds polymeric F-actin. Phalloidin used in the experiment was conjugated with bright orange fluorescent dye TRITC.

Working solutions of Calcein, AM (C.AM) and PI were prepared separately and then mixed for convenient use. To make a solution of C.AM, a lyophilized dye was reconstituted in 50 μL DMSO to bring the initial concentration to 1 mM, then diluted 1:1000 and aliquoted for further use. The final concentration was 1 μM. To make a solution of PI, a powder dye was dissolved in deionized water. Initial concentration was 1 mg/mL or 1.5 mM. Then diluted 1:1000 and aliquoted. The final concentration was 1.5 μM. To dilute both dyes, warm PBS was used. C.AM and PI were mixed in 1 vial considering the amount of 1 mL of mixed solution was needed to cover 1 standard microscope slide with cells. Before staining, cells were fixed with PFA 4% solution for 20 minutes. Cells were then incubated for 30 minutes with fluorescent dyes and washed twice with PBS. To store samples, one drop of ProLong Antifade mountant solution (Thermo Fisher Scientific) was placed on top of the slide and covered with a coverslip. Samples were visualized on Nikon inverted microscope. For staining experiments cell was exposed to the same flow rate, and small chamber for a microscopic glass slide was used with the following dimensions: width = 1.27 cm, height = 0.0254 cm, length = 4.55 cm.

3.8. Comparison with existing microarray data from GEO repository.

Microarray data from the experiment was compared with other microarray data sets downloaded from Gene Expression Omnibus (GEO) repository [2]. Used gene expression sets are indicated in the table below.

[2] https://www.ncbi.nlm.nih.gov/sites/GDSbrowser

Table 3. Secondary microarray data used from GEO repository.

#	Study	Organism	Data Set Record	Samples used	Library/ Platform	Reference
1	TGFβ1 effect on ovarian FBs	H. sapiens	GDS5351	GSM989481, (83), (85), (88), (90), (92)	Affymetrix Human Genome U133 Plus 2.0	Yeung et al. (2013) [113]
2	TGFβ1 effect on gingival FBs	H. sapiens	GDS5811	GSM1586720, (24), (22), (26)	Affymetrix Human Gene 1.0 ST Array	Kuk et al. (2015) [114]
3	FBs vs FB-derived iPSCs	H. sapiens	GDS4400	GSM823565, (66), (71), (72)	Affymetrix Human Genome U133A 2.0	Liu et al. (2012) [115]
4	MSCs vs chondrocytes from osteoarthritic knee	H. sapiens	GDS3785	GSM490983, (84), (85), (86)	Affymetrix Human Genome U133 Plus 2.0 Array	Bernstein et al. (2010) [116]
5	iPSC-derived neurons from schizophrenia study	H. sapiens	GDS3938	GSM630788, (89), (90)	Affymetrix Human Gene 1.0 ST Array	Brennand et al. (2011) [117]
6	iPSC-der cardiomyocytes from cardiomyopathy study	H. sapiens	GDS4435	GSM862170, (71)	Affymetrix Human Gene 1.0 ST Array	Sun et al. (2012) [118]
7	NK cells from isolated human peripheral blood	H. sapiens	GSE85592	GSM2278897, (98)	Affymetrix Human Transcriptome Array 2.0	Contributors Cerdeira, A.S. et al. (2016)

Genes from all microarray data were filtered in TAC 3.0 and analyzed with ToppFun of ToppGene Suite and ConsensusPathDB-human. Data was plotted in Microsoft Excel 2016. Additional information regarding data processing is presented in the Appendix.

3.9. Statistical analysis.

Data were collected, analyzed in triplicates, and shown as mean ± standard deviation or standard error of the mean where indicated. ANOVA was used to calculate *p* values in $2^{-\Delta\Delta C_T}$ and SST-RMA analysis. Fold change and *p* value cut-offs were used as indicated in the Results section.

Chapter 4. Results

This chapter addresses the following objectives: fibroblasts survive under the fluid flow at 6 dynes/cm^2; expression of genes significantly changes under fluid flow; gene expression profile under the flow is similar, to some extent, to gene expression profiles after the induction of TGF-β and trans-differentiation; and co-treatment with PI-103 and fluid flow affects expression of genes responsible for development.

4.1. NHDF survival and morphology under shear stress.

The first objective was to establish the flow protocol for fibroblasts in the chamber and assess cell morphology and viability. Visualization of cells after taking glass plates out of the chamber revealed that about the same number of cells remained on the plate with a morphology similar to control groups. Excessive proliferation of cells was not noticed. Cell alignment, previously reported in the literature for different cell types, along or perpendicular the flow was not noted as well (Fig. 9).

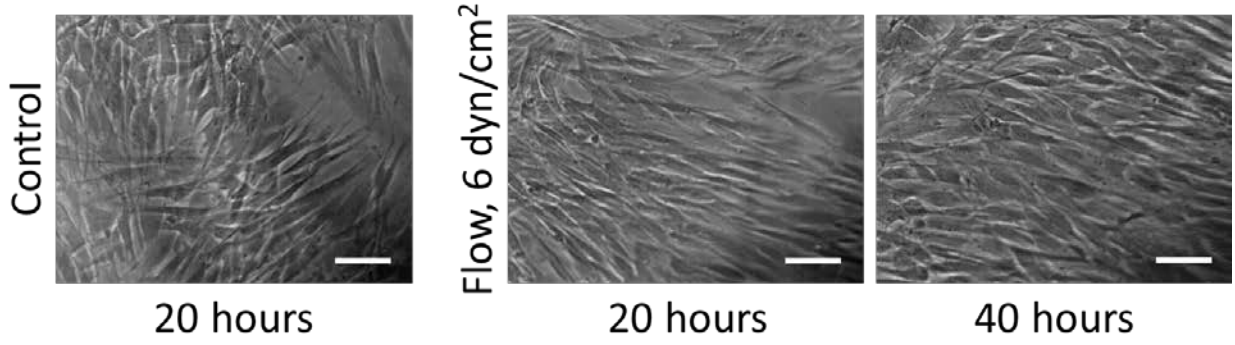

Figure 9. FBs in control group and after 20hrs and 40hrs of exposure to fluid flow. FBs remained adherent to glass slide after 20 hours and 40 hours of exposure. Pictures were taken from the middle of the slide. Scale bar – 100 μm. Flow direction ↑.

Monolayer integrity was not compromised by 10 dyn/cm^2 flow. Ruptured integrity occurred, occasionally, when air bubbles were presented in the loop. This may have occurred due to excessive bubbling, failure to remove bubbles completely with the initial flow priming, or leaks in the system.

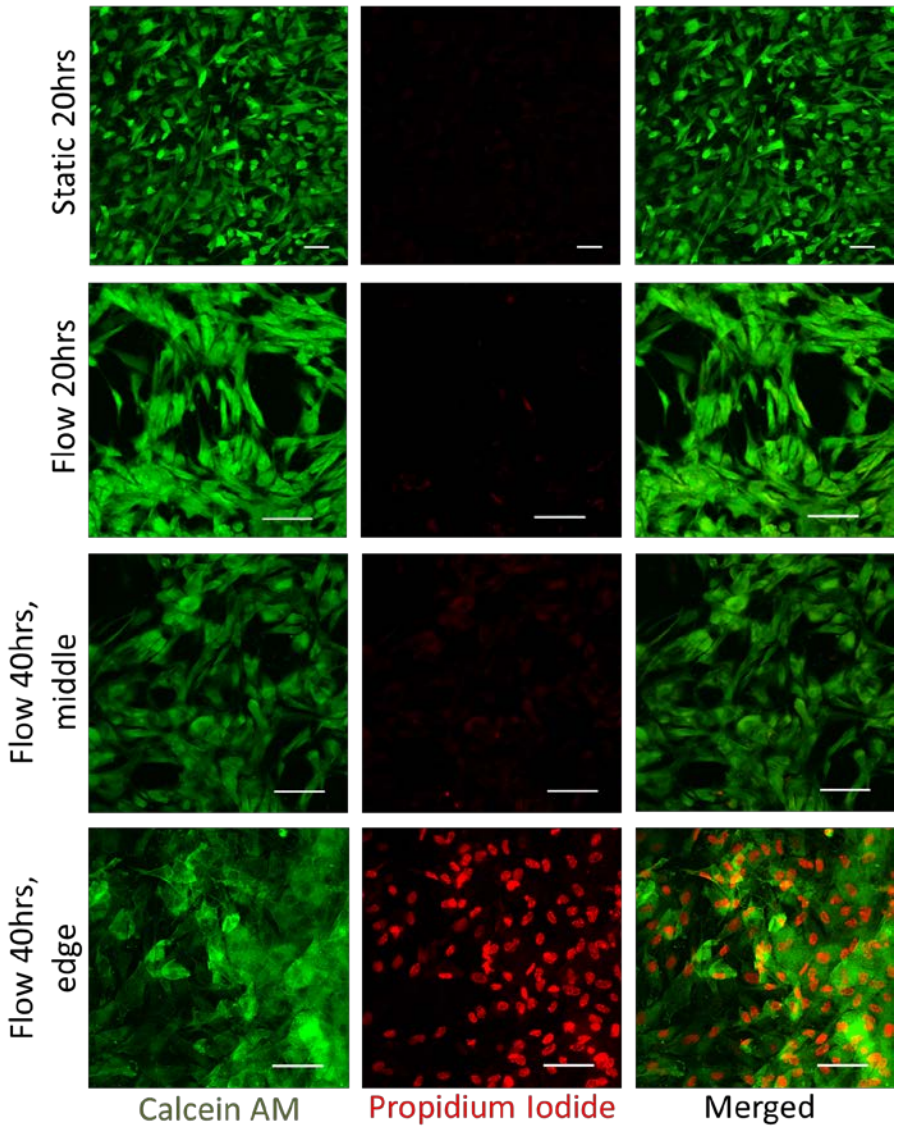

Figure 10. Live/dead staining of FBs in control group and after 20 and 40 hours of flow exposure. Upper panel represents cells in Flow 20hrs group C.AM, PI, and merged image. Middle panel – Flow 40hrs group where cells sit exactly in the middle of the slide. Lower panel shows cells from the edges and corners next to silicon gasket. Scale bar – 100 µm. Flow direction ↑.

Small areas free of cells were observed, potentially due to gaps in seeding or cell detachment. Live/dead staining confirmed that most of the cells, around 95%, remained alive after 20 hours and 40 hours of flow exposure (Fig. 10). There were slightly more dead cells in areas next to the gasket in 40hrs group. This may be due to disturbed uneven flow at the edges. Phalloidin staining indicated a very distinguishing cytoskeleton feature. Cells from all groups depicted a similar cytoskeleton organization as seen by Phalloidin staining (Fig. 11). Small unoccupied areas were visible on nearly each slide.

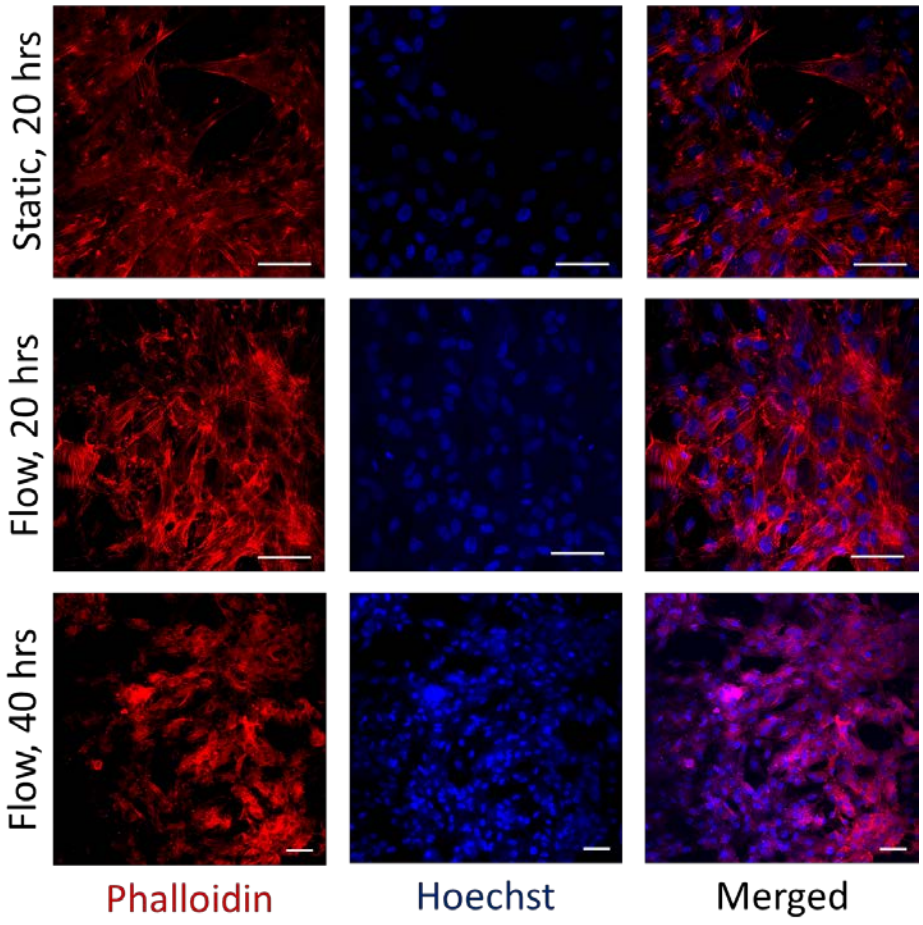

Figure 11. Hoechst/Phalloidin-TRITC staining of FBs in control group and after 20 and 40 hours of flow exposure. Nearly all cells demonstrated distinctive nuclear staining with Hoechst. Actin filaments are aligned neither parallel nor perpendicular to the flow. Scale bar – 100 μm. Flow direction ↑.

4.2. Gene expression changes under the flow.

4.2.1. Microarray data analysis.

Microarrays were run for triplicate RNA samples from Static, Flow 20hrs, and Flow 40hrs conditions. The heat map and hierarchical clustering are presented in Fig 12. The heat map shows good agreement between replicates as seen by clustering (top section of Figure 12).

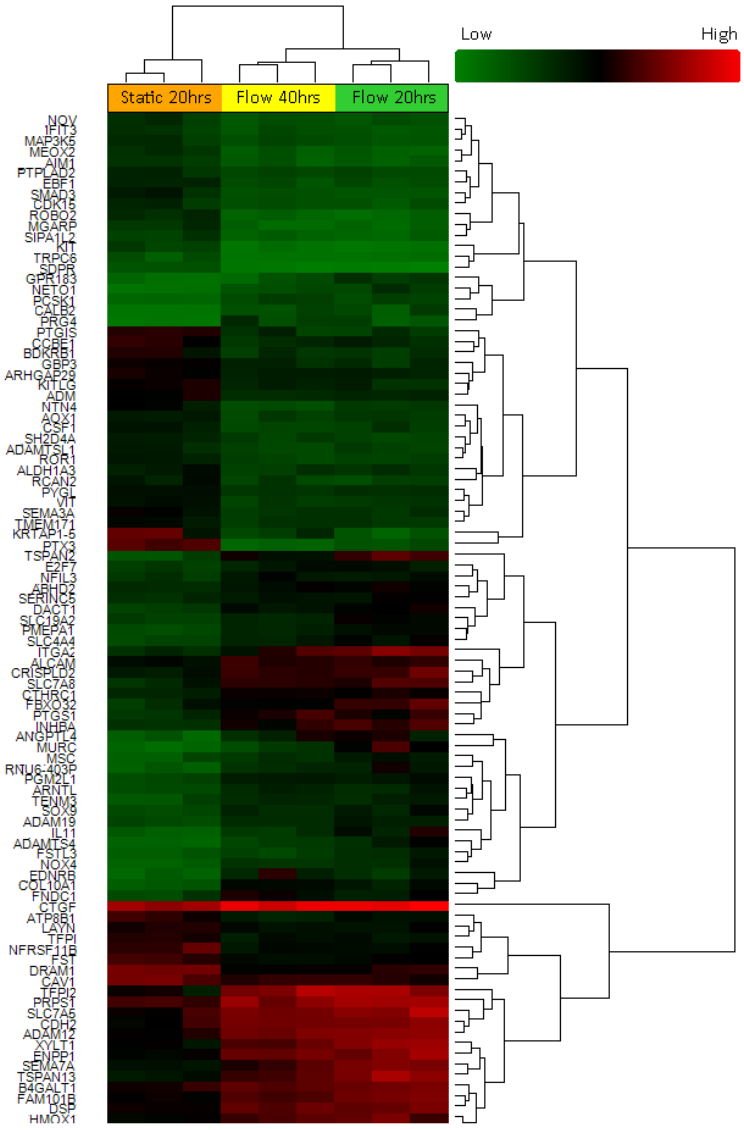

Figure 12. Hierarchical clustering and heat map of 96 differentially expressed genes in all three sets of experiment. Green color indicates low bi-weight average signal, red color – high. The heat map and clustering was obtained in TAC 3.0.

Three groups of differentially expressed genes were used for the analysis (p<0.01, fold change cut-off >3, <-3): Static vs Flow 20hrs, Static vs Flow 40hrs, and Flow 20hrs vs Flow 40hrs. Below are volcano plots for these three conditions (Fig. 13).

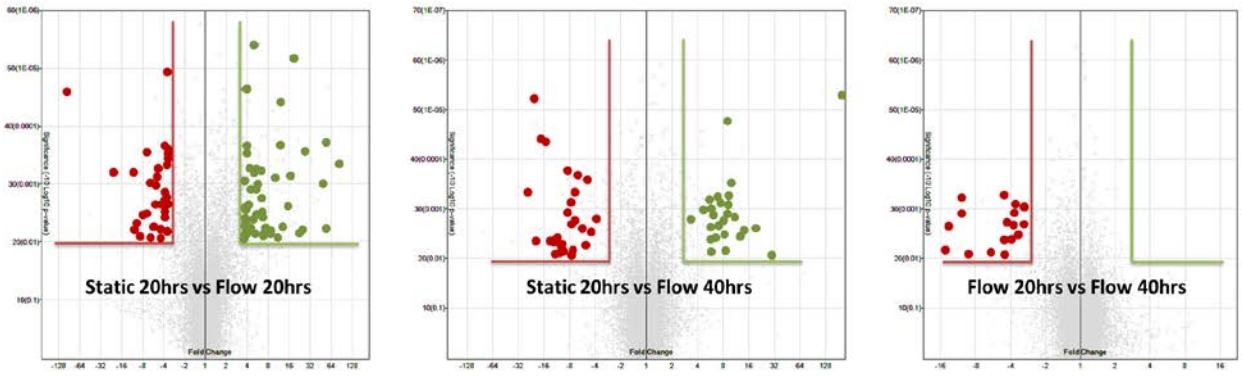

Figure 13. Volcano plots showing differentially expressed genes at p<0.01, fold change cut-off >3, <-3. Y-axis indicates p-value, X-axis – fold change.

The number of genes modulated in Static vs Flow 20hrs was 175 with 112 upregulated and 63 downregulated gene expression (64/36%). After a longer exposure to flow for 40 hours, the number of differentially expressed genes was 91 with upregulated/downregulated ratio 51/49%. Fewer genes were modulated in Flow 20hrs vs Flow 40hrs: 17 genes, all of which were downregulated.

Gene Ontology (GO): Biological Process (BP) analysis in ConsensusPathDB-human [3] (CPDB) demonstrated 409 GO:BP terms (p<0.01) in Static vs Flow 20hrs. ToppFun of ToppGene Suite [4] returned 114 GO categories with a p-value cut-off <0.01. The top 30 categories are shown in Table 4.

[3] http://cpdb.molgen.mpg.de
[4] https://toppgene.cchmc.org/enrichment.jsp

Pathway analysis performed in Wikipathways, Reactome, and KEGG demonstrated that 117 genes (70% from the total input) were present in at least one pathway. Picked pathways of interest with the highest *p*-value are shown in Table 5. Analysis indicated substantial involvement of TGF-β signaling, differentiation and development pathways. The *p*-value indicates that observed level of annotation for a group of genes is significant within the context of annotation for all genes within the genome. For more information refer to Boyle et al. (2004) [119].

Table 4. Static vs Flow 20hrs. Top 30 Gene Ontology: Biological Process categories. Column 3 and 4 indicate the number of genes from input and number of genes associated with the category, respectively. GO:BP terms are organized by *p*-value.

	ID	Name	*p* -Value	# in Input	# in Annotation
1	GO:2000026	Regulation of multicellular organismal development	1.49E-09	44	1901
2	GO:0040011	Locomotion	3.80E-09	41	1740
3	GO:0022603	Regulation of anatomical structure morphogenesis	3.99E-09	32	1131
4	GO:0036293	Response to decreased oxygen levels	2.84E-08	16	322
5	GO:0006928	Movement of cell or subcellular component	3.91E-08	41	1888
6	GO:0070482	Response to oxygen levels	5.79E-08	16	339
7	GO:0060429	Epithelium development	1.20E-07	32	1307
8	GO:0051270	Regulation of cellular component movement	1.56E-07	25	861
9	GO:0040012	Regulation of locomotion	1.78E-07	25	867
10	GO:0045937	Positive regulation of phosphate metabolic process	1.84E-07	29	1127
11	GO:0010562	Positive regulation of phosphorus metabolic process	1.84E-07	29	1127
12	GO:0051240	Positive regulation of multicellular organismal process	5.28E-07	35	1616
13	GO:2000145	Regulation of cell motility	5.38E-07	23	794
14	GO:0051094	Positive regulation of developmental process	5.61E-07	31	1329
15	GO:0030334	Regulation of cell migration	6.76E-07	22	743
16	GO:0009967	Positive regulation of signal transduction	7.07E-07	33	1488
17	GO:0001666	Response to hypoxia	7.72E-07	14	313
18	GO:0048870	Cell motility	9.29E-07	32	1433
19	GO:0051674	Localization of cell	9.29E-07	32	1433
20	GO:0016477	Cell migration	1.14E-06	30	1302
21	GO:0019220	Regulation of phosphate metabolic process	1.37E-06	36	1760
22	GO:0051247	Positive regulation of protein metabolic process	1.47E-06	34	1613
23	GO:0051174	Regulation of phosphorus metabolic process	1.62E-06	36	1773
24	GO:0045595	Regulation of cell differentiation	1.85E-06	35	1706
25	GO:0009887	Animal organ morphogenesis	2.16E-06	27	1130
26	GO:0008284	Positive regulation of cell proliferation	2.17E-06	24	927
27	GO:0072359	Circulatory system development	2.19E-06	26	1062
28	GO:0072358	Cardiovascular system development	2.19E-06	26	1062
29	GO:0030335	Positive regulation of cell migration	2.26E-06	16	446
30	GO:0023056	Positive regulation of signaling	2.87E-06	34	1662

Table 5. Static vs Flow 20hrs. Top pathways from ConsensusPathDB-human online data base. Top 10 pathways organized by *p*-value.

	Pathway	Source	*p* -value	Genes from Input/Set size
1	Differentiation Pathway	Wikipathways	6.68E-07	6/48
2	Signaling by Activin	Reactome	1.2E-06	4/13
3	Developmental Biology	Reactome	0.000103	13/586
4	Axon guidance	Reactome	0.00019	11/459
5	Human Complement System	Wikipathways	0.000312	5/90
6	TGF-β receptor signaling	PID	0.000322	4/50
7	TGF-β Signaling Pathway	Wikipathways	0.000465	4/55
8	TGF-β rec. sign. activ. SMADs	Reactome	0.0012	3/32
9	Axon guidance - H. sapiens	KEGG	0.0015	5/127
10	Hair Follicle Development	Wikipathways	0.00264	3/42

The same GO analysis was done for the Static vs Flow 40hrs group. Signal normalization and analysis in TAC 3.0 software generated a table with 91 differentially expressed genes (fold change cut-off >3 and <-3, $p<0.01$). Top 10 pathways are illustrated in Table 7. ToppFun GO:BP analysis showed over 500 terms, CPDB overrepresentation analysis – over 430 categories. Top 30 level 2 categories are shown in Table 6.

Table 6. Static vs Flow 40hrs. Top pathways from ConsensusPathDB-human online data base. Top 10 pathways organized by *p*-value.

	Pathway	Source	*p* -value	Genes from Input/Set size
1	Differentiation Pathway	Wikipathways	2.54E-07	6/48
2	Signaling by Activin	Reactome	6.27E-07	4/13
3	Antagonism of Activin by Follistatin	Reactome	6.77E-07	3/4
4	Hematopoietic cell lineage	KEGG	0.000124	5/87
5	Reg. of Commissural axon pathfindin	Reactome	0.000186	2/4
6	Endochondral Ossification	Wikipathways	0.000423	4/64
7	Spinal Cord Injury	Wikipathways	0.000477	5/116
8	Oxidative Stress	Wikipathways	0.000619	3/30
9	Prostaglandin Synthesis and Regulati	Wikipathways	0.000619	3/30
10	TGF Beta Signaling Pathway	Wikipathways	0.00362	3/55

Table 7. Static vs Flow 40hrs. Top 30 Gene Ontology: Biological Process categories. Column 3 and 4 indicate the number of genes from input and number of genes associated with the category, respectively. GO:BP terms are organized by *p*-value

	ID	Name	*p*-value	# from Inp	# in Annotation
1	GO:2000026	regulation of multicellular organismal development	1.76E-20	44	1901
2	GO:0040011	locomotion	4.31E-20	42	1740
3	GO:0006928	movement of cell or subcellular component	9.11E-19	42	1888
4	GO:0022603	regulation of anatomical structure morphogenesis	6.89E-17	32	1131
5	GO:0060429	epithelium development	4.23E-15	32	1307
6	GO:0051240	positive regulation of multicellular organismal process	5.63E-15	35	1616
7	GO:0048870	cell motility	7.92E-15	33	1433
8	GO:0051674	localization of cell	7.92E-15	33	1433
9	GO:0051270	regulation of cellular component movement	2.55E-14	26	861
10	GO:0016477	cell migration	2.80E-14	31	1302
11	GO:0045595	regulation of cell differentiation	2.88E-14	35	1706
12	GO:0040012	regulation of locomotion	3.00E-14	26	867
13	GO:0045937	positive regulation of phosphate metabolic process	3.44E-14	29	1127
14	GO:0010562	positive regulation of phosphorus metabolic process	3.44E-14	29	1127
15	GO:0051094	positive regulation of developmental process	4.87E-14	31	1329
16	GO:0019220	regulation of phosphate metabolic process	7.31E-14	35	1760
17	GO:0051174	regulation of phosphorus metabolic process	9.09E-14	35	1773
18	GO:0051247	positive regulation of protein metabolic process	2.29E-13	33	1613
19	GO:2000145	regulation of cell motility	3.06E-13	24	794
20	GO:0030334	regulation of cell migration	6.45E-13	23	743
21	GO:0009967	positive regulation of signal transduction	9.90E-13	31	1488
22	GO:0001932	regulation of protein phosphorylation	1.42E-12	30	1406
23	GO:0032270	positive regulation of cellular protein metabolic process	1.56E-12	31	1514
24	GO:0023056	positive regulation of signaling	3.13E-12	32	1662
25	GO:0036293	response to decreased oxygen levels	3.13E-12	16	322
26	GO:0072359	circulatory system development	3.18E-12	26	1062
27	GO:0072358	cardiovascular system development	3.18E-12	26	1062
28	GO:0010647	positive regulation of cell communication	4.44E-12	32	1684
29	GO:0070482	response to oxygen levels	6.81E-12	16	339
30	GO:0006468	protein phosphorylation	8.57E-12	34	1954
31	GO:0042325	regulation of phosphorylation	8.99E-12	30	1512

All four tables above share numerous categories and pathways. The same analysis was performed for Flow 20hrs vs Flow 40hrs group. Interestingly, zero GO:BP terms were returned. Comparison between Flow 20hrs and Flow 40hrs changes control group from Static to Flow 20hrs and does not provide a clear representation of processes occurred within the time of exposure to flow.

Several differentially expressed genes were involved in regulation of tissue development and organ morphogenesis. Locomotion and migratory activity were the second highest weighted category. Cell signaling and communication terms were presented as well. Both positive and negative response to oxygen level and metabolic process categories returned from ToppFun and CPDB analysis. Analysis of common genes between all major GO:BP categories revealed a complex network of genes with first and second neighbors, proteins, and complexes. The network was filtered to leave interconnected nodes without second neighbors. The simplified network is illustrated in Fig. 14.

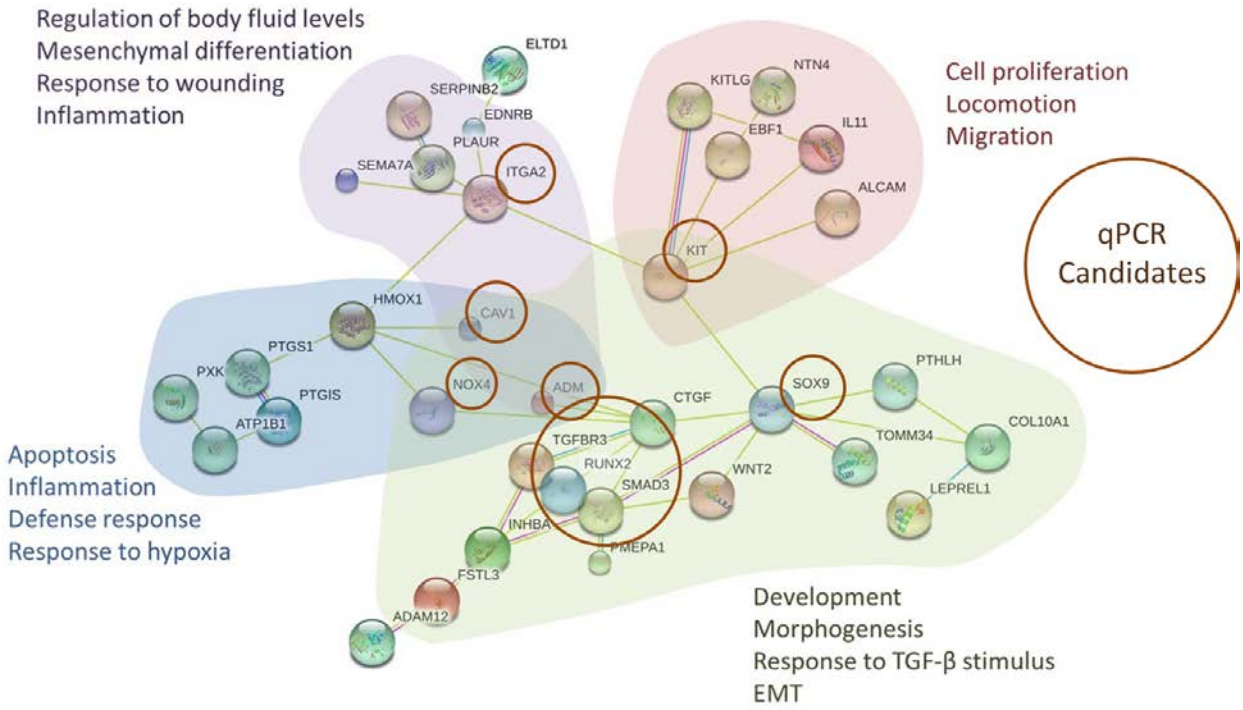

Figure 14. Subnet of full network of potential genes of interests. Nodes organized in subgroups according to common GO categories and highlighted with a different background color. Circles represent candidates for qPCR. Different lines represent different degrees of interaction.

For PCR analysis, the list of ten genes of interest (ITGA2, KIT, CAV1, ADM, SOX9, TGFBR3, RUNX2, SMAD3, PTX3, NOX4) were identified from microarray results. This list was enriched with six other genes (COL1A1, SNAI1, POU5F1, CDH24, CDH1, PDGFRA), chosen based on the previous research, to make a full list of 16 genes. Gene full names and a brief description are shown in Table 8. PCR and $2^{-\Delta\Delta C_T}$ analysis confirmed the same trend of gene expression obtained from a microarray. Four genes were upregulated, seven downregulated, expression of four genes (SNAIL, COL1A1, POU5F1, CDH24) statistically remained unchanged, and one gene (CDH1) was not expressed in all experiments (Fig 15). Shear stress upregulated gene expression of two transcription factors RUNX2 and SOX9, as well as NOX4 and ITGA2 genes significantly (p<0.01). Flow-dependent downregulation occurred in ADM, CAV1, PTX3, TGFBR3, SMAD3, and KIT gene expression. Pan-fibroblast marker PDGFRA was significantly (p<0.05) downregulated by flow after 20 and 40 hours by 2.41 and 2.42 folds, respectively.

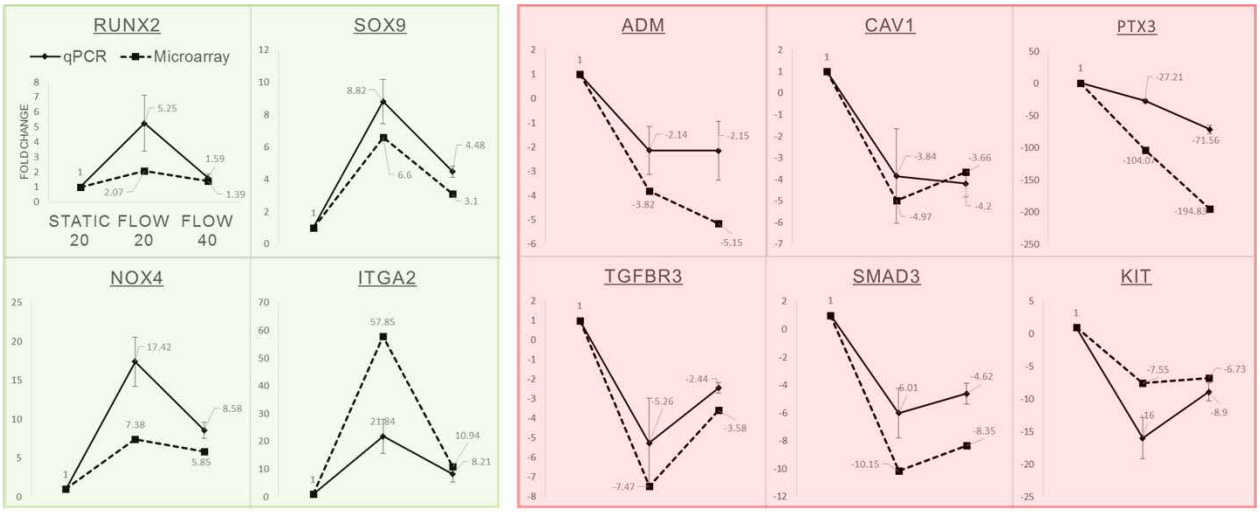

Figure 15. Confirmation of microarray expression of genes of interest by qPCR. $2^{-\Delta\Delta C_T}$ analysis confirmed the same gene expression trend of all flow modulated genes. Left panel represents four upregulated genes (green background), right - six downregulated genes (red background).

4.2.2. GEO microarray data set comparison.

Below is the comparison of fibroblast gene expression profiles after fluid flow and TGFβ1 treatment, as well as comparison of gene expression profiles of fibroblasts and other cell type derived from either fibroblasts or iPSCs. Figures of comparison also demonstrate similar genes, which were modulated in both studies and their fold change.

4.2.2.1. Flow effect (NHDF) vs effect of TGFβ1 treatment (gingival FBs).

Our microarray data and data from the TGFβ1 effect on gingival FBs were compared [114] (Fig. 16). Additional information is presented in Figure 31 and Table 9 in the Appendix.

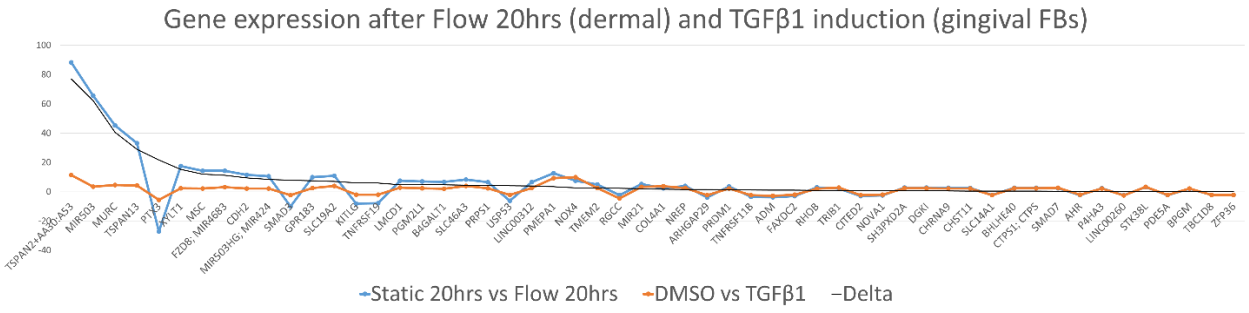

Figure 16. Comparison of Flow 20hrs and TGFβ1 effect on gene expression in dermal and gingival fibroblasts. Y-axis indicates fold change, X-axis – gene names. Connections between dots are provided for a better visualization and do not indicate continuous changes of values. When number of common genes exceeds 300, trends become indistinguishable. Therefore, all dots in the same trend are linked. Delta line represents the absolute difference between expressions of each gene in two data sets. Number of similar genes between two data sets is 54.

The total number of tested genes in our microarray data was 67528, with 799 genes differentially expressed after 20 hours of flow exposure at fold change cut-off >2 or <-2 and *p*-value <0.05. The number of differentially expressed genes in the TGFβ1 studies was 109 out of 29096 tested. Between Flow 20hrs (799 genes) and TGFβ1 (109 genes), the number of common

genes was 54. The expression of these 54 genes is represented in Figure 16. The trend of gene expression between Flow 20hrs and TGFβ1 was similar for each gene. For Flow 40hrs versus TGFβ1, number of common genes was 32 (between 335 and 109 differentially expressed, respectively). Still, the trend of gene expression was similar to Flow 40hrs. None of the common genes were expressed differently in two data sets (Fig. 17).

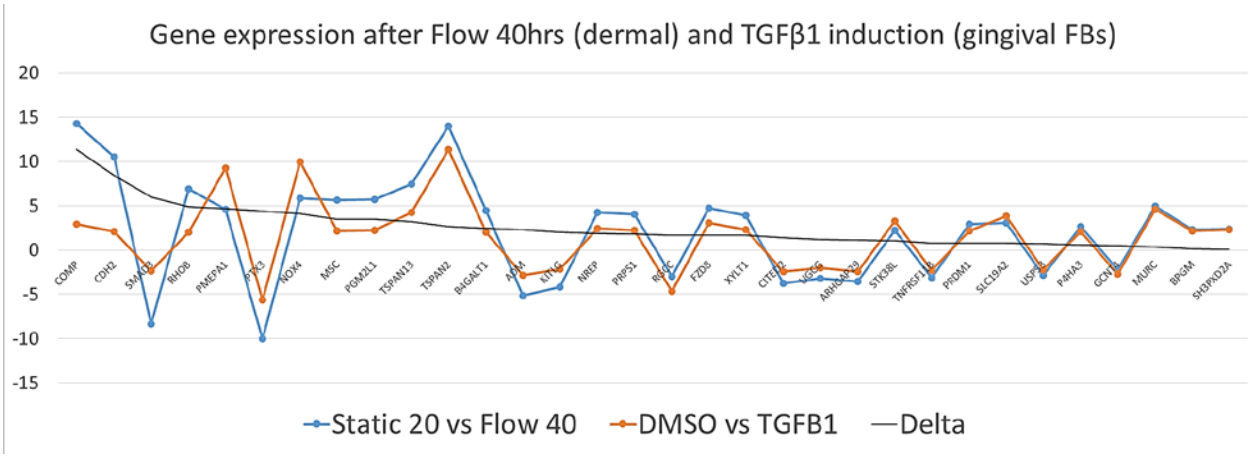

Figure 17. Comparison of Flow 40hrs and TGFβ1 effect on gene expression in dermal and gingival fibroblasts.

The platform used in this TGFβ1 study was Affymetrix Human Gene 1.0 ST with 30000 genes. Fluid flow microarray data was also compared with a TGFβ1 study that was performed on a different platform that could analyze more genes. Microarray data of TGFβ1 effect on ovarium fibroblasts analyzed on a platform with 54613 gene identifiers exists and available through GEO repository [113].

4.2.2.2. Flow effect (NHDF) vs effect of TGFβ1 treatment (ovarian FBs).

Flow exposed fibroblast gene expression from this study was compared to the effect of TGFβ1 treatment on ovarian fibroblasts. The results were similar with minor differences. The total number of 1523 genes were modulated by TGFβ1 treatment. Among them, 114 genes were in common with Flow 20hrs experiment (Fig. 18).

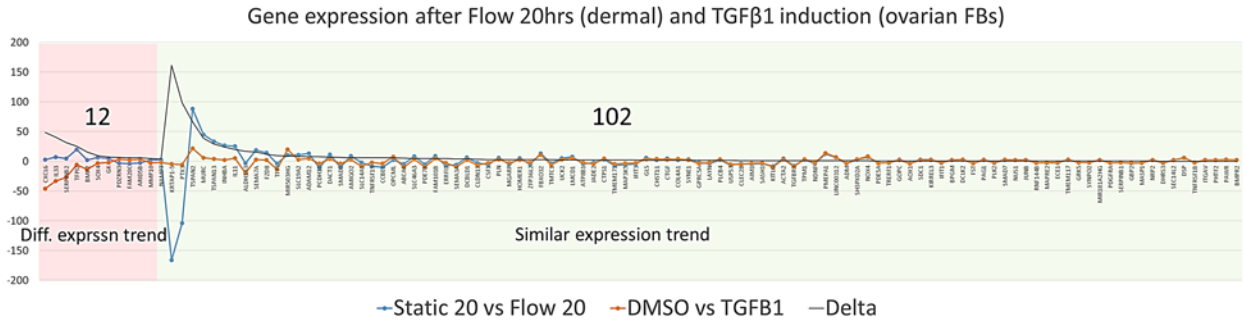

Figure 18. Comparison of Flow 20hrs and TGFβ1 effect on gene expression in ovarian FBs. Red background indicates the portion of genes with a different trend of expression. Green background – similar trend. Numbers above the lines (12 and 102) are the number of genes in each trend. The total number of genes – 114. Diff. exprssn trend – different expression trend, opposite to similar expression trend. Y-axis – fold change, X-axis – gene names, which are barely seen due to a scale, the original comparison was performed in Microsoft Excel with interactive plots and changeable scale.

This figure differs from two figures above (Fig. 16 and 17) because different trend of expression (red portion with 12 genes) is added to the similar trend of expression (green portion with 102 genes) between two studies. Trend of different expression indicates that expression of a gene was opposite in a secondary data set compared to shear stress induction, more information with the example is provided in Figure 31 in the Appendix. For Flow 40hrs versus TGFβ1 effect on ovarium fibroblasts, 335 and 1523 differentially expressed genes were compared. Number of common genes was 57, all from the same trend of expression (Fig. 19).

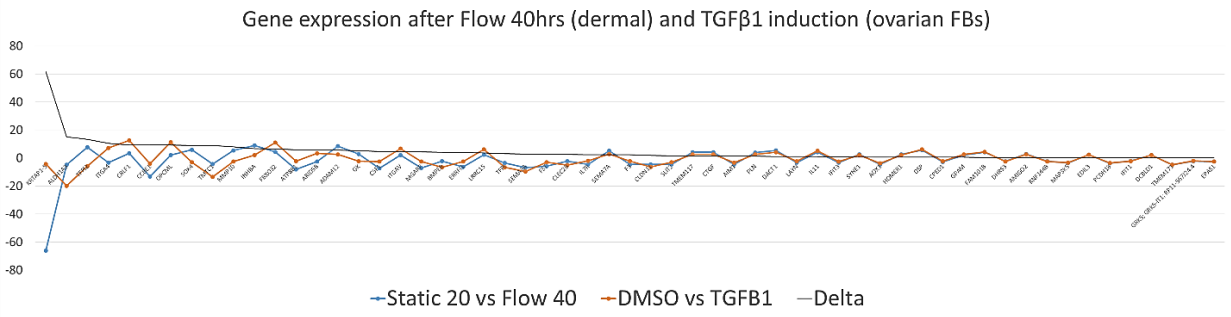

Figure 19. Comparison of Flow 40hrs and TGFβ1 effect on gene expression in ovarian FBs.

Another comparison was performed on how gene expression differs under the flow effect and between FBs and FBs-derived iPSCs. The only study that exists in GEO repository was performed on lung fibroblasts and iPSCs derived from lung fibroblasts.

4.2.2.3. Flow effect (NHDF) vs lung FB-derived iPSCs gene expression profile.

The two flow conditions were compared with the gene expression profile of lung FB-derived iPSCs (Fig. 20).

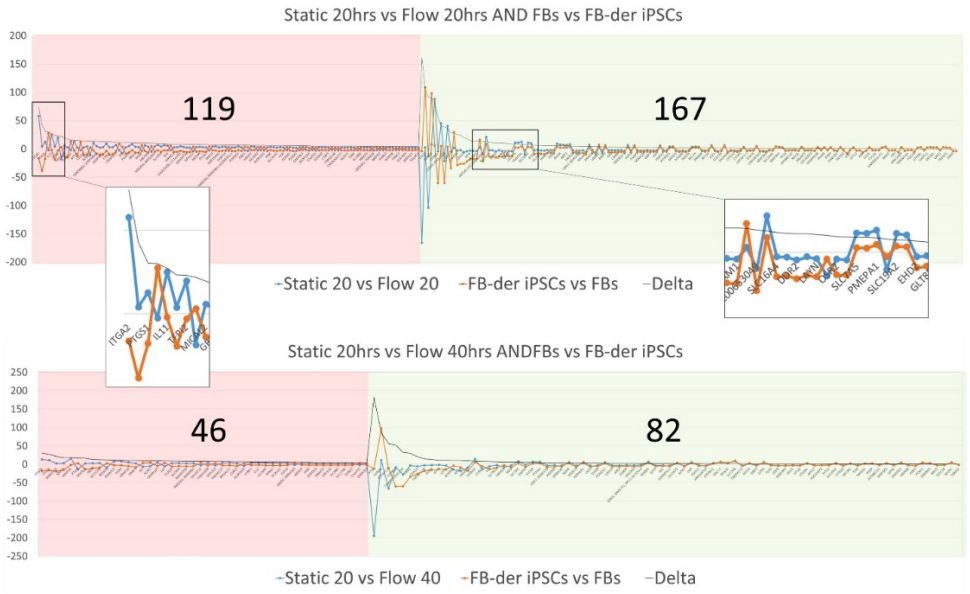

Figure 20. Comparison of Flow 20hrs, 40hrs and gene expression profile of FB-der iPSCs in dermal and lung fibroblasts. Due to many genes, portions of trends are presented for demonstration of a bigger scale. Red background indicates the portion of genes with a different trend of expression. Green – similar trend.

Numbers above the lines are the numbers of genes on each side. Graphs demonstrate a lot of difference as well as the similarity between gene expression profiles in the experiment and derivation of iPSCs from lung FBs.

The comparison was done betwen our static data set and a negative control, the natural killer cell microarray data set performed on the same platform, HTA 2.0.

4.2.2.4. Flow effect (NHDF) vs natural killer (NK) cells gene expression profile.

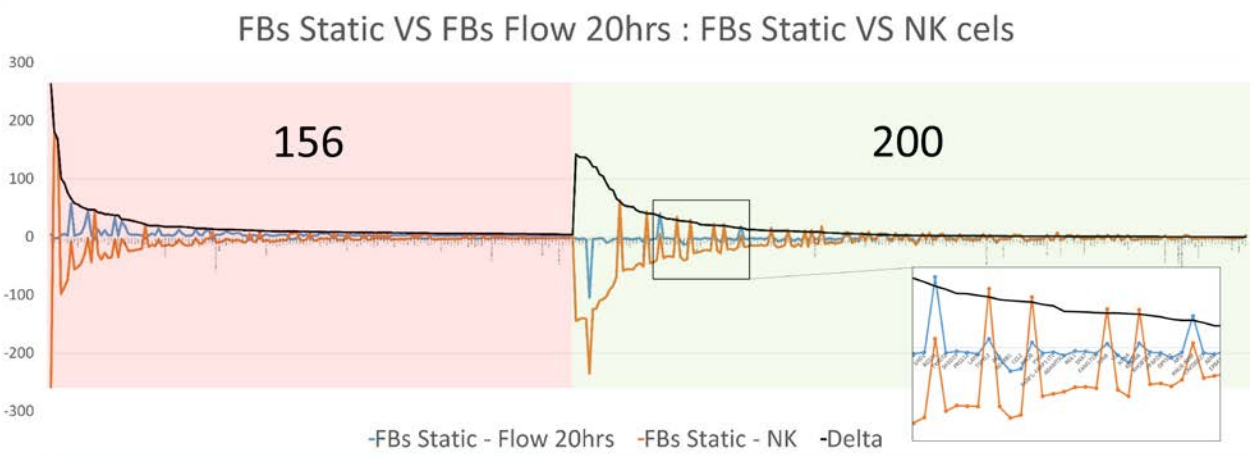

Figure 21. Comparison of Flow 20hrs, 40hrs and gene expression profile of NK cells gene expression profile.

It was anticipated that there would be little similarity between fibroblast gene expression profile after fluid flow and gene expression profile of natural killer cells due to their different origin. Therefore, natural killers were chosen as a negative control. As shown in Figure 21, expression of 356 genes still was similar (expression trend of 200 genes was the same, other 156 - different) to the flow experiment.

4.3. PI-103 inhibitor treatment effect on gene expression.

Addition of PI-103 for 20hrs demonstrated involvement of PI3K/AKT/mTOR pathways in flow-dependent gene regulation. Simultaneous influence of inhibitor and shear stress caused different expression responses within genes of interest. Five different responses are described below. For a convenient analysis, these genes are additionally represented on one page in Figure 32 the Appendix.

4.3.1. Genes affected by PI-103 only.

For several genes, gene regulation was not influenced by flow preconditioning but significantly affected by PI-103 (Fig. 22).

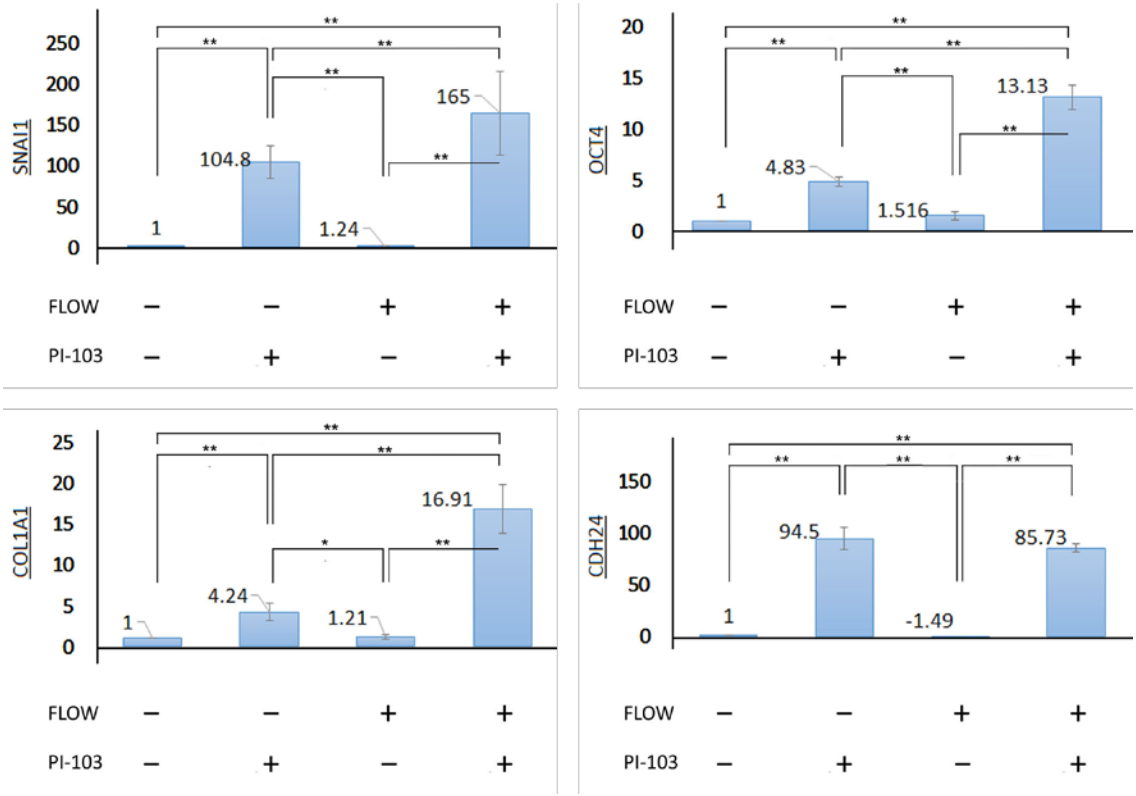

Figure 22. Expression of genes not affected by flow but modulated by PI-103.

Shear stress did not have a significant effect on the expression of all genes in this group compared to static culture. Expression of four genes was not responsive to fluid flow but was significantly upregulated after incubation with PI-103 for 20 hours. The presence of the inhibitor in the flow loop for 20 hours further accelerated the difference in expression between the control group (static + inhibitor) and experiment group (flow + inhibitor) for OCT4, SNAI1, and COL1A1 (p<0.01) and remained at the same level for CDH24. SNAI1 expression showed the greatest increase upon PI-103 treatment under flow and static conditions (165 and 105 fold increase, respectively). COL1A1 had the greatest difference between static and flow preconditioned cells to PI-103 (4 fold and 17 fold increase, respectively) SNAI1 is the only gene in this group presented based on values from 6 total replicates of 2 flow samples to reduce SEM. All other genes represent 9 total replicates from 3 samples.

4.3.2. Genes affected by PI-103 under static conditions.

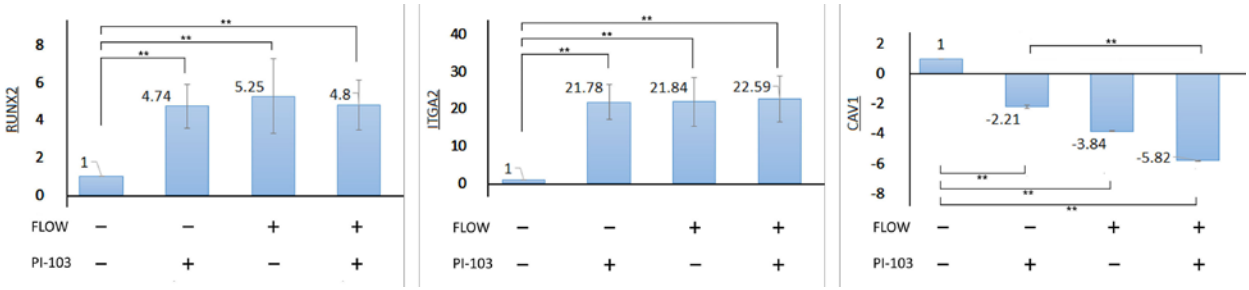

Figure 23. Expression of genes not affected by PI-103 but affected by shear stress.

Expression of RUNX2, ITGA2, and CAV1 did not change under flow + inhibitor treatment after 20 hours compared to the static + inhibitor. Flow and PI-103 seemed to have a strong significant (p<0.001) similar effect on the expression of RUNX2 and ITGA2 and less but still significant (p<0.01) effect on CAV1 indicating that flow and PI3K/AKT may share some common signaling.

4.3.3. Inhibitor overrides flow effect on gene expression.

Despite flow-dependent modulation, PI-103 treatment reversed the direction of gene regulation for two genes, ADM and PDGFRA (Fig. 24).

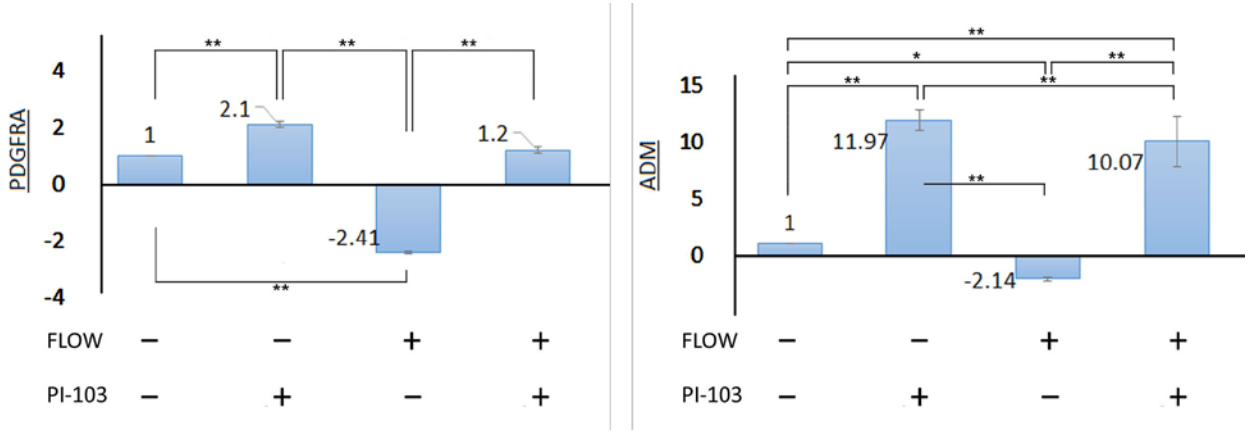

Figure 24. Genes for which PI-103 treatment superseded the flow effect.

Shear stress alone downregulated the expression of PDGFRA and ADM ($p<0.01$ and $p<0.05$, respectively). The addition of inhibitor overrode the expression of these genes after 20 hours. PDGFRA is a pan-fibroblastic marker and its downregulation by flow is particularly interesting and discussed in the next chapter.

4.3.4. Inhibitor impairs flow effect on gene expression.

The largest group contains 5 genes out of total 16. While the flow effect is not overridden entirely, it was greatly or completely brought to the level of static control without PI-103 (Fig. 25).

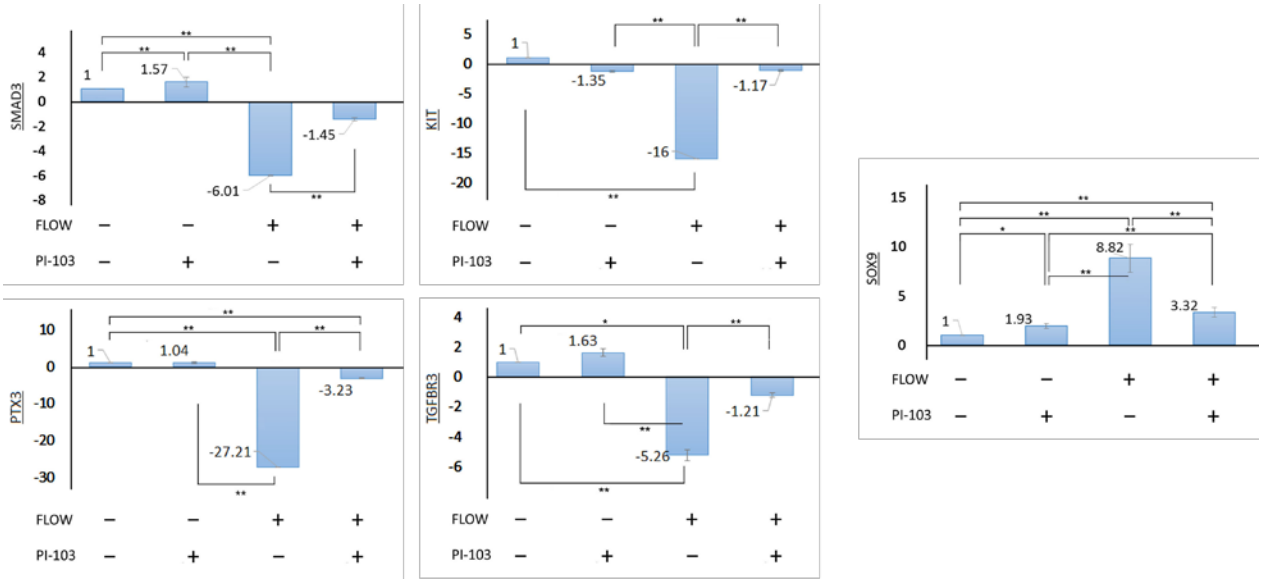

Figure 25. Genes for which PI-103 treatment diminished the flow effect.

Shear stress alone decreased the expression of four genes, SMAD3, KIT, PTX3, and TGFBR3, and upregulated the expression of SOX9 in comparison with static control after 20 hours. The combination of flow and inhibitor greatly impaired the effect of flow by driving the expression of all genes in this group to either control level (SMAD3, KIT, and TGFBR3) or very close to a control level (SOX9, PTX3) after 20 hours.

4.3.5. Inhibitor enhances flow effect on gene expression.

One gene had a unique flow + inhibitor response among all other genes of interest (Fig. 26).

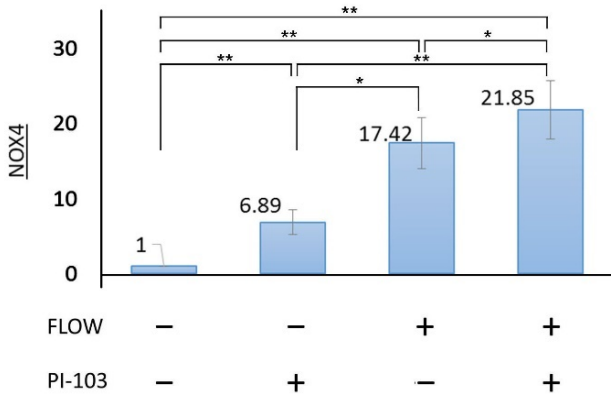

Figure 26. PI-103 stimulated flow-dependent expression of NOX4.

The smallest and last group contains one gene, NOX4, whose expression was upregulated under flow solely (p<0.001) and inhibitor in static after 20 hours (p<0.01). Combined treatment with flow and inhibitor upregulated the gene expression synergistically compared to a static control without inhibitor (p<0.001). This may point to the large involvement of NOX4 in response under flow and PI-103.

Chapter 5. Discussion and summary

The major findings of the study are:

- Fibroblasts survive at elevated levels of shear stress of 6 dyn/cm^2 for 20 and 40 hours of exposure.
- Fluid flow modulates expression of several hundred genes in human dermal fibrobalsts.
- Treatment with PI-103 indicated involvement of TGF-β and PI3K/AKT pathways in flow modulation of gene expression.

These findings are discussed below in the following 6 sections:

- Fibroblasts are viable and do not change morphology under the flow after 20 and 40 hours – Section 5.1.
- Shear stress does not modulate mesenchymal-to-epithelial transition at the gene level – Section 5.2.
- Positive regulation of expression of chondrogenic and osteogenic markers – Section 5.3.
- Involvement of flow in regulation of some physiological functions in fibrobalsts – Section 5.4.
- Fluid flow effect on the expression of genes, which are conserved during differentiation. Difference score summarizes comparison between 9 microarray data sets – Section 5.5.
- Upregulation of some pluripotency markers may not be an indication of fibroblasts trans-differentiation after co-exposure to fluid flow and PI-103 inhibitor – Section 5.6.

5.1. Adaptation response of NHDF to shear stress.

It was demonstrated that under fluid flow of 6 dyn/cm^2 fibroblasts remained highly viable after 20 hours and 40 hours of exposure. As per what was discussed in the Background chapter, 6 dyn/cm^2 is not a typical shear stress dermal fibroblasts are normally exposed to in vivo. Average normal shear stress caused by interstitial fluid flow vary in the range from 0.05 dyn/cm^2 to 0.3 dyn/cm^2 [102], slightly increasing in wounds and injuries for a short period, typically, shorter than 4 hours [75,98]. Nonetheless, dermal fibroblast morphology and size under fluid flow remained indistinguishable from control cells expanded on the same glass plate in a static culture. The number of FB differentially expressed genes from microarray study more likely to contain a subset of genes responsible for cell survival. Expression of some of these genes is discussed in sections 5.4 and 5.6 below, also supported by the existing literature. Additional work is needed to fully elucidate the effect of shear stress magnitude. It is unclear why fibroblasts would need that level of shear stress resistance if they do not typically experience shear stress of 6 dyn/cm^2 in vivo. High resistance could be important for wound healing, when fibroblasts are able to remain adherent and viable in the site of injury. Nonetheless, this hypothesis requires experimental validation.

The number of cells remained on the glass plate after 20 hours and 40 hours of exposure compared to control group demonstrated that fibroblasts under flow did not undergo, visually, an increase in cell death or excessive proliferation, suggesting that inner cellular mechanisms diminished stress level of prolonged exposure to fluid flow and kept fibroblasts alive. However, cell proliferation, as well as cell alignment, were not measured and are considered for future experiments. Visualization of F-actin staining revealed that cytoskeleton organization was not different from static culture as well as perpendicular or parallel alignment to flow did not occur as demonstrated in fibroblasts under low rate interstitial flow by Ng et al. (2003) [91].

Myofibroblast marker ACTA2 was not among genes of interest and its expression was not confirmed by qPCR, however analysis in TAC Software indicated that ACTA2 expression was upregulated by 4.63 fold (p=0.0418) after 20 hours of exposure and 3.5 fold after 40 hours with a p-value 0.098. Alongside with fibroblasts morphology and cytoskeleton organization, this may suggest that fluid flow is capable to trigger fibroblast-to-myofibroblasts differentiation between 0 and 20 hours of exposure but is not capable of maintaining it after 20 hours. This is another direction for future work to test this hypothesis.

To summarize this section, it is clear that fluid flow modulated expression of a subset of genes that maintain cell survival. It is unknown what would happen if fibroblasts were left in the chamber exposed to fluid flow for a longer period (over 40 hours). Sections 5.2 to 5.6 discuss possible ways for FB to go in this regard based on their gene expression in 20hrs and 40hrs experiment.

5.2. Shear stress does not modulate the expression of epithelial and mesenchymal markers but downregulates fibroblastic ones.

In the Literature review chapter, it was mentioned that there are two possible paths of fibroblast to change phenotype on their way to differentiation into a different cell type. One of them is a direct trans-differentiation that skips the pluripotency stage, and another one is through mesenchymal to epithelium transition. In their 2010 paper, Polo et al. reviewed two independent studies of fibroblast differentiation and claimed that MET was an unavoidable step during the conversion of fibroblasts into iPSCs [120]. This path starts with downregulation of typical mesenchymal or fibroblast-specific markers, such as N-cadherin (CDH2) or platelet-derived growth factor receptor α (PDGFRA) and upregulation of epithelial markers, such as SNAI1 and

E-cadherin (CDH1) during the first step. The next step continues with downregulation of epithelial markers and upregulation of four major Yamanaka factors (OKSM).

The hypothesis was tested that fluid flow could trigger MET and modulate the expression of markers of different germ lines. Microarray analysis and qPCR confirmed the following expression profile. SNAI1, an epithelial marker, was not affected by shear stress either after 20 hours or 40 hours. E-cadherin qPCR amplification plots were nothing but straight lines in all experimental and control runs suggesting that expression of epithelial markers was not responsive to fluid flow of 6 dyn/cm^2. OCT4 (POU5F1) had the same as SNAI1 expression profile and was not different between control and two flow groups. PDGFRA, a pan-fibroblast marker, was downregulated by 2.41 and 2.42 fold in flow 20hrs vs static and flow 40hrs vs static experiments, respectively (qPCR confirmed microarray analysis for PDGFRA, $p<0.01$). N-cadherin expression data is available from microarray analysis only but indicated a high upregulation after 20 and 40 hours, respectively, 11.4 fold ($p=0.0131$) and 10.53 fold ($p=0.0167$). Interestingly, PI-103 inhibitor, which is known for its antitumorigenic properties by promoting MET and suppressing EMT [121], eliminated gene expression restrictions under flow and positively modulated expression of SNAI1, and OCT4 and blocked flow-induced downregulation of PDGFRA. Inhibitor data of CDH2 expression in not available.

Summarizing this section, fluid flow effect after both 20hrs and 40hrs negatively regulated expression of some fibroblastic markers, upregulated mesenchymal marker expression and had a neutral effect on epithelial markers suggesting that MET was not modulated by shear stress and fluid flow alone is incapable of initiating MET within 40 hours of fibroblast exposure to 6 dyn/cm^2. Moreover, fluid flow caused effect that prevented fibroblasts from MET as it turned out from PI-103 studies and, possibly promoted EMT, which was previously confirmed in endothelial cells

[122,123]. The hypothesis that fluid flow promotes EMT is also supported by data published by Hwangbo et al. (2016), they demonstrated that TGFβ1-activated SMAD signaling during EMT prevents CAV1-mediated internalization and degradation of TGF-β receptors, including TGFBR3 [124].

5.3. Shear stress positively modulates SOX9 and RUNX2 expression in NHDF.

SOX9 and RUNX2 genes are major regulators of chondrogenesis and osteogenesis, respectively. Fluid flow positively regulated both in the experiment, while PI-103 inhibitor diminished SOX9 upregulation and did not affect RUNX2 expression. Upregulation of these two genes may be an evidence of fibroblast epigenetic state (chromatin openings) to differentiate into different cell type of the same, mesenchymal, origin, which requires additional confirmation. Microarray analysis (qPCR data in not available) also revealed the upregulation of genes of two types of collagen both after 20 and 40 hours that facilitate chondrocyte differentiation, first was collagen type 10 α1, a short chain collagen expressed by hypertrophic chondrocytes during endochondral ossification [GeneCards], second one was collagen type 4 α1, a marker of chondrogenesis. PI-103 inhibitor study also demonstrated that SOX9, SNAI1, and OCT4 are downstream targets for TGF-β/PI3K/AKT pathway, but CDH1, and RUNX2 are not.

To summarize this section, fluid flow modulates expression of some gene of differentiation, specifically, chondrocytes and osteocytes markers, possibly due to epigenetic state, which may be considered in prospect differentiation protocols. However, epigenetic state of dermal fibroblasts is needed to be studied to confirm this statement. Data also demonstrates that expression of SOX9, RUNX2, and COL4A1 after 20 hours was significantly higher than after 40 hours indicating that somewhere in between 0 and 40 hours fibroblasts started to compensate gene

modulation through unknown mechanisms of adaptation, possible this effect could be caused by interference with modulation of cell survival signaling. This shows that for future differentiation protocols, the lone effect of fluid flow on fibroblasts is more pronounced at 20 hours time-point rather than at 40 hours.

5.4. Fluid flow alleviates the expression of genes related to anti-fibrotic, anti-inflammatory, anti-apoptotic, anti-proliferative and anti-migratory effect in NHDF.

During the wound healing process, fibroblasts are responsible for migration to the site of injury to produce ECM components, such as COL1A1, and secret cell regulatory cytokines, such as TGF-β, which recruit immune cells, monocytes, and neutrophils, to infiltrate the wound [125]. SMAD3-depleted murine models showed accelerated wound healing effect that was achieved by immune cells absence at a site of injury [125,126]. The absence of SMAD3 also correlated with low levels of TGFβ1 [125] and impaired cell migration[127]. KIT gene is capable of impairing migration via PI3K-AKT and MEK-ERK pathways according to Vajravelu et al. (2015), which is also confirmed by Tan et al. (2015) [128,129]. Wahl et al. (1993) stated that SMAD3 deletion impairs chemotaxis of monocytes to TGFβ1 without affecting the expression of integrins and ICAMs, which was confirmed by Ashcroft et al. in 2000 [126,130]. This may explain ITGA2 gene expression dynamics in the experiment. Although ITGA2 is a PI3K pathway downstream gene [131], its expression was independent of changes in SMAD and PI3K/AKT signaling in the experiment. Another evidence of the anti-fibrotic potential of flow, as well as anti-proliferative, is downregulation of PDGFRA, which was confirmed by microarray and qPCR in the experiment. Studies suggest that PDGFRA mediates TGF-β induced fibrosis [132]. Interesting interactions were found in the literature regarding PDGFRA, NOX4, and PTX3 expression. Wagner et al. demonstrated that PDGF-induced mitogenic activity involves the NOX4-dependent production of reactive oxygen species, which

activate AKT and play a role in regulation of proliferation [133]. Also, NOX4 expression may influence PTX3 expression. Kunes et al. (2012) indicated that inflammatory response is achieved by explosive production of ROS, which is the primary role of NOX4 [134]. PTX3 has been shown to be an inflammation marker and can be used for therapeutic purposes [134–136].

Dominant-negative expression of SMAD3 and positive SMAD7 is also required for inhibition of COL1A1 expression [137,138]. In flow experiment, expression of COL1A1 was not modulated by flow but was upregulated after PI-103 treatment, suggesting that expression of some types of collagen (COL1A1) is synchronized with changes in SMAD3 expression. Microarray data analysis indicated significant (p=0.0259) upregulation of SMAD7 by 2.31 fold after 20 hours of exposure to flow, after 40 hours p-value was too high (0.074) to consider significant changes in expression. Thus, shear stress may facilitate ECM synthesis impairment. However, elevated levels of COL10A1 and COL4A1 expression in the experiment remain unclear and require further investigation (PCR data for SMAD7, COL10A1, COL4A1 is not available).

An interesting question remains – why the presence of SMAD3 is needed when it facilitates so many pathological processes? Ashcroft et al. (1999) suggest that cells are balancing between apoptosis and survival by regulating expression of key genes, one of them is SMAD3 that positively modulates controlled cell death (Fig. 27) [125].

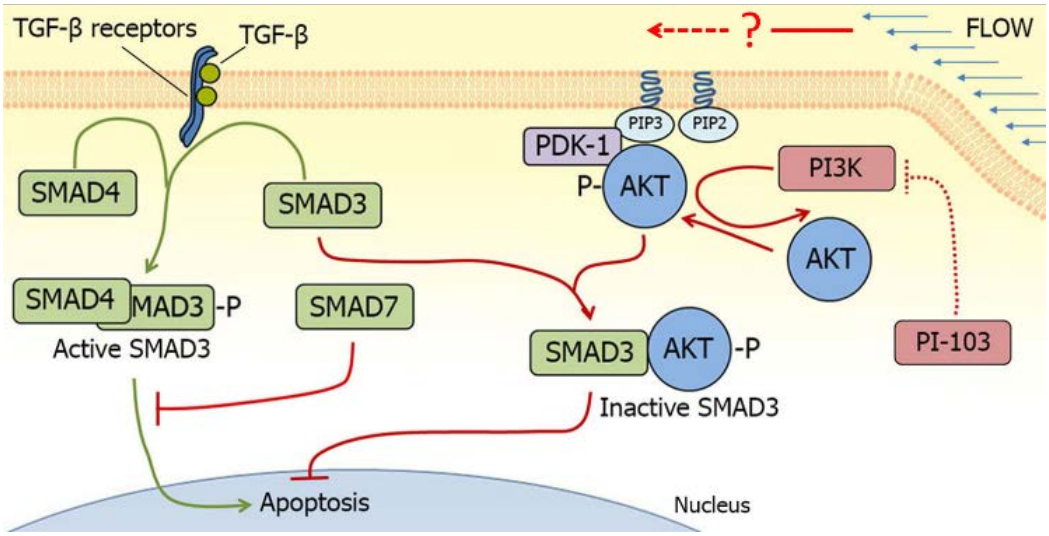

Figure 27. Interaction of SMAD3 and AKT regulates the balance between cell survival and TGF-β-induced apoptosis in static condition. After an activation of TGF-β receptors, pSMAD3 forms a complex with SMAD4 and translocate to the nucleus. SMAD7 and pAKT inhibits the function of SMAD3. The participation of flow in this signaling interaction is unclear (modified from [139]).

Summarizing this section, microarray, qPCR, and PI-103 treatment data of expression of SMAD3, NOX4, PTX3, ITGA2, and PDGFRA suggest that under fluid flow FBs resist to high levels of stress by negatively regulating inflammation, ECM remodeling, fibrosis and cell death. The addition of more stress factors (prolonged exposure to fluid flow for 40 hours) adjusts TGF-β signaling which may shift the balance towards apoptosis. Probably, if negative impact on cells persist, eventually this would lead to SMAD3-modulated apoptosis when resistance potential of fibroblasts is depleted (refer to the increasing expression of NOX4, Fig. 29). However, this hypothesis needs to be confirmed by additional studies.

5.5. Fluid flow modulates expression of genes, which are conserved during differentiation.

This chapter summarizes a large comparison of eight different microarray data sets obtained from GEO repository with microarray data from the flow experiment. A detailed description of the comparison process is presented in Table 9 in the Appendix. Briefly, the

intention of the calculated score was to show how close fluid flow drives fibroblasts to another cell type if fibroblasts have chosen a fate of trans-differentiation under fluid flow.

The difference between two effects was compared. 1) control, effect that fluid flow caused – FBs Static vs FBs Flow 20hrs, and FBs Static vs FBs Flow 40hrs and 2) effect caused by FBs treatment, or difference in gene expression profiles between two cell types (e.g., FBs vs TGFβ1-induced FBs). For convenience, the similarity is presented as a score, or similarity score, and represents the percentage of common genes between two effects (flow effect vs treatment effect), or flow effect and difference in gene expression profile. Calculated similarity score is in Fig. 28. For score calculation refer to Figure 31 in the Appendix.

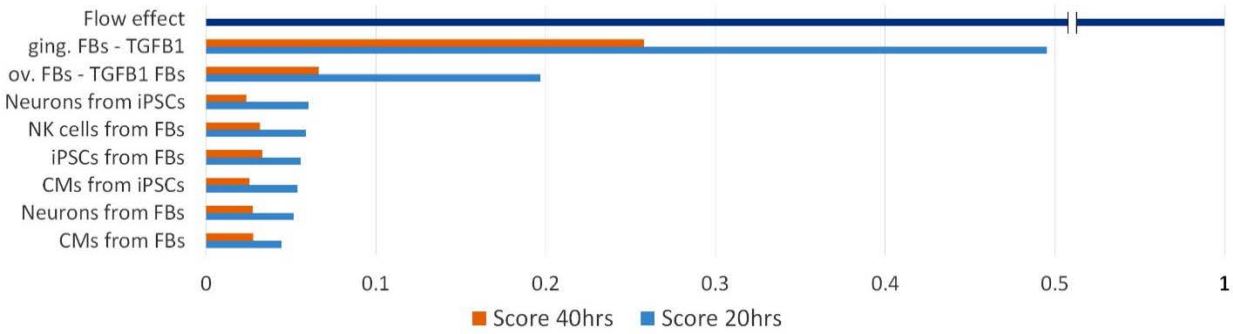

Figure 28. Similarity score for eight comparisons (for additional information refer to Appendix).

The score shows how big a difference is between flow effect and treatment effect on a scale from 0 to 1, where 1 indicates a 100% similarity to a flow effect, and 0 means complete difference with flow effect. As it turned out, the highest score (similarity) was observed between flow effect at 20 hours and TGFβ1 treatment effect on gingival fibroblasts. This confirms statements discussed in the literature review chapter that shear stress involves TGF-β pathway. Interestingly, expression of TGFβ1 gene according to microarray data was not significantly modulated (1.61 fold change,

p=0.1019 after 20 hours; after 40 hours – 1.89, *p*=0.0363). Apparently, flow induces TGFβ1 through different downstream targets of TGFβ1 and TGF-β pathway but not through upregulation of TGFβ1 gene expression.

Summarizing this section, comparison analysis confirms that fluid flow effect is more pronounced at 20 hours rather than at 40 hours time-point as the number of common genes shortened. Although thorough analysis of the involvement of each gene is required, the data suggest that genes responsible for regulation of development are conserved across all microarrays compared, including current experimental data, while genes responsible for signaling are prone to be conditional. Unique and duplicated genes for both conditions are listed in the Appendix.

5.6. Upregulation of OCT4 (POU5F1), as a reciprocal regulation of AKT, may not indicate pluripotency after co-exposure to flow and PI-103.

AKT phosphorylates OCT4 to initiate OCT4/SOX2 heterodimer formation [140]. Lin et al. demonstrated that AKT-mediated phosphorylation promoted the interaction of OCT4 with other pluripotency markers, promoted self-renewal of embryonal carcinoma cells, and suppressed their differentiation [141]. They also confirmed that in embryonal carcinoma cells, levels of phosphorylated OCT4 by AKT correlated with resistance to apoptosis and tumorigenic potential [141].

AKT and OCT4 expression are mutually orchestrated. Taking into account an increased upregulation of OCT4 in the experiment and dynamics of ADM, PTX3, and NOX4 expression, it is assumed that PI-103 treatment dramatically increased the level of non-physiological negative impact on FBs under the flow. This suggests that OCT4 upregulation is another compensatory mechanism of cell survival. However, this hypothesis requires additional confirmation.

5.7. Limitations.

There are some limitations of the study, which need to be considered for future work:

- The custom-built flow loop, except for peristaltic pump, is challenging to run. The total number of flow runs was over 60. Almost half of them were discarded from the experiment due to different reasons, such as leaks or excessive bubbling. Better control will more likely affect the standard deviation of the results.
- Flow loop oxygen calculations were made with many assumptions (refer to Appendix section **Oxygen calculations**) and may differ from the actual oxygen concentration in the flow loop. Use of an oxygen sensor should be considered to continuously measure O_2 levels.
- Heterogeneity of the fibroblast population should be quantified prior to the experiment. It is possible that nearly all commercially available fibroblast cultures contain a subpopulation of adipocytes, preadipocytes, and mesenchymal stem cells or their progenitors, or a mixture of them.
- Control samples (Static 40hrs) were collected but never analyzed due to microarray platform limitation to process many samples simultaneously. Thus, the cost is another limitation.
- Expression of some markers were not confirmed with qPCR due to project timeline.
- Gene expression results of key genes need additional confirmation with protein expression.
- All trans-differentiation techniques require more than two days for cells to differentiate. That suggests that fibroblasts should be exposed to flow for a period

longer than 40 hours. The main limitation is high chance of contamination due to passing the media change time-point.

5.8. Future work.

The findings discussed in sections 5.1-5.6 leave some of the questions open for additional experiments. We have identified that under fluid flow, at a gene level, cells are not prone to differentiate into either iPSCs or progenitors of different cell lines, though some of the markers were upregulated. It is possible that resistance to high level of shear stress is a significant roadblock of initiation of differentiation. Thus, same experiments with lower magnitude of shear stress is needed, as well as prolonged exposure to flow for non-inhibitory study, e.g. 60 hours, and 40 hour for inhibitory study followed by microarray study for a comparison. The second part of this experiment is seen to be a quantification of protein expression, specifically, phosphorylated levels of SMADs and other signaling molecules of TGF-β and PI3K/AKT pathways. Putting gene expression and protein expresion pieces together would insert another known part into a puzzle of pathway interactions since the entire picture of signaling interplay under the flow is unclear.

Interestingly, SOX9 and RUNX2, master developmental genes for chondrogenesis and osteogenesis, are very flow-responsive. Further understanding of their regulation will probably provide more answers. Future experiments may be focused on either SOX9 or RUNX2 knock-down by small interfering RNA or other inhibitors.

In the experiment, OCT4 was the only Yamanaka factor of interest that was not upregulated by flow and was significantly modulated in the inhibitor study. To complete the full picture, gene expression of other Yamanaka factors (KLF4, SOX2, NANOG) would shed some light on the regulation of master pluripotency markers under fluid flow and PI-103 co-treatment.

Overall, shear stress can alter the expression of genes responsible for survival and development. NHDF is a very resistant cell type capable of surviving in conditions that seemed to be not evolutionary natural for it. This should be considered, as any treatment applied to NHDF would more likely trigger a cascade of self-defensive mechanisms, which will protect cells from a potential negative impact of treatment to prevent apoptosis or necrosis. Also, fibroblasts respond to shear stress by modulating many of their functions including regulation of development. Although, FBs trans-differentiation under the flow requires additional experiments and validation, fluid flow may be considered as a preconditioning factor in de- or trans-differentiation protocols for cell production.

References

1. Outani, H. *et al.* Direct Induction of Chondrogenic Cells from Human Dermal Fibroblast Culture by Defined Factors. *PLOS ONE* 8, e77365 (2013).
2. Xue, Y. *et al.* Direct Conversion of Fibroblasts to Neurons by Reprogramming PTB-Regulated MicroRNA Circuits. *Cell* 152, 82–96 (2013).
3. Takahashi, K. *et al.* Induction of Pluripotent Stem Cells from Adult Human Fibroblasts by Defined Factors. *Cell* 131, 861–872 (2007).
4. Yamanaka, S. A Fresh Look at iPS Cells. *Cell* 137, 13–17 (2009).
5. Gareau, T. *et al.* Shear stress influences the pluripotency of murine embryonic stem cells in stirred suspension bioreactors. *J. Tissue Eng. Regen. Med.* 8, 268–278 (2014).
6. Lara, G. G. *et al.* Fluid Flow Modulation of Murine Embryonic Stem Cell Pluripotency Gene Expression in the Absence of LIF. *Cell. Mol. Bioeng.* 6, 335–345 (2013).
7. Bindu A, H. & B, S. Potency of Various Types of Stem Cells and their Transplantation. *J. Stem Cell Res. Ther.* 1, (2011).
8. Goldberg, A. D., Allis, C. D. & Bernstein, E. Epigenetics: A Landscape Takes Shape. *Cell* 128, 635–638 (2007).
9. Epigenetic Landscape | The Embryo Project Encyclopedia. Available at: https://embryo.asu.edu/pages/epigenetic-landscape. (Accessed: 7th July 2016)
10. Wegener, M., Bader, A. & Giri, S. How to mend a broken heart: adult and induced pluripotent stem cell therapy for heart repair and regeneration. *Drug Discov. Today.* doi:10.1016/j.drudis.2015.02.010
11. Junker, J. P. E., Sommar, P., Skog, M., Johnson, H. & Kratz, G. Adipogenic, chondrogenic and osteogenic differentiation of clonally derived human dermal fibroblasts. *Cells Tissues Organs* 191, 105–118 (2010).
12. Takahashi, K. & Yamanaka, S. Induction of Pluripotent Stem Cells from Mouse Embryonic and Adult Fibroblast Cultures by Defined Factors. *Cell* 126, 663–676 (2006).
13. Csöbönyeiová, M., Polák, Š. & Danišovič, L. Perspectives of induced pluripotent stem cells for cardiovascular system regeneration. *Exp. Biol. Med.* (2015). doi:10.1177/1535370214565976
14. Dell'Era, P. Cardiac disease modeling using induced pluripotent stem cell-derived human cardiomyocytes. *World J. Stem Cells* 7, 329 (2015).
15. Malik, N. & Rao, M. S. A Review of the Methods for Human iPSC Derivation. *Methods Mol. Biol. Clifton NJ* 997, 23–33 (2013).
16. Han, D. W. *et al.* Direct Reprogramming of Fibroblasts into Neural Stem Cells by Defined Factors. *Cell Stem Cell* 10, 465–472 (2012).
17. Caiazzo, M. *et al.* Direct generation of functional dopaminergic neurons from mouse and human fibroblasts. *Nature* 476, 224–227 (2011).

18. Kim, J. *et al.* Direct reprogramming of mouse fibroblasts to neural progenitors. *Proc. Natl. Acad. Sci.* 108, 7838–7843 (2011).

19. Pang, Z. P. *et al.* Induction of human neuronal cells by defined transcription factors. *Nature* 476, 220–223 (2011).

20. Vierbuchen, T. *et al.* Direct conversion of fibroblasts to functional neurons by defined factors. *Nature* 463, 1035–1041 (2010).

21. Yang, N., Ng, Y. H., Pang, Z. P., Südhof, T. C. & Wernig, M. Induced Neuronal Cells: How to Make and Define a Neuron. *Cell Stem Cell* 9, 517–525 (2011).

22. Ieda, M. *et al.* Direct reprogramming of fibroblasts into functional cardiomyocytes by defined factors. *Cell* 142, 375–386 (2010).

23. Fu, J.-D. & Srivastava, D. Direct Reprogramming of Fibroblasts into Cardiomyocytes for Cardiac Regenerative Medicine. *Circ. J.* (2015).

24. Fu, J.-D. *et al.* Direct Reprogramming of Human Fibroblasts toward a Cardiomyocyte-like State. *Stem Cell Rep.* 1, 235–247 (2013).

25. Nam, Y.-J. *et al.* Reprogramming of human fibroblasts toward a cardiac fate. *Proc. Natl. Acad. Sci. U. S. A.* 110, 5588–5593 (2013).

26. Wada, R. *et al.* Induction of human cardiomyocyte-like cells from fibroblasts by defined factors. *Proc. Natl. Acad. Sci.* 110, 12667–12672 (2013).

27. Piryaei, A. *et al.* Ultrastructural maturation of human bone marrow mesenchymal stem cells-derived cardiomyocytes under alternative induction of 5-azacytidine. *Cell Biol. Int.* 39, 519–530 (2015).

28. Gao, Q. *et al.* A Cocktail Method for Promoting Cardiomyocyte Differentiation from Bone Marrow-Derived Mesenchymal Stem Cells. *Stem Cells Int.* 2014, (2014).

29. Choi, Y. S. *et al.* Differentiation of human adipose-derived stem cells into beating cardiomyocytes. *J. Cell. Mol. Med.* 14, 878–889 (2010).

30. Cao, N. *et al.* Conversion of human fibroblasts into functional cardiomyocytes by small molecules. *Science* aaf1502 (2016). doi:10.1126/science.aaf1502

31. Margariti, A. *et al.* Direct reprogramming of fibroblasts into endothelial cells capable of angiogenesis and reendothelialization in tissue-engineered vessels. *Proc. Natl. Acad. Sci.* 109, 13793–13798 (2012).

32. Sayed, N. *et al.* Transdifferentiation of Human Fibroblasts to Endothelial Cells. Clinical Perspective. *Circulation* 131, 300–309 (2015).

33. Ginsberg, M. *et al.* Efficient Direct Reprogramming of Mature Amniotic Cells into Endothelial Cells by ETS Factors and TGFβ Suppression. *Cell* 151, 559–575 (2012).

34. Watabe, T. *et al.* TGF-beta receptor kinase inhibitor enhances growth and integrity of embryonic stem cell-derived endothelial cells. *J. Cell Biol.* 163, 1303–1311 (2003).

35. Szabo, E. *et al.* Direct conversion of human fibroblasts to multilineage blood progenitors. *Nature* 468, 521–526 (2010).

36. Sorrell, J. M. & Caplan, A. I. Fibroblast heterogeneity: more than skin deep. *J. Cell Sci.* 117, 667–675 (2004).

37. Fernandes, K. J. L. *et al.* A dermal niche for multipotent adult skin-derived precursor cells. *Nat. Cell Biol.* 6, 1082–1093 (2004).

38. Jinno, H. *et al.* Convergent genesis of an adult neural crest-like dermal stem cell from distinct developmental origins. *Stem Cells Dayt. Ohio* 28, 2027–2040 (2010).

39. Driskell, R. R. & Watt, F. M. Understanding fibroblast heterogeneity in the skin. *Trends Cell Biol.* 25, 92–99 (2015).

40. Sorrell, J. M., Baber, M. A. & Caplan, A. I. Site-matched papillary and reticular human dermal fibroblasts differ in their release of specific growth factors/cytokines and in their interaction with keratinocytes. *J. Cell. Physiol.* 200, 134–145 (2004).

41. Lee, J. & Tumbar, T. Hairy tale of signaling in hair follicle development and cycling. *Semin. Cell Dev. Biol.* 23, 906–916 (2012).

42. Sennett, R. & Rendl, M. Mesenchymal-epithelial interactions during hair follicle morphogenesis and cycling. *Semin. Cell Dev. Biol.* 23, 917–927 (2012).

43. Biernaskie, J. *et al.* SKPs derive from hair follicle precursors and exhibit properties of adult dermal stem cells. *Cell Stem Cell* 5, 610–623 (2009).

44. Toma, J. G. *et al.* Isolation of multipotent adult stem cells from the dermis of mammalian skin. *Nat. Cell Biol.* 3, 778–784 (2001).

45. Paus, R. & Cotsarelis, G. The biology of hair follicles. *N. Engl. J. Med.* 341, 491–497 (1999).

46. Ito, M. & Sato, Y. Dynamic ultrastructural changes of the connective tissue sheath of human hair follicles during hair cycle. *Arch. Dermatol. Res.* 282, 434–441 (1990).

47. Yang, C.-C. & Cotsarelis, G. Review of hair follicle dermal cells. *J. Dermatol. Sci.* 57, 2 (2010).

48. Feutz, A.-C., Barrandon, Y. & Monard, D. Control of thrombin signaling through PI3K is a mechanism underlying plasticity between hair follicle dermal sheath and papilla cells. *J. Cell Sci.* 121, 1435–1443 (2008).

49. Amoh, Y. & Hoffman, R. M. Isolation and culture of hair follicle pluripotent stem (hfPS) cells and their use for nerve and spinal cord regeneration. *Methods Mol. Biol. Clifton NJ* 585, 401–420 (2010).

50. Amoh, Y., Li, L., Katsuoka, K., Penman, S. & Hoffman, R. M. Multipotent nestin-positive, keratin-negative hair-follicle bulge stem cells can form neurons. *Proc. Natl. Acad. Sci. U. S. A.* 102, 5530–5534 (2005).

51. Janmaat, C. J. *et al.* Human Dermal Fibroblasts Demonstrate Positive Immunostaining for Neuron- and Glia- Specific Proteins. *PLOS ONE* 10. (2015).

52. Dominici, M. *et al.* Minimal criteria for defining multipotent mesenchymal stromal cells. The International Society for Cellular Therapy position statement. *Cytotherapy* 8, 315–317 (2006).

53. Haniffa, M. A., Collin, M. P., Buckley, C. D. & Dazzi, F. Mesenchymal stem cells: the fibroblasts' new clothes? *Haematologica* 94, 258–263 (2009).

54. Jääger, K. & Neuman, T. Human dermal fibroblasts exhibit delayed adipogenic differentiation compared with mesenchymal stem cells. *Stem Cells Dev.* 20, 1327–1336 (2011).

55. Ali, A. T., Hochfeld, W. E., Myburgh, R. & Pepper, M. S. Adipocyte and adipogenesis. *Eur. J. Cell Biol.* 92, 229–236 (2013).

56. Sudo, K. *et al.* Mesenchymal progenitors able to differentiate into osteogenic, chondrogenic, and/or adipogenic cells in vitro are present in most primary fibroblast-like cell populations. *Stem Cells Dayt. Ohio* 25, 1610–1617 (2007).

57. Ingber, D. E. Cellular mechanotransduction: putting all the pieces together again. *FASEB J.* 20, 811–827 (2006).

58. Hamill, O. P. & Martinac, B. Molecular Basis of Mechanotransduction in Living Cells. *Physiol. Rev.* 81, 685–740 (2001).

59. Schwartz, M. A. & DeSimone, D. W. Cell adhesion receptors in mechanotransduction. *Curr. Opin. Cell Biol.* 20, 551–556 (2008).

60. Orr, A. W., Helmke, B. P., Blackman, B. R. & Schwartz, M. A. Mechanisms of Mechanotransduction. *Dev. Cell* 10, 11–20 (2006).

61. Wang, J. H.-C., Thampatty, B. P., Lin, J.-S. & Im, H.-J. Mechanoregulation of gene expression in fibroblasts. *Gene* 391, 1–15 (2007).

62. Davies, P. F. Flow-mediated endothelial mechanotransduction. *Physiol. Rev.* 75, 519–560 (1995).

63. Chiquet, M., Tunç-Civelek, V. & Sarasa-Renedo, A. Gene regulation by mechanotransduction in fibroblasts. *Appl. Physiol. Nutr. Metab.* 32, 967–973 (2007).

64. Choquet, D., Felsenfeld, D. P. & Sheetz, M. P. Extracellular matrix rigidity causes strengthening of integrin-cytoskeleton linkages. *Cell* 88, 39–48 (1997).

65. Schmidt, C., Pommerenke, H., Dürr, F., Nebe, B. & Rychly, J. Mechanical stressing of integrin receptors induces enhanced tyrosine phosphorylation of cytoskeletally anchored proteins. *J. Biol. Chem.* 273, 5081–5085 (1998).

66. Tzima, E. *et al.* A mechanosensory complex that mediates the endothelial cell response to fluid shear stress. *Nature* 437, 426–431 (2005).

67. Mohan, S., Mohan, N. & Sprague, E. A. Differential activation of NF-kappa B in human aortic endothelial cells conditioned to specific flow environments. *Am. J. Physiol.* 273, C572-578 (1997).

68. Tamada, M., Sheetz, M. P. & Sawada, Y. Activation of a signaling cascade by cytoskeleton stretch. *Dev. Cell* 7, 709–718 (2004).

69. Bershadsky, A., Kozlov, M. & Geiger, B. Adhesion-mediated mechanosensitivity: a time to experiment, and a time to theorize. *Curr. Opin. Cell Biol.* 18, 472–481 (2006).

70. van Kooten, T. G., Schakenraad, J. M., Van der Mei, H. C. & Busscher, H. J. Development and use of a parallel-plate flow chamber for studying cellular adhesion to solid surfaces. *J. Biomed. Mater. Res.* 26, 725–738 (1992).

71. Gupta, R. *et al.* The effect of shear stress on fibroblasts derived from Dupuytren's tissue and normal palmar fascia. *J. Hand Surg.* 23, 945–950 (1998).

72. Steward, R. L., Cheng, C.-M., Ye, J. D., Bellin, R. M. & LeDuc, P. R. Mechanical stretch and shear flow induced reorganization and recruitment of fibronectin in fibroblasts. *Sci. Rep.* 1, (2011).

73. Garanich, J. S., Mathura, R. A., Shi, Z.-D. & Tarbell, J. M. Effects of fluid shear stress on adventitial fibroblast migration: implications for flow-mediated mechanisms of arterialization and intimal hyperplasia. *Am. J. Physiol. Heart Circ. Physiol.* 292, H3128-3135 (2007).

74. Archambault, J. M., Elfervig-Wall, M. K., Tsuzaki, M., Herzog, W. & Banes, A. J. Rabbit tendon cells produce MMP-3 in response to fluid flow without significant calcium transients. *J. Biomech.* 35, 303–309 (2002).

75. Ng, C. P., Hinz, B. & Swartz, M. A. Interstitial fluid flow induces myofibroblast differentiation and collagen alignment in vitro. *J. Cell Sci.* 118, 4731–4739 (2005).

76. Park, J. S. *et al.* The effect of matrix stiffness on the differentiation of mesenchymal stem cells in response to TGF-β. *Biomaterials* 32, 3921–3930 (2011).

77. Martines, E., McGhee, K., Wilkinson, C. & Curtis, A. A parallel-plate flow chamber to study initial cell adhesion on a nanofeatured surface. *IEEE Trans. Nanobioscience* 3, 90–95 (2004).

78. Shi, Z. D., Wang, H. & Tarbell, J. M. Interstitial flow induces MMP-1 expression and SMC migration in 3-D collagen I gels via an ERK1/2-c-Jun pathway and mechanosenation by heparan sulfate proteoglycans and focal adhesions. in *Proceedings of the 2010 IEEE 36th Annual Northeast Bioengineering Conference (NEBEC)* 1–2 (2010). doi:10.1109/NEBC.2010.5458236

79. Korin, N., Bransky, A., Dinnar, U. & Levenberg, S. A parametric study of human fibroblasts culture in a microchannel bioreactor. *Lab. Chip* 7, 611–617 (2007).

80. Dan, L., Chua, C.-K. & Leong, K.-F. Fibroblast response to interstitial flow: A state-of-the-art review. *Biotechnol. Bioeng.* 107, 1–10 (2010).

81. Kouzarides, T. Chromatin modifications and their function. *Cell* 128, 693–705 (2007).

82. Chen, L.-J., Wei, S.-Y. & Chiu, J.-J. Mechanical regulation of epigenetics in vascular biology and pathobiology. *J. Cell. Mol. Med.* 17, 437–448 (2013).

83. Illi, B. *et al.* Shear Stress–Mediated Chromatin Remodeling Provides Molecular Basis for Flow-Dependent Regulation of Gene Expression. *Circ. Res.* 93, 155–161 (2003).

84. Heo, S.-J. *et al.* Biophysical Regulation of Chromatin Architecture Instills a Mechanical Memory in Mesenchymal Stem Cells. *Sci. Rep.* 5, (2015).

85. Runyan, C. E., Poncelet, A.-C. & Schnaper, H. W. TGF-beta receptor-binding proteins: complex interactions. *Cell. Signal.* 18, 2077–2088 (2006).

86. Ghosh, A. K., Yuan, W., Mori, Y., Chen Sj, null & Varga, J. Antagonistic regulation of type I collagen gene expression by interferon-gamma and transforming growth factor-beta. Integration at the level of p300/CBP transcriptional coactivators. *J. Biol. Chem.* 276, 11041–11048 (2001).

87. Chiquet, M., Renedo, A. S., Huber, F. & Flück, M. How do fibroblasts translate mechanical signals into changes in extracellular matrix production? *Matrix Biol.* 22, 73–80 (2003).

88. Yang, G., Crawford, R. C. & Wang, J. H.-C. Proliferation and collagen production of human patellar tendon fibroblasts in response to cyclic uniaxial stretching in serum-free conditions. *J. Biomech.* 37, 1543–1550 (2004).

89. Heinemeier, K., Langberg, H., Olesen, J. L. & Kjaer, M. Role of TGF-beta1 in relation to exercise-induced type I collagen synthesis in human tendinous tissue. *J. Appl. Physiol. Bethesda Md 1985* 95, 2390–2397 (2003).

90. Maeda, T. *et al.* Conversion of Mechanical Force into TGF-β-Mediated Biochemical Signals. *Curr. Biol.* 21, 933–941 (2011).

91. Ng, C. P. & Swartz, M. A. Fibroblast alignment under interstitial fluid flow using a novel 3-D tissue culture model. *Am. J. Physiol. Heart Circ. Physiol.* 284, H1771-1777 (2003).

92. Baum, J. & Duffy, H. S. Fibroblasts and Myofibroblasts: What are we talking about? *J. Cardiovasc. Pharmacol.* 57, 376–379 (2011).

93. Wang, S. & Tarbell, J. M. Effect of fluid flow on smooth muscle cells in a 3-dimensional collagen gel model. *Arterioscler. Thromb. Vasc. Biol.* 20, 2220–2225 (2000).

94. Bonvin, C., Overney, J., Shieh, A. C., Dixon, J. B. & Swartz, M. A. A multichamber fluidic device for 3D cultures under interstitial flow with live imaging: development, characterization, and applications. *Biotechnol. Bioeng.* 105, 982–991 (2010).

95. Radisic, M. *et al.* Medium perfusion enables engineering of compact and contractile cardiac tissue. *Am. J. Physiol. Heart Circ. Physiol.* 286, H507-516 (2004).

96. Shi, Z.-D. & Tarbell, J. M. Fluid flow mechanotransduction in vascular smooth muscle cells and fibroblasts. *Ann. Biomed. Eng.* 39, 1608–1619 (2011).

97. Galie, P. A., Russell, M. W., Westfall, M. V. & Stegemann, J. P. Interstitial fluid flow and cyclic strain differentially regulate cardiac fibroblast activation via AT1R and TGF-β1. *Exp. Cell Res.* 318, 75–84 (2012).

98. Laine, G. A. & Allen, S. J. Left ventricular myocardial edema. Lymph flow, interstitial fibrosis, and cardiac function. *Circ. Res.* 68, 1713–1721 (1991).

99. Petrov, V. V., Fagard, R. H. & Lijnen, P. J. Stimulation of collagen production by transforming growth factor-beta1 during differentiation of cardiac fibroblasts to myofibroblasts. *Hypertens. Dallas Tex 1979* 39, 258–263 (2002).

100. Glaros, T., Larsen, M. & Li, L. Macrophages and fibroblasts during inflammation, tissue damage and organ injury. *Front. Biosci. Landmark Ed.* 14, 3988–3993 (2009).

101. Akhmetshina, A. *et al.* Activation of canonical Wnt signalling is required for TGF-β-mediated fibrosis. *Nat. Commun.* 3, 735 (2012).

102. Shi, Z.-D., Ji, X.-Y., Qazi, H. & Tarbell, J. M. Interstitial flow promotes vascular fibroblast, myofibroblast, and smooth muscle cell motility in 3-D collagen I via upregulation of MMP-1. *Am. J. Physiol. - Heart Circ. Physiol.* 297, H1225–H1234 (2009).

103. Shi, Z.-D., Wang, H. & Tarbell, J. M. Heparan sulfate proteoglycans mediate interstitial flow mechanotransduction regulating MMP-13 expression and cell motility via FAK-ERK in 3D collagen. *PloS One* 6, e15956 (2011).

104. MacKenna, D. A., Dolfi, F., Vuori, K. & Ruoslahti, E. Extracellular signal-regulated kinase and c-Jun NH2-terminal kinase activation by mechanical stretch is integrin-dependent and matrix-specific in rat cardiac fibroblasts. *J. Clin. Invest.* 101, 301–310 (1998).

105. Tao, L., Liu, J., Li, Z., Dai, X. & Li, S. Role of the JAK-STAT pathway in proliferation and differentiation of human hypertrophic scar fibroblasts induced by connective tissue growth factor. *Mol. Med. Rep.* 3, 941–945 (2010).

106. Li, G., Li, Y.-Y., Sun, J.-E., Lin, W. & Zhou, R. ILK–PI3K/AKT pathway participates in cutaneous wound contraction by regulating fibroblast migration and differentiation to myofibroblast. *Lab. Invest.* 96, 741–751 (2016).

107. Shafa, M. *et al.* Impact of stirred suspension bioreactor culture on the differentiation of murine embryonic stem cells into cardiomyocytes. *BMC Cell Biol.* 12, 53 (2011).

108. Shafa, M. *et al.* Derivation of iPSCs in stirred suspension bioreactors. *Nat. Methods* 9, 465–466 (2012).

109. Alexander Obrejanu. Fluid Flow Induced Modulation of Smad2 and Akt Phosphorylation in Arterial Endothelial Cells. (2012).

110. Wang, C., Lu, H. & Schwartz, M. A. A novel in vitro flow system for changing flow direction on endothelial cells. *J. Biomech.* 45, 1212–1218 (2012).

111. Livak, K. J. & Schmittgen, T. D. Analysis of Relative Gene Expression Data Using Real-Time Quantitative PCR and the $2^{-\Delta\Delta CT}$ Method. *Methods* 25, 402–408 (2001).

112. Yu, J. *et al.* Multi-platform assessment of transcriptional profiling technologies utilizing a precise probe mapping methodology. *BMC Genomics* 16, (2015).

113. Yeung, T.-L. *et al.* TGF-β modulates ovarian cancer invasion by upregulating CAF-derived versican in the tumor microenvironment. *Cancer Res.* 73, 5016–5028 (2013).

114. Kuk, H., Hutchenreuther, J., Murphy-Marshman, H., Carter, D. & Leask, A. 5Z-7-Oxozeanol Inhibits the Effects of TGFβ1 on Human Gingival Fibroblasts. *PloS One* 10, e0123689 (2015).

115. Liu, G.-H. *et al.* Progressive degeneration of human neural stem cells caused by pathogenic LRRK2. *Nature* 491, 603–607 (2012).

116. Bernstein, P. *et al.* Expression pattern differences between osteoarthritic chondrocytes and mesenchymal stem cells during chondrogenic differentiation. *Osteoarthritis Cartilage* 18, 1596–1607 (2010).

117. Brennand, K. J. *et al.* Modelling schizophrenia using human induced pluripotent stem cells. *Nature* 473, 221–225 (2011).

118. Sun, N. *et al.* Patient-specific induced pluripotent stem cells as a model for familial dilated cardiomyopathy. *Sci. Transl. Med.* 4, 130ra47–130ra47 (2012).

119. Boyle, E. I. *et al.* GO::TermFinder—open source software for accessing Gene Ontology information and finding significantly enriched Gene Ontology terms associated with a list of genes. *Bioinforma. Oxf. Engl.* 20, 3710–3715 (2004).

120. Polo, J. M. & Hochedlinger, K. When Fibroblasts MET iPSCs. *Cell Stem Cell* 7, 5–6 (2010).

121. Zou, Z.-Q. *et al.* A novel dual PI3Kalpha/mTOR inhibitor PI-103 with high antitumor activity in non-small cell lung cancer cells. *Int. J. Mol. Med.* 24, 97–101 (2009).

122. Elliott, W. H., Tan, Y., Li, M. & Tan, W. High Pulsatility Flow Promotes Vascular Fibrosis by Triggering Endothelial EndMT and Fibroblast Activation. *Cell. Mol. Bioeng.* 8, 285–295 (2015).

123. Krenning, G. *et al.* Endothelial Plasticity: Shifting Phenotypes through Force Feedback. *Stem Cells Int.* 2016, e9762959 (2016).

124. Hwangbo, C. *et al.* Syntenin regulates TGF-β1-induced Smad activation and the epithelial-to-mesenchymal transition by inhibiting caveolin-mediated TGF-β type I receptor internalization. *Oncogene* 35, 389–401 (2016).

125. Ashcroft, G. S. *et al.* Mice lacking Smad3 show accelerated wound healing and an impaired local inflammatory response. *Nat. Cell Biol.* 1, 260–266 (1999).

126. Ashcroft, G. S. & Roberts, A. B. Loss of Smad3 modulates wound healing. *Cytokine Growth Factor Rev.* 11, 125–131 (2000).

127. Zhang, X., Yang, J., Zhao, J., Zhang, P. & Huang, X. MicroRNA-23b Inhibits the Proliferation and Migration of Heat-Denatured Fibroblasts by Targeting Smad3. *PloS One* 10, (2015).

128. Tan, J. *et al.* C-kit signaling promotes proliferation and invasion of colorectal mucinous adenocarcinoma in a murine model. *Oncotarget* 6, 27037–27048 (2015).

129. Vajravelu, B. N. *et al.* C-Kit Promotes Growth and Migration of Human Cardiac Progenitor Cells via the PI3K-AKT and MEK-ERK Pathways. *PloS One* 10, (2015).

130. Sm, W. *et al.* Role of transforming growth factor beta in the pathophysiology of chronic inflammation. *J. Periodontol.* 64, 450–455 (1993).

131. Dozmorov, M. G. *et al.* 5α-androstane-3α,17β-diol selectively activates the canonical PI3K/AKT pathway: a bioinformatics-based evidence for androgen-activated cytoplasmic signaling. *Genomic Med.* 1, 139–146 (2008).

132. Bonner, J. C., Badgett, A., Lindroos, P. M. & Osornio-Vargas, A. R. Transforming growth factor beta 1 downregulates the platelet-derived growth factor alpha-receptor subtype on human lung fibroblasts in vitro. *Am. J. Respir. Cell Mol. Biol.* 13, 496–505 (1995).

133. Wagner, B. *et al.* Mitogenic Signaling via Platelet-Derived Growth Factor β in Metanephric Mesenchymal Cells. *J. Am. Soc. Nephrol.* 18, 2903–2911 (2007).

134. Kunes, P. *et al.* Pentraxin 3(PTX 3): An Endogenous Modulator of the Inflammatory Response, Pentraxin 3(PTX 3): An Endogenous Modulator of the Inflammatory Response. *Mediat. Inflamm. Mediat. Inflamm.* 2012, 2012, (2012).

135. Inoue, K., Kodama, T. & Daida, H. Pentraxin 3: A Novel Biomarker for Inflammatory Cardiovascular Disease. *Int. J. Vasc. Med.* 2012, (2012).

136. Choi, B. *et al.* Pentraxin-3 Silencing Suppresses Gastric Cancer-related Inflammation by Inhibiting Chemotactic Migration of Macrophages. *Anticancer Res.* 35, 2663–2668 (2015).

137. Flanders, K. C. Smad3 as a mediator of the fibrotic response. *Int. J. Exp. Pathol.* 85, 47–64 (2004).

138. Cho, J.-W., Il, K.-J. & Lee, K.-S. Downregulation of type I collagen expression in silibinin-treated human skin fibroblasts by blocking the activation of Smad2/3-dependent signaling pathways: potential therapeutic use in the chemoprevention of keloids. *Int. J. Mol. Med.* 31, 1148–1152 (2013).

139. Remy, I., Montmarquette, A. & Michnick, S. W. PKB/Akt modulates TGF-beta signalling through a direct interaction with Smad3. *Nat. Cell Biol.* 6, 358–365 (2004).

140. Dai, X., Liu, P., Lau, A. W., Liu, Y. & Inuzuka, H. Acetylation-dependent regulation of essential iPS-inducing factors: a regulatory crossroad for pluripotency and tumorigenesis. *Cancer Med.* 3, 1211–1224 (2014).

141. Lin, Y. *et al.* Reciprocal Regulation of Akt and Oct4 Promotes the Self-Renewal and Survival of Embryonal Carcinoma Cells. *Mol. Cell* 48, 627–640 (2012).

142. Streeter, I. & Cheema, U. Oxygen consumption rate of cells in 3D culture: the use of experiment and simulation to measure kinetic parameters and optimise culture conditions. *The Analyst* 136, 4013–4019 (2011).

143. Naciri, M., Kuystermans, D. & Al-Rubeai, M. Monitoring pH and dissolved oxygen in mammalian cell culture using optical sensors. *Cytotechnology* 57, 245–250 (2008).

144. Zupke, C., Sinskey, A. J. & Stephanopoulos, G. Intracellular flux analysis applied to the effect of dissolved oxygen on hybridomas. *Appl. Microbiol. Biotechnol.* 44, 27–36 (1995).

145. Vendruscolo, F., Rossi, M., Jos&#xe9, R., Schmidell, W. & Ninow, J. L. Determination of Oxygen Solubility in Liquid Media. *Int. Sch. Res. Not.* 2012, (2012).

146. De Santa Barbara, P. *et al.* Direct Interaction of SRY-Related Protein SOX9 and Steroidogenic Factor 1 Regulates Transcription of the Human Anti-Müllerian Hormone Gene. *Mol. Cell. Biol.* 18, 6653–6665 (1998).

147. Moustakas, A., Souchelnytskyi, S. & Heldin, C.-H. Smad regulation in TGF-β signal transduction. *J. Cell Sci.* 114, 4359–4369 (2001).

148. Yamamoto, M., Toya, Y., Jensen, R. A. & Ishikawa, Y. Caveolin Is an Inhibitor of Platelet-Derived Growth Factor Receptor Signaling. *Exp. Cell Res.* 247, 380–388 (1999).

149. Parton, R. G. & Simons, K. The multiple faces of caveolae. *Nat. Rev. Mol. Cell Biol.* 8, 185–194 (2007).

150. Hanai, J. *et al.* Interaction and Functional Cooperation of PEBP2/CBF with Smads Synergistic Induction of the Immunoglobulin Germline Cα Promoter. *J. Biol. Chem.* 274, 31577–31582 (1999).

151. Zhang, Y.-W. *et al.* A RUNX2/PEBP2αA/CBFA1 mutation displaying impaired transactivation and Smad interaction in cleidocranial dysplasia. *Proc. Natl. Acad. Sci.* 97, 10549–10554 (2000).

152. Garlanda, C., Bottazzi, B., Bastone, A. & Mantovani, A. Pentraxins at the crossroads between innate immunity, inflammation, matrix deposition, and female fertility. *Annu. Rev. Immunol.* 23, 337–366 (2004).

153. Schröder, K. *et al.* Nox4 is a protective reactive oxygen species generating vascular NADPH oxidase. *Circ. Res.* 110, 1217–1225 (2012).

154. Zhu, P. *et al.* Nox4-dependent ROS modulation by amino endoperoxides to induce apoptosis in cancer cells. *Cell Death Dis.* 4, (2013).

155. Niwa, H., Miyazaki, J. & Smith, A. G. Quantitative expression of Oct-3/4 defines differentiation, dedifferentiation or self-renewal of ES cells. *Nat. Genet.* 24, 372–376 (2000).

156. Kotkamp, K. *et al.* Pou5f1/Oct4 Promotes Cell Survival via Direct Activation of mych Expression during Zebrafish Gastrulation. *PLOS ONE* 9, (2014).

Appendix

Oxygen calculations (supplementary information for section 3.2).

The amount of medium for cell expansion was based on the optimal oxygen accessibility for NHDFs calculated by using Flick's law of diffusion. This law formulates oxygen delivery to the cell culture through a permeable membrane:

$$Flux = -P(c_2 - c_1), \quad (4)$$

where P is the permeability for gas at a given temperature; $c_2 - c_1$ is concentration difference of the gas across the membrane. The law describes an oxygen flux based on its gradient between high concentration and low concentration areas. In one dimension, the Flick's second law is:

$$J = -D\frac{\Delta\varphi}{\Delta\chi}, \quad (5)$$

where J is the diffusion flux, D is the diffusion coefficient in the dimension of m^2/s, φ is the concentration, and χ is the height of medium level above the cells.

The first step was to assemble a loop and then apply a chamber with the cell to it. The loop was sitting in a biosafety cabinet at room temperature (without a glass plate with cell) before placing it in an incubator for approximately 10-20 minutes. To calculate the initial amount of air in the entire loop the following formula was used:

$$V_{Total\ air} = (V_B - V_{B\ Medium}) + (V_{PD} - V_{PD\ Medium}) + V_{Tubing}, \quad (6)$$

where, $V_{Total\ air}$ is the total amount of air in the system, V_B is the amount of air in the bottle, $V_{B\ Medium}$ is volume of medium in the bottle, V_{PD} is volume of air in the pulse dampener, $V_{PD\ Medium}$ is volume of medium in the pulse dampener, V_{Tubing} is volume of air in the tubing.

Calculation of oxygen level in the parallel plate flow chamber was made with assumptions. It was assumed that oxygen gradient was enough (low in the medium, high in the air) to drive gas

diffusion through medium due to cell oxygen consumption. The amount of oxygen produced during cell expiration was neglected. The depletion of air in the pulse dampener was also neglected. The pressure that was created in the tubing right after parallel plate flow chamber after pump priming was assumed to be immediately released through air filters. Solubility was calculated for DMEM medium with 0% FBS and at 25°C.

The average amount of air in the system was calculated as 305420 mm^3, part of oxygen theoretically available for cells was 62611 mm^3 (21%). Assuming that air filters were open for spontaneous oxygen exchange, the latest number indicates the amount of oxygen constantly circulating in the system at any time of the experiment. At 25°C and normal pressure, the solubility of oxygen in DMEM medium without FBS is 7 mg per liter. Adjusted amount of soluble oxygen in 180 cm^3 of the medium used in a loop is 1.26 mg. With 62611 mm^3 of oxygen in the loop, available dissolved oxygen in the medium is $2.6 \cdot 10^{-4}$ moles.

It is known that FBS decreases oxygen solubility in medium and oxygen concentration is a dynamic value because of cell respiration. These assumptions were used due to technical limitations of monitoring oxygen level in a loop at the time of the experiment. However, considering NHDF oxygen consumption rate as $1.19 \cdot 10^{-17}$ mol $cell^{-1}$ s^{-1} [142], doubling time of 41.8 hours, longest time point of exposure of 40 hours and number of cells with density of 16000 cell/cm^2 on 11x6 cm glass plate (gasket reduces the edges of plate for cells to occupy), the amount of oxygen consumed by all cells at the end of 40 hours flow experiment is $4.9 \cdot 10^{-6}$ moles, which is significantly lower than calculated amount of dissolved oxygen constantly presented in a loop. Sources used for oxygen calculations: [142–145].

Table 8. Description of genes of interests **(supplementary information for section 3.5).**

Gene name	*Brief description*
SOX9	Encodes protein transcription factor SRY (Sex-Determining Region Y)-Box 9. Acts during chondrocyte differentiation [146], plays a pivotal role in the male sexual development and normal skeletal development [NCBI]. The key transcription factor may regulate the expression of many genes involved in chondrogenesis [GeneCards].
SMAD3	Encodes protein SMAD3 (Mothers Against DPP Homolog 3). Mediates the signals from the transforming growth factor beta (TGF-β) superfamily ligands. Regulate cell proliferation, differentiation, and death. Essential in tumor growth [147].
ITGA2	Encodes cluster of differentiation 49b (CD49b)-integrin α subunit. Makes up half of the α2β1 integrin duplex. Integrins are involved in cell adhesion and participate in cell-surface mediated signaling [NCBI].
KIT	Proto-oncogene c-Kit or tyrosine-protein kinase Kit encodes CD117, which is a receptor tyrosine kinase type III, which binds to stem cell factor (c-KIT ligand, KITLG). Plays a role in cell survival, proliferation and differentiation. Marker of hematopoietic progenitors. Cell mobilizing marker, which indirectly defines progenitors' potential to migrate from the bone marrow into the bloodstream [NCBI].
CAV1	Encodes protein caveolin-1. The main component of the caveolae plasma membrane. Inhibits PDGF receptor kinase activity [148]. Roles vary: lipid regulation, cell signaling, mechanosensation. Chronic exposure to the flow stimulates upregulation of caveolin-1 in endothelial cells [149].
ADM	Encodes adrenomedullin. Plays a role in angiogenesis and increasing the tolerance of cells to oxidative stress and the negative effect of hypoxia [NCBI].
TGFBR3	Encodes betaglycan, a cell surface chondroitin sulfate / heparan sulfate proteoglycan, may inhibit TGF-β signaling. Could be involved in capturing and retaining TGF-beta for presentation to the signaling receptors [GeneCards].
RUNX2	Encodes runt-related transcription factor 2. RUNX2 is a key transcription factor for osteoblast differentiation. Directly interacts with SMAD3 [111], [112].
PTX3	Encodes pentraxin-related protein PTX3. Pentraxin is rapidly produced and released by many cell types in response to primary inflammatory signals and activates the classical pathway of complement activation and facilitates pathogen recognition [152].

NOX4	Encodes enzyme NADPH oxidase 4 that functions as the catalytic subunit of the NADPH oxidase complex. The protein acts as an oxygen sensor and reduces molecular oxygen by generating ROS or reactive oxygen species [GeneCards]. Protein is claimed to protect the vasculature against inflammatory stress [114]. Cancer cells intensively producing NOX4 undergo apoptosis [154]. ROS may play a role in signaling, cell growth and proliferation [NCBI]
COL1A1	Encodes α-1 type 1 collagen, a major component of fibrillar type 1 collagen. Strengthens and supports body tissues including skin. Provides rigidity and elasticity. Plays a role in PDGFR signaling, specifically, interacts with PDGFRB [NCBI].
SNAI1	Encodes Zinc finger protein SNAI1. Member of a family of transcription factors that repress adhesion molecule CDH1 (E-cadherin) and regulate EMT during embryonic development (NCBI). One of the key markers of EMT and is critical for mesoderm formation. SNAI1 is a regulator element in many cellular processes. Thus functions vary, e.g. maintenance of embryonic mesoderm, growth arrest, survival, cell migration [GeneCards].
POU5F1	Encodes POU domain, class 5, transcription factor 1 or octamer-binding protein 4 (OCT4). Plays a key role in embryonic development and stem cell pluripotency. A key marker of undifferentiated cells. Quantitative expression defines cell plasticity to differentiate [155]. Promotes cell survival [156].
CDH24	Encodes cadherin 24, a calcium-dependent cell adhesion protein. Mediates strong adhesion between cells [GeneCards].
CDH1	Encodes Cadherin 1, Type 1, E-cadherin (Epithelial). Regulates cell-cell adhesion, mobility, and proliferation of epithelial cells. Has strong tumor suppression function [GaneCards].
PDGFRA	Encodes platelet-derived growth factor receptor, alpha polypeptide, and a cell surface tyrosine kinase receptor for members of the platelet-derived growth factor family [NCBI]. CAV1 inhibits PDGFR signaling, specifically, PDGFRA activity [109]. Studies suggest that this gene plays a role in organ development, wound healing, and tumor progression and mediates signaling cascades, e.g. AKT signaling pathway [GeneCards].

Source 1: GeneCards: The Human Gene Database (GeneCards) at http://www.genecards.org
Source 2: The National Center for Biotechnology Information (NCBI) at http://www.ncbi.nlm.nih.gov/

Primer design (supplementary information for section 3.5).

To design primers, IDT Real-time PCR Tool [5] was used. Gene was entered in the form of RefSeq, e.g. for SMAD3 – NM_001145102.1. All RefSeq entries are available through NCBI [6] or Refgene [7] websites. Alternatively, FASTA format is allowed to be used for specific sequences. Chosen parameters for the primers were as following: min, optimum, maximum amplicon sizes were 80, 100, 120 respectively. Box for 'Exons' was checked off to ensure that designed primer was complementary to available exon only. Then coding sequences (CDS) were generated.

Primer3 [8] online tool was then used to test generated sequences. First, gene FASTA format or entire gene sequence was inserted into a box on top of the page. Boxes 'Pick left primer' and 'Pick right primer' contained generated sequences from IDT Real-time PCR Tool. Most of the rest parameters were left by default (blank), except for Primer Size: 12 80 22, Primer Temperature 58 60 62, Max Tm Difference 2.0. Primer GC% content: 40 50 60. Product size range 80-120. Recommended primers were then picked based on parameters that were close to desired input values. Around ten different sequences were tested for each gene and two the most suitable sequences were submitted through IDT website for a purchase. After delivery, all primers were reconstituted to a concentration of 47 µM and diluted 1:10 to the final batch concentration of 4.7 µM. Primers were stored in the fridge for no longer than three months, for a longer storage freezer is recommended.

All pairs of primers were tested by ViiA 7 Real-Time PCR System (Thermo Fisher Scientific) by generating standard melt curves. Nine out of ten pairs indicated presence of one

[5] https://www.idtdna.com/scitools/Applications/RealTimePCR/
[6] http://www.ncbi.nlm.nih.gov/gene/
[7] http://refgene.com/gene/
[8] http://bioinfo.ut.ee/primer3/

product in the sample (melt curve for SOX9 had multiple peaks). The second pair of primers for SOX9 was tested and showed the presence of one product. Thus, IDT Real-time PCR Tool with additional testing in Primer3 is a robust tool to design favorable primers.

$2^{-\Delta\Delta C_T}$ analysis (supplementary information for section 3.5).

The analysis was performed according to K. J. Livak and T. D. Schmittgen (2001) [111] in Microsoft Excel 2016 with available standard tools without additional plug-ins. PCR for two reference genes, RPOL2A and PRLP0, was run for all samples. C_T value for reference genes for all sample did not exceed 1.5 C_T. The geometric mean of C_T for reference genes (C_T RefGen) was calculated first for each triplicate of each sample. To obtain a ΔC_T Cntrl value, C_T RefGen was subtracted from a C_T value of gene of interest (C_T GOI), e.g. SMAD3, from a control experiment. Same calculations were used to obtain a ΔC_T Exprmt value for flow experiments. For $\Delta\Delta C_T$ value, ΔC_T Cntrl was subtracted from ΔC_T Exprmt, then individual $2^{-\Delta\Delta C_T}$ values were calculated. The general formula was:

$$2^{-(C_T\ GOI - C_T\ RefGen)_{Experiment} - (C_T\ GOI - C_T\ RefGen)_{Control}}, \qquad (7)$$

where C_T *GOI* is the C_T value of gene of interest, C_T *RefGen* is the C_T value of the geometric mean of two reference genes.

The values of $2^{-\Delta\Delta C_T}$ are always greater than 0 and do not clearly represent a negative fold change of gene expression. To calculate a negative fold change when $2^{-\Delta\Delta C_T}$ was <1, the following formula was used: $1/2^{-\Delta\Delta C_T}$. Example: $2^{-\Delta\Delta C_T}$ of CAV1 was 0.164. This means the expression of caveolin was downregulated in the flow experiment. Negative fold change was 1/0.164=6.098 (value from microarray analysis was negative 4.97). To decrease the standard error, individual values for $2^{-\Delta\Delta C_T}$ were used instead of averaged ones. In Microsoft Excel, convenient function to use to present a commonly acceptable fold change from $2^{-\Delta\Delta C_T}$ values is IF Function (Fig. 29).

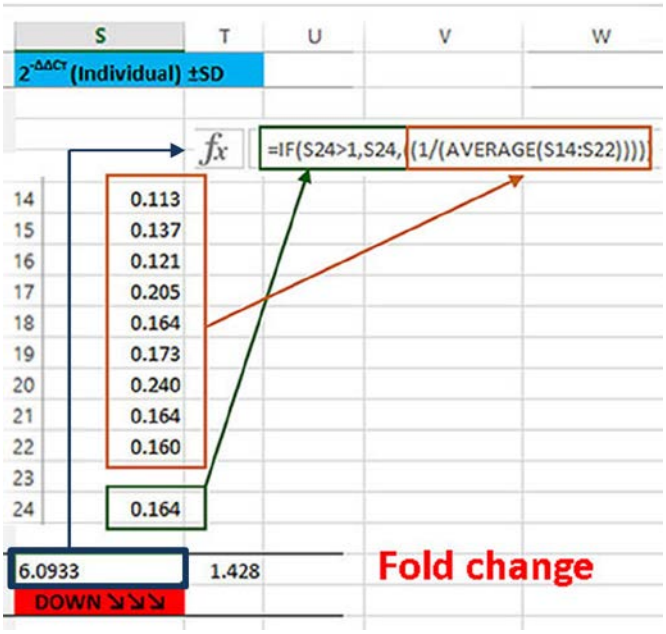

Figure 29. Example of ME2016 function to calculate fold expression based on $2^{-\Delta\Delta C_T}$ values. The average value was with the function IF (on top). As value 0.164 was less than 1, function IF calculated the second condition and divided one by the average of values from cells S14:S22. The result was 6.0933. The cell below was color-coded with Conditional Formatting (standard tool in Excel) and tailored to the cell S24. Thus, the program checked S24 cell and applied the corresponding color depending if the value was greater or less than 1. Color codes help to indicate upregulation or downregulated and prevent a subjective error because a negative sign is never used. One-way ANOVA between experimental ΔC_T and flow ΔC_T (control) was used to calculate *p*-value. In this particular example for CAV1, $p=9.5\cdot10^{-11}$.

Function IF and color-coding help to automate calculations. By only manual changing C_T GOI values, the program automatically calculates fold change with a color indicating the direction of gene modulation. Data from $2^{-\Delta\Delta C_T}$ analysis reflected the same trends from microarray analysis.

RIN values of RNA samples according to 2100 Bioanalyzer (supplementary information for section 4.2).

All samples collected according to mirVana protocol demonstrated high RIN (RNA Integrity Number) values (Fig. 30).

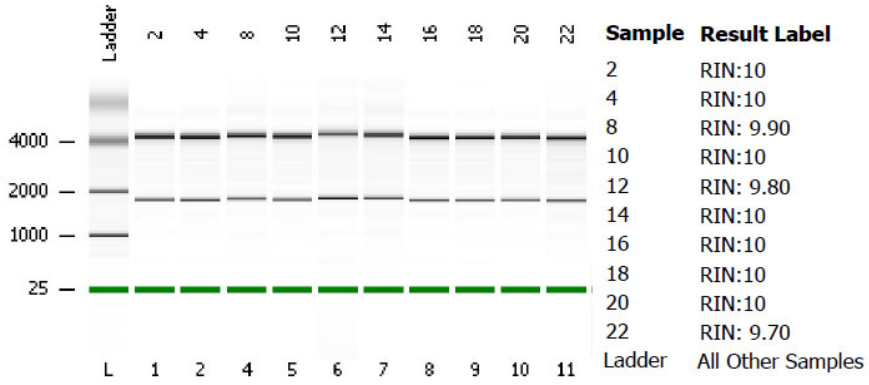

Figure 30. RIN values of samples of RNA from 2100 Bioanalyzer. Most of the samples indicated the highest quality with RIN=10, while three samples had high values close to 10.

All other RNA samples were considered of a high quality. Nine samples, one triplicate per one of three conditions (Static, Flow 20hrs, Flow 40hrs) were used to generate and analyze microarray data.

GEO access and microarray data processing (supplementary information for section 4.2.2).

Gene Expression Omnibus (GEO) offers more than 4300 microarray studies. It has become a useful tool to compare a newly generated data with the existing one from a submitted research. The search of a suitable data set starts with GEO Data Set Browser. The section under the list of sets provides a brief description, including the platform and cited paper. Sample Subsets button reveals links for a corresponding sample alongside with the description. Each sample contains a summary and a supplementary file or files, usually a file with .CEL extension. All needed .CEL files were downloaded, and RMA analysis was run in Affymetrix Expression Console, available from the official Affymetrix website. Generated .CHP files was imported into Affymetrix TAC Software 3.0 and analyzed with a fold change cut-off >2 or <-2 and $p<0.05$. Gene lists were filtered based on the genes of interest and expression of common genes was compared in Microsoft Excel 2016. Gene expression was plotted based on the fold change difference and similarity of trends of expression. Figure 31, as an example, depicts a small portion of plotted gene expression data.

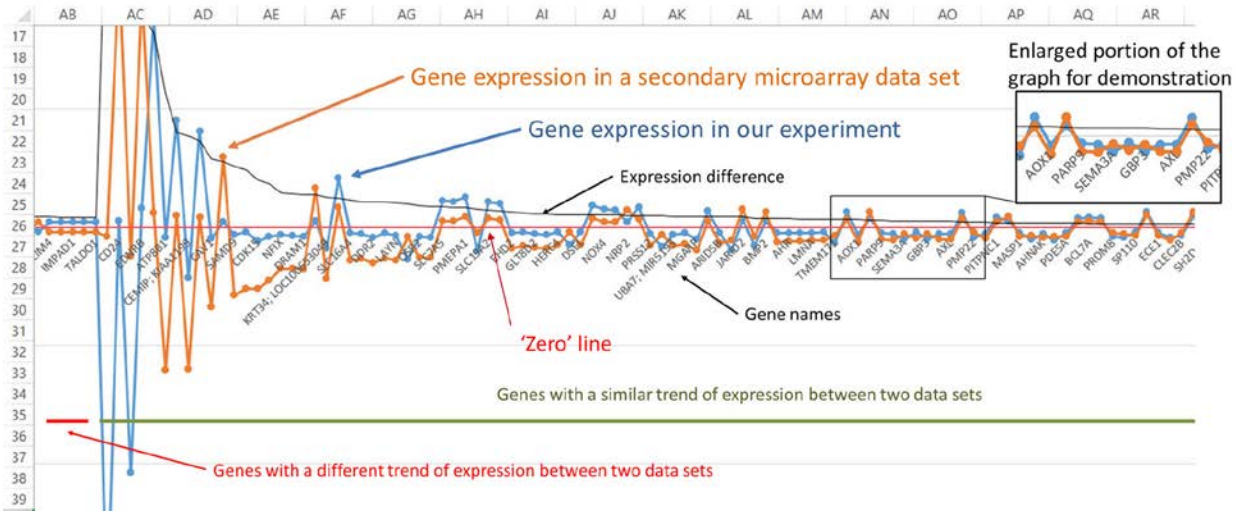

Figure 31. Example of comparison of gene expression between two different data sets from GEO repository.

Supplementary files can be pulled from different studies and compare with each other as long as platform or library used is the same, otherwise raw data submitted as a .TXT file has to be processed in a separate software with programming component to assign thousands of identifiers from different platforms and run RMA or similar normalization analysis. Software, such as MatLab or R-Studio, provides a suitable technical solution, which was beyond the scope and timeline of the current project.

The trend from Figure 31 was considered similar if both numbers of fold change were above or below zero line (upregulation of downregulation), and different if one was below and another one was above the line and vice versa. To test trend similarity we used IF Function in Microsoft Excel 2016 and multiplied two values of fold change of the same gene from two comparisons. For similar trend the product was always greater than zero (e.g. 5.6 * 7.8 and -5.6 * -13.1 are >0, thus trend is similar, -4.3 * 5.2 and 6.2 * -5.5 are <0, thus trend is different). Delta is an absolute difference between two values of fold change (ABS Function in Microsoft Excel 2016). Double sorting, the first by Delta values and the second by trend (we used letters to assign trend in cells) followed by inserting a combined diagram with three lines for fold change from two comparisons and a Delta column generates a diagram as depicted in figures 16-21.

Score for figure 28 was calculated by dividing the number of common genes by the number of differentially expressed genes in non-control comparison. Example: the number of differentially expressed genes in static versus flow 20 hours (control) experiment was 799, the number of differentially expressed genes in iPSCs from FBs comparison was 5049, the number of common genes was 282, thus Difference Score =282/5049=0.5585.

Categories of comparison from Fig. 28 are clarified in the order of their appearance below.

Table 9. Description of comparison categories for Figure 28 **(supplementary information for section 4.2.2).**

#	Comparison	Description
1	Flow effect	Represents comparison between fibroblasts in static culture and fibroblasts after 20 hours and 40 hours of flow in the experiment. This category normalized other ones. Score for both flow conditions equals one.
2	ging. FBs – TGFβ1	Comparison between gingival fibroblasts and gingival fibroblasts induced with TGFβ1. Same platform and study.
3	ov. FBs – TGFβ1	Same as previous but fibroblasts were derived from the ovary. Same platform and study.
4	Neurons from iPSCs	Represents comparison between iPSC-derived neurons and FB-derived iPSCs from healthy donors. Different platforms, the comparison was performed on samples from two different microarray data sets.
5	NK cells from FBs	Comparison between natural killer cells expression profile from a secondary study and fibroblasts in a static condition in the experiment. The only comparison with control data set from flow experiment.
6	iPSCs from FBs	Comparison between gene expression profiles of lung fibroblasts and lung fibroblast-derived iPSCs. Same platform and study.
7	CMs from iPSCs	Represents comparison between iPSC-derived cardiomyocytes and FB-derived iPSCs from healthy donors. Different platforms, the comparison was performed on samples from two different microarray data sets.
8	Neurons from FBs	Comparison between iPSC-derived neurons and lung fibroblasts. Different platforms, the comparison was performed on samples from two different microarray data sets.
9	CMs from FBs	Comparison between iPSC-derived cardiomyocytes and lung fibroblasts. Different platforms, the comparison was performed on samples from two different microarray data sets.

Lists of unique and duplicated genes are provided below:

Table 11. List of genes from the Discussion (section 5.5) and Figure 28.

Control condition	Gene names in HGNC symbol format
Flow 20, Unique genes, N=160	ABCA1, ABHD5, ACLY, AGTRAP, ALDH6A1, AMIGO2, AMOT, ANKRD44, APBB2, APCDD1, APCDD1L, APOBEC3D, ARHGAP35, AS3MT; BORCS7-ASMT, BCL7A, BDKRB2; BDKRB1, BRAF, BTBD2, C14orf1, C4orf26, CALM3; CALM1; CALM2, CBLN2, CCDC102B, CDC42EP4, CEMIP, CNKSR3, COL10A1, CSGALNACT2, CXCL6, CYB5A, DACT1, DHCR7, DNAJC3, E2F7, EBF1, EDEM3, ELTD1, EMX2, EMX2OS, EPM2AIP1; TRANK1, ERN1, FAM102B, FAM196B, FAM57A, FARP1; FARP1-IT1, FICD,FLJ30064,FLOT1, FNBP1, FNDC1, FTSJ1, FYCO1, GABBR2
Flow 20, Duplicated genes, N=476	ABCA6, ABHD2, ABLIM3, ACKR3, ACOX2, ACTA2, ADAM12, ADAM19, ADAMTS6, ADAMTSL1, ADM, AHNAK, AHR, AIM1, AK5, ALCAM, ALDH1A3, ALDH3A2, AMOT; MIR4329, AMPH, ANKRD10-IT1, ANKRD28, AOX1, APOBEC3C, APOL2, APOL6, APPL2, ARHGAP29, ARID5B, ARL6IP5, ARNTL, ARSJ, AS3MT, ASAP2, ATP10D, ATP1B1, AXL, B3GALT2, B4GALT1, BAG2, BBS2, BCKDHB, BDH2; SLC9B2, BDKRB1, BDKRB2, BHLHE40, BLOC1S2, BMP2, BMPR2, BPGM, C15orf41, C1orf21, CALB2, CALHM2, CARHSP1, CAV1, CBLB, CCBE1, CCDC71L, CCL2, CCNG1, CD24, CD274, CD3EAP, CDC42EP3, CDH2, CDK14, CDK15, CDK17, CDON,

	CEMIP; KIAA1199, CHMP1B, CHRNA9, CHST11, CHURC1-FNTB; FNTB, CITED2, CLDN11, CLEC2B, CNN3, COL4A1, CPEB4, CRABP2, CREB3L2, CRISPLD2, CRYZ, CSF1, CSRP1, CTGF, CTHRC1, CTPS1; CTPS, CXCL5, CYTH3, CYYR1, DAAM2, DACT1, DCAF13, DCBLD1, DCLK1, DCLK2, DDR2, DEK, DGKI, DHCR24, DHRS3, DHRS7, DNAJB5, DNAJB9, DOCK11, DOCK4, DPYSL2, DRAM1, DSEL, DSP, ECE1, EDEM1, EDNRB, EHBP1, EMP2, ENPP1, ENPP2, EPB41L2, ERCC6; PGBD3; ERCC6-PGBD3, ERRFI1, ESM1, ESYT1, ETV6, EVI2B, F2RL2, FABP5, FAM101B, FAM168A, FAM171B, FAM20C, FAM214B, FAXDC2, FBXO32, FHOD3, FKBP14, FLRT2, FLT1, FMNL3, FOXP1, FRMPD3, FRY, FST, FSTL3, FZD7, FZD8; MIR4683, GALNT12, GAS6, GBP2, GCLC, GLS, GLT8D2, GNG5P2, GOLGA6L10; GOLGA6L9; GOLGA6L5P; GOLGA8Q, GOLGA6L9; GOLGA6L17P; GOLGA6L10; GOLGA6L5P, GOLIM4, GOLT1B, GOPC, GPR1, GPR135; L3HYPDH, GPR180, GPR183, GPRC5A; MIR614, GREB1L, GRIA3, GRK5, GSTO1, GUCY1B3, HEG1, HERC4, HGF, HIPK2, HIPK3, HIST1H2BC; HIST1H2BB, HIST2H2BE, HOMER1, HS3ST3B1, IDH1, IDH2, IFI16, IFIT1, IFIT3, IFIT5, IL11, IMPAD1, INHBA, INSIG1, ITGA2, ITGAV, ITPRIP, ITPRIPL2, IVNS1ABP, JADE2, JARID2, JUNB, KDM6B, KIAA1217, KIAA1549L, KIRREL, KIRREL3, KIT, KITLG, KRT34; LOC100653049, KRTAP1-1, KRTAP1-4; KRTAP1-3; KRTAP1-1; KRTAP1-5, KRTAP1-5, LAYN, LDB2, LINC00152; MIR4435-1HG, LINC00260, LINC00312, LINC01128; RP11-206L10.11, LMCD1, LMNA, LMO4, LRIG1, LRRN3, LTA4H, LTBP1, MAP3K4, MAP3K5, MAPRE2, MARCKS, MASP1, MED8, MEF2D, MEIS2, METTL7A, MGARP, MICAL2, MIR125B1, MIR181B1, MIR199A1, MIR21; VMP1, MIR31HG, MIR503, MLXIP, MMP14, MMP16, MNS1, MOB1B, MOSPD1, MPV17L2, MRGPRF, MSANTD3-TMEFF1; TMEFF1, MT1F, MT1G, MT1H, MT1JP, MT1X, MT2A, MTX3, MURC, MYO10, NADK2, NAMPT, NAT9, NCOA2, NDNF, NDRG3, NEDD4, NFIA, NFIX, NIPSNAP1; THOC5, NOV, NOVA1, NOX4, NPAS2, NREP, NRG1, NRP2, NTN4, OAS2, OPCML, OR56B1; TRIM22, OSBPL1A, OSBPL9, OSR2, PAG1, PALLD, PARD3B, PARP14, PARP9, PAWR, PCDH18, PCDH9, PCSK1, PDCD1LG2, PDE5A, PDE7B, PDGFRA, PDLIM7, PDPN, PDZRN3, PEG10, PGM2L1, PGM3, PHTF2, PIK3R1, PITPNC1, PLAUR, PLCB4, PLCH1, PLK2, PLK3, PLN, PLOD2, PMEPA1, PMP22, PNP, POPDC3, PORCN, PPP1R14C, PPP2R3A, PPP3CA, PRDM1, PRDM8, PREX1, PRIM2, PRIM2; LOC100996481, PRPS1, PRR5L, PRRX1, PRSS12, PSIP1, PTGIS, PTGS1, PTHLH, PTK7, PTPRK, PTX3, PXK, RALGPS2, RARG, RASSF8, RAVER2, RBM24, RCAN2, RCAN2, REV3L, RGCC, RGL1, RGS16, RHOB, RHOBTB3, RNF128, RNF144B, RNF213, ROBO2, ROR1, RUNX2, RUSC2, RYBP, S100A10, SAMD9, SAMD9L, SAMHD1, SASH1, SAV1, SCG5, SDC1, SDPR, SEC14L2, SEC61G, SEMA3A, SEMA7A, SERINC5, SERPINB1, SERPINB2; SERPINB10, SGMS2, SH2D4A, SH3PXD2A, SH3PXD2B, SIPA1L1, SIPA1L2, SIRPA, SKP2, SLC14A1, SLC16A4, SLC17A5, SLC19A2, SLC20A2, SLC22A4, SLC25A32, SLC26A2, SLC30A1, SLC30A4, SLC33A1, SLC35E1, SLC35F2, SLC38A5, SLC39A7, SLC41A2, SLC43A3; PRG2, SLC4A4, SLC7A14, SLC7A5, SLC7A6, SLC7A8, SLC9A1, SLC9B2, SMAD3, SMAD7, SOX4, SP110,SPDL1, SPHK1, SRGAP2B; SRGAP2C, SRPX2, SSR3, STAT6, STK38L, SUCLG2, SWAP70, SYNE1, SYNPO2, SYT11, SYT14, SYTL2, TAGLN, TALDO1, TANC2, TBC1D8, TBX5, TCEB3, TENM3, TFPI, TFPI2, TGFBR3, THAP2, TMEM104, TMEM117, TMEM14A, TMEM171, TMEM2, TMOD1, TMTC1, TNFRSF11B, TNFRSF12A, TNFRSF19, TOMM34, TOMM40, TOX, TP53, TPM1, TPST1, TRANK1, TRERF1, TRIB1, TRIM21, TRPC6, TSPAN13, TSPAN2, TTF2, UBA7; MIR5193, UBE2M, UBE2MP1, UBE2Q2P1, UCK2, USP53, VDR, VIT, VLDLR, VPS25, WNT5B, YRDC, ZFP36, ZFP36L2, ZNF267, ZNF281, ZNF778
Flow 40, Unique genes, N=58	AMIGO2, ANKRD10; ANKRD10-IT1, ANKRD10+N1:N1151, ANKRD44, BAIAP2L1; BRI3, C14orf1, CALM2; CALM1; CALM3, CALM3, CCDC102B, CEMIP; KIAA1199, CNKSR3, COL10A1, CRLF1, DNAJC3, E2F7, EBF1, ELTD1, FAM168A, FLRT2; LOC100506718, FNDC1, FOXQ1, GPCPD1, GPR124, GRK5; GRK5-IT1; RP11-567J24.4, IFI27, KANK4, LINC00327, LINC01060; RP11-219G10.3, MCOLN1, MEOX2, MIR222, MMP10, MSTO1, MSTO1; MSTO2P, NEIL3, OR52N3P; TRIM22, OR56B1; TRIM22, OR5B21, PENK, PER3, PKP4, PRIM2; LOC100996481, RNU6-403P, RP11-527N22.2, RP4-794H19.4, RPS6KA2, RRAS2, SAT1, SF3B3, SOX9, SPDL1; CCDC99, SPTLC3, TLR3, TMEFF1, TP53I3, UBA7; MIR5193, UGGT2, XG; XGY2; XGPY2
Flow 40, Duplicated genes, N=283	ABCA1, ABHD2, ADAM12, ADAM19, ADAMTS4, ADAMTS6, ADAMTSL1, ADM, AIM1, ALCAM, ALDH1A3, AMOT, ANKH, ANKRD10-IT1, ANTXR1, AOX1, APOBEC3C, APPL2, ARHGAP18, ARHGAP29, ARID5B, ARNTL, ARSJ, ASAP2, ATF6B; TNXB, ATP8B1, AXL, B3GALT2, B4GALT1, BAALC, BAG2, BDH2; SLC9B2, BDKRB1, BDKRB2; BDKRB1, BLVRB, BMP2K, BMPER, BPGM, BRI3, BTN3A1, C15orf41, C1orf21, CALB2, CAV1, CAV2; CAV1, CBLB, CCBE1, CCL2, CCNG1, CDC42EP3, CDH2, CDK15, CEMIP, CHMP1B, CITED2, CLDN11, CLEC2B, CLU, COL8A1, COMP, CPED1, CREB3L2, CRISPLD2, CSF1, CSRP1, CSRP2, CTGF, CTHRC1, CTSK, CUL4B, CYB5A, DACT1, DCBLD1, DDR2, DHRS3, DHRS7, DRAM1, DSP, DTX3L, DUSP4, EDIL3, EDNRB, EHBP1, ELN, EMP2, ENPP1, ENPP2, EPAS1, EPM2AIP1; TRANK1, ERRFI1, ETV6, EVI2B, F3, FAM101B, FBN2, FBXO32, FHOD3, FOXP1, FST, FSTL3, FZD7, FZD8, GALNT12, GBP3, GCNT1, GCNT4, GK, GLT8D2, GOLGA6L10; GOLGA6L9; GOLGA6L5P; GOLGA8Q, GOLGA6L9; GOLGA6L17P; GOLGA6L10; GOLGA6L5P, GPAM, GPR1, GRIK2, GRK5, HEG1, HMOX1, HOMER1, IFIT1, IFIT3, IFNE, IL11, IL7R, INHBA, IPCEF1; CNKSR3, ITGA2, ITGA4, ITGAV, KIT, KITLG, KRTAP1-4; KRTAP1-3; KRTAP1-1; KRTAP1-5, KRTAP1-5, LAYN, LIMS3L; LIMS3, LOXL4, LRRC15, LTBP1, MAP3K4, MAP3K5, MB21D2, MEIS2, MEST, MGARP, MGARP; NDUFC1, MICAL2, MIR29A, MIR31HG, MLLT11, MMP14, MMP16, MMP2, MSANTD3-TMEFF1; TMEFF1, MSC, MTX3, MURC, MXRA5, NCAM2, NDUFA12, NFIL3, NOV, NOX4, NQO1, NR4A2, NREP, NTN4, OAS2, OAS3; OAS2, OLR1, P4HA3, PARD3B, PARP14, PARP9, PCDH18, PCSK1, PGM2L1, PITPNC1, PLAUR, PLN, PMEPA1, POPDC3, PORCN, PPA1, PPP1R14C, PPP3CA, PRDM1, PRDM8, PRELP, PRIM2, PRL, PRPS1, PRR5L, PRRX1, PRSS12, PRSS23, PSMB9, PSMD2, PSME1, PTGIS, PTGS1, PTHLH, PTK7, PTX3, PYGL, RASSF8, RCAN2, RGCC, RGS16, RHOB, RNF144B, RNF150, ROBO2, ROR1, RPS19, RYBP, S100A10, SALL1, SAMHD1, SDPR, SEMA3A, SEMA7A, SERINC5, SGCD, SGMS2, SH2D4A, SH3PXD2A, SIPA1L1, SIPA1L2, SKP2, SLC16A2, SLC17A5, SLC19A2, SLC22A3, SLC22A4, SLC30A7, SLC35F2, SLC38A5, SLC39A7, SLC4A4, SLC7A5, SLC7A8, SLC9B2, SLIT2, SMAD3, SOX4, SPDL1, SPON1, SPTBN1, SRPX2, STC1, STK38L, STOM, SWAP70, SYNE1, SYT14, SYTL2, TBX3, TBX5, TENM2, TFPI, TFPI., FPI2, THBS4, TMEM171, TMOD1, TMTC1, TNFRSF11B, TNXB, TNXB; TNXA, TOM1L1, TOX, TRANK1, TRIM22, TRPC6, TSPAN13, TSPAN2, TSPYL2, UBA7, UGCG, USP53, VGLL3, VIT, VLDLR, XYLT1

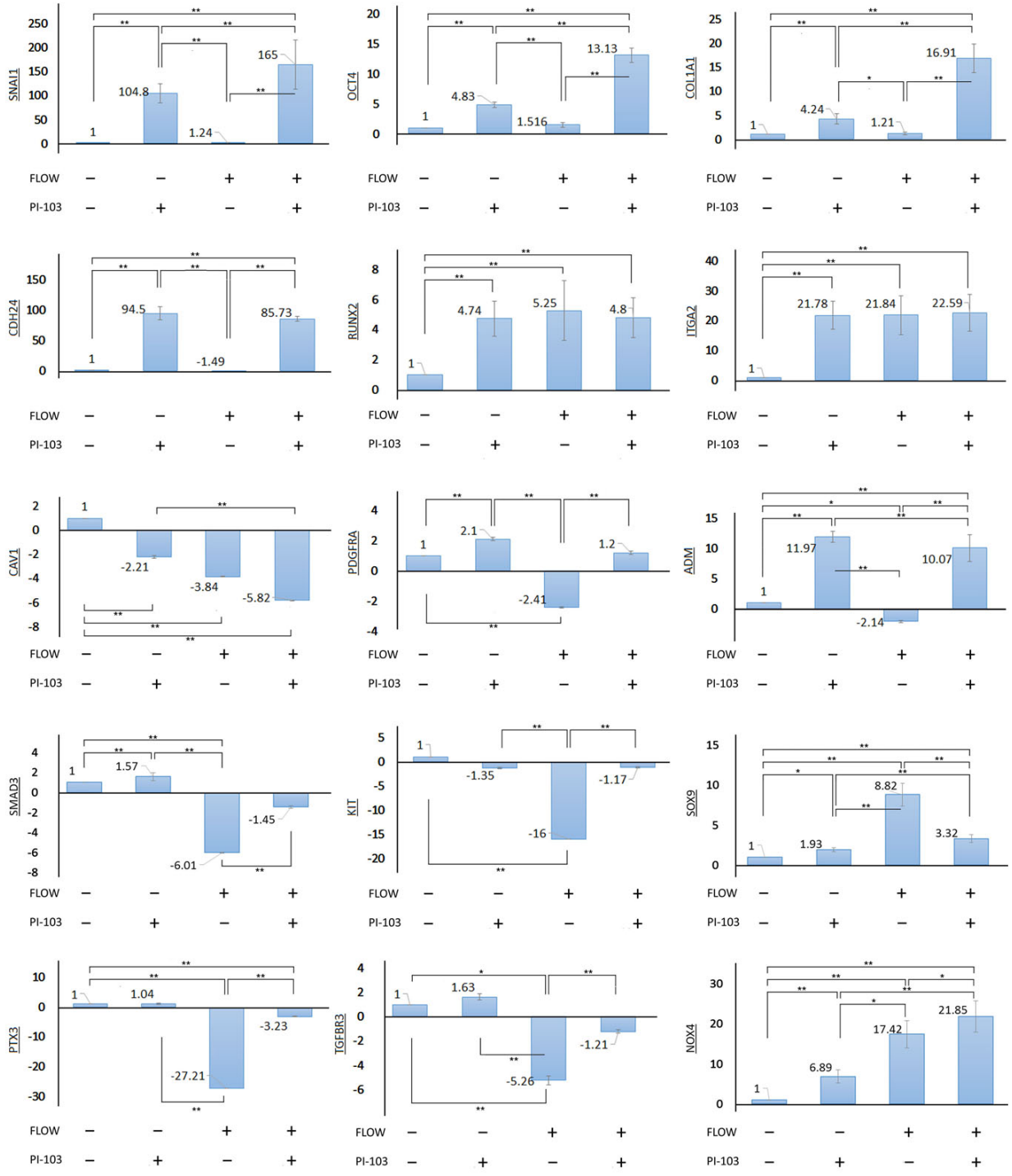

Figure 32. Summary of expression of all genes according to Results chapter **(supplementary information for section 5.5).**